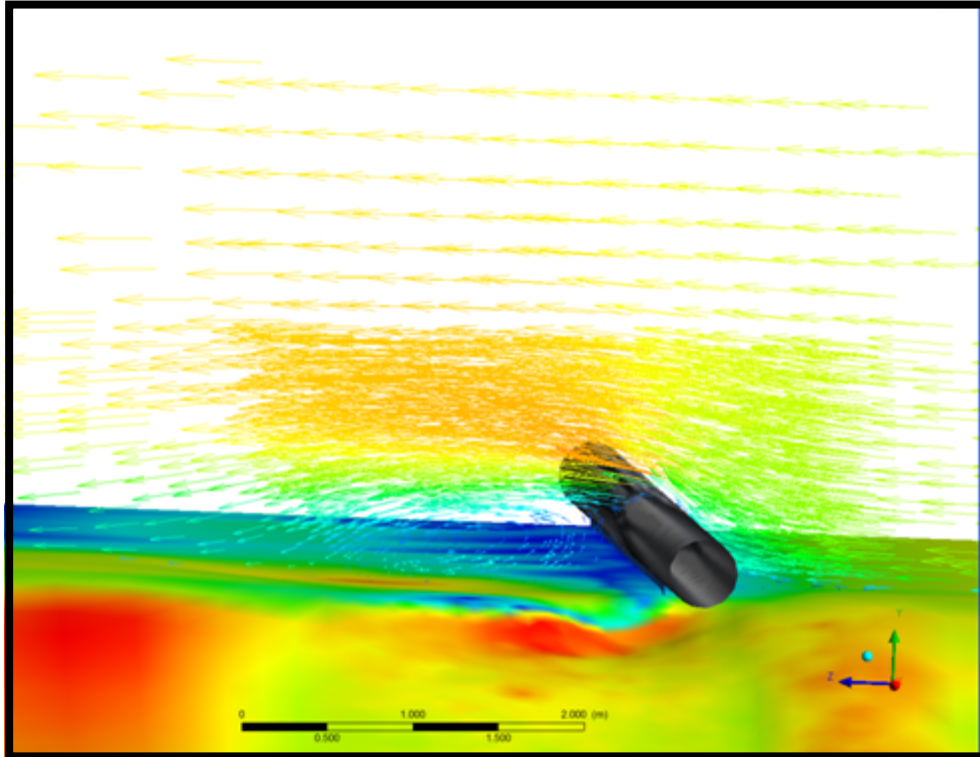




Risk Assessment for Pipelines In Deepwater (RAPID) Joint Industry Project



PREPARED FOR:

**Bureau of Ocean Energy Management, Regulation, and Enforcement
(BOEMRE)**

**THIS STUDY WAS FUNDED BY THE BOEMRE, U.S. DEPARTMENT OF THE INTERIOR, WASHINGTON, D.C.,
UNDER CONTRACT NUMBER M08PC20039**

Mik Else

Safety Research Engineer | U.S. Dept. of Interior | Bureau of
Offshore Energy Management, Regulation, and Enforcement
381 Elden Street, MS 4021 | Herndon, VA 20170-4879

PREPARED BY:



This report was prepared under contract between the Bureau of Ocean Energy Management, Regulation, and Enforcement (BOEMRE) and SeaQ Joint Venture (Sea Engineering, Incorporated). This report has been technically reviewed by the BOEMRE and approved for publication. Approval does not signify that the contents necessarily reflect the views and policies of the agency, nor does mention of trade names or commercial products constitute endorsement or recommendation for use. It is, however, exempt from review and compliance with the BOEMRE editorial standards.

Table of Contents

ABSTRACT.....	6
SECTION 1 INTRODUCTION	7
1.1 PIPELINE RISK AND THE ROLE OF DEEP-SEA FURROWS.....	7
1.2 STUDY OBJECTIVES.....	8
1.3 REPORT STRUCTURE	9
SECTION 2 LITERATURE REVIEW	10
2.1 ASSESSMENT OF PIPELINE RISK IN FURROW FIELDS.....	10
2.2 THREE-DIMENSIONAL SCOUR BELOW OFFSHORE PIPELINS IN STEADY CURRENTS.....	11
SECTION 3 COMPUTATIONAL FLUID DYNAMICS	13
3.1 GENERAL OVERVIEW OF THE MODELING PROCESS	13
3.2 DESCRIPTION OF MATHEMATICAL MODELS.....	14
3.3 MODEL GEOMETRY AND BOUNDARY CONDITIONS FOR CONSTRUCTED SPANS	17
SECTION 4 BATHYMETRIC DATA RESOLUTION	19
4.1 METHODS OF INVESTIGATION FOR DATA RESOLUTION ANALYSIS	19
4.2 BATHYMETRIC RESOLUTION EFFECTS ON BED PROFILES	22
4.3 BATHYMETRIC RESOLUTION EFFECTS ON BED SHEAR.....	24
SECTION 5 SPAN HYDRODYNAMICS AND BED EROSION	27
5.1 SPAN HYDRODYNAMICS.....	27
5.2 METHODS OF INVESTIGATION FOR 6-DAY BED EROSION	29
5.3.1 <i>Global Trend</i>	31
5.3.2 <i>Local Trends</i>	32
5.3.3 <i>Calculating Horizontal Propagation Rates</i>	35
SECTION 6 CONCLUSIONSRECOMMENDATIONS	37
6.1 DESIGN CONSIDERATIONS	39
6.1.1 <i>Recommendations Preceding Pipeline Placement</i>	39
6.1.2 <i>Recommendations Following Pipeline Placement</i>	42
6.2 FUTURE RESEARCH TOPICS	45
SECTION 7 REFERENCES	48

List of Figures

Figure2- 1. Flow chart of the procedure developed by SeaQ to assess pipeline risk in furrow fields.....	50
Figure2-2. Spatial distribution of pipeline risk factors in the Atlantis region at the end of a two year period.....	51
Figure2-3. Spatial distribution of pipeline risk factors in the Atlantis region at the end of a ten year period.....	52
Figure2-4. Diagram of the experimental setup used by Cheng et al.....	52
Figure 3- 1. Diagram of the physical setup used for CFD models. The velocity inlet is the face 3.4 m upstream from the pipeline, and the pressure outlet is the face 6.9 m downstream from the pipeline.	53
Figure 4-1. Histogram of shoulder slopes for 1 ft bathymetric resolution. Angles computed between first two points at each shoulder.....	54
Figure 4-2. Histogram of shoulder slopes for 1 ft bathymetric resolution. Angles computed as average of 5 points at each shoulder.	54
Figure 4-3. Histogram of shoulder slopes for 1 ft bathymetric resolution. Angles computed as average of 10 points at each shoulder.	54
Figure 4-4. Comparison of constructed bed profiles to the seabed for Span 1 (0.4 degree shoulder slope).	55
Figure 4-5. Comparison of constructed bed profiles to the seabed for Span 2 (0.9 degree shoulder slope).	56
Figure 4-6. Comparison of constructed bed profiles to the seabed for Span 3 (5.4 degree shoulder slope).	57
Figure 4-7. Average Difference (cm) between the constructed beds and the seabed over the first 2 feet of the span.....	58
Figure 4-8. Global bed shear stress (Pa) patterns for Span 1. Constructs from varying data resolution are displayed in each sub window: top is the 1-foot resolution construct; bottom left is the 5-foot resolution construct; bottom right is the 10-resolution construct. The pipeline is colored gray to elucidate its position. Regions of high shear stress are represented by hot colors, while areas of low shear stress are depicted by cool colors.....	59
Figure 4-9. Global bed shear stress (Pa) patterns for Span 2. Constructs from varying data resolution are displayed in each sub window: top is the 1-foot resolution construct; bottom left is the 5-foot resolution construct; bottom right is the 10-resolution construct. The pipeline is colored gray to elucidate its position. Regions of high shear stress are represented by hot colors, while areas of low shear stress are depicted by cool colors.....	60
Figure 4-10. Global bed shear stress (Pa) patterns for Span 3. Constructs from varying data resolution are displayed in each sub window: top is the 1-foot resolution construct; bottom left	

is the 5-foot resolution construct; bottom right is the 10-resolution construct. The pipeline is colored gray to elucidate its position. Regions of high shear stress are represented by hot colors, while areas of low shear stress are depicted by cool colors..... 61

Figure 4-11. Bed shear stress (Pa) profiles for Span 1 directly under the pipe for 1, 5 and 10 foot data resolution constructs. 62

Figure 4-12. Bed shear stress (Pa) profiles for Span 2 directly under the pipe for 1, 5 and 10 foot data resolution constructs. 62

Figure 4-13. Bed shear stress (Pa) profiles for Span 3 directly under the pipe for 1, 5 and 10 foot data resolution constructs. 63

Figure 4-14. Maximum calculated shear stress (Pa) on the sediment bed for all constructs. 63

Figure 5-1. Schematic of flow characteristics around a pipeline on the seabed. a) Flow streamlines over the pipeline showing flow separation and downstream recirculation. b) Pressure distribution around the pipeline..... 64

Figure 5-2. Figure 2. Velocity vectors and seabed shear stress contours (Pa) along an example pipeline span. The pipeline is in contact with the bed in the far side of the image and the near side is the span..... 65

Figure 5-3. Velocity contour (m/s) cross section in the at the pipeline shoulder 66

Figure 5-4. Pressure contour (Pa) cross section in the at the pipeline shoulder. 67

Figure 5-5. Velocity vectors (m/s) cross section and bed shear stress (Pa) in the wake of the pipeline shoulder. 68

Figure 5-6. Velocity vectors (m/s) cross section and bed shear stress (Pa) over the pipeline shoulder region. Top half of the figure is where the pipeline is on the sediment bed, the middle is the shoulder region, and the lower half is the span region. 69

Figure 5-7. Bed shear stress (Pa) contours over the pipeline shoulder region. Top half of the figure is where the pipeline is on the sediment bed, the middle is the shoulder region, and the lower half is the span region..... 70

Figure 5-8. Global shear stress (Pa) pattern on Span 2 using a current speed of 25 cm/s. The bed shear stress was below the critical shear stress of sand (0.2 Pa) over the sediment bed. 71

Figure 5-9. Global bed shear stress (Pa) on eroding bed for the initial bed form (top left), bed after 1 day (top right), bed after 2 days (bottom left), and bed after 3 days (bottom right) of 75 cm/s current speeds. 72

Figure 5-10. Global bed shear stress (Pa) on eroding bed after 3 days (top left), 4 days (top right), 5 days (bottom left), and 6 days (bottom right) of 75 cm/s current speeds. 73

Figure 5-11. Global bed shear stress (Pa) on eroding bed for the initial bed form (top left), bed after 2 days (top right), bed after 4 days (bottom left), and bed after 6 days (bottom right) of 50 cm/s current speeds. 74

Figure 5-12. Global bed shear stress (Pa) on eroding bed for the initial bed form (right), and the bed after 6 days of 35 cm/s current speeds. 75

Figure 5-13. Time series of bed profiles for the 75 cm/s simulations. Profiles were taken at 10 and 25 cm upstream from the pipeline axis, directly below the pipeline axis, and 10 cm downstream from the pipeline axis. 76

Figure 5-14. Time series of bed profiles for the 75 cm/s simulations. Profiles were taken at 25, 50, 100, and 200 cm downstream from the pipeline axis. 77

Figure 5-15. Time series of bed profiles for the 50 cm/s simulations. Profiles were taken at 10 and 25 cm upstream from the pipeline axis, directly below the pipeline axis, and 10 cm downstream from the pipeline axis. 78

Figure 5-16. Time series of bed profiles for the 50 cm/s simulations. Profiles were taken at 25, 50, 100, and 200 cm downstream from the pipeline axis. 79

Figure 5-17. Time series of bed profiles for the 35 cm/s simulations. Profiles were taken at 10 and 25 cm upstream from the pipeline axis, directly below the pipeline axis, and 10 cm downstream from the pipeline axis. 80

Figure 5-18. Time series of bed profiles for the 35 cm/s simulations. Profiles were taken at 25, 50, 100, and 200 cm downstream from the pipeline axis. 81

Figure 5-19. The mean (right) and maximum (left) drop in bed height (m) for the 75 cm/s simulations. 82

Figure 5-20. The mean (right) and maximum (left) drop in bed height (m) for the 50 cm/s simulations. 82

Figure 5-21. The mean (right) and maximum (left) drop in bed height (m) for the 35 cm/s simulations. 83

Figure 5-22. Time changing bed shear stress (Pa) profiles for the 75 cm/s simulations at 10 cm upstream from the pipeline axis (left), and directly below the pipeline axis (right). 84

Figure 5-23. Time changing bed shear stress (Pa) profiles for the 75 cm/s simulations at 10 (left), and 25 cm downstream from the pipeline (right). 84

Figure 5-24. Time changing bed shear stress (Pa) profiles for the 50 cm/s simulations at 10 cm upstream from the pipeline axis (left), and directly below the pipeline axis (right). 85

Figure 5-25. Time changing bed shear stress (Pa) profiles for the 50 cm/s simulations at 10 (left), and 25 cm downstream from the pipeline (right). 85

Figure 5-26. Time changing bed shear stress (Pa) profiles for the 35 cm/s simulations at 10 cm upstream from the pipeline axis (left), and directly below the pipeline axis (right). 86

Figure 5-27. Time changing bed shear stress (Pa) profiles for the 35 cm/s simulations at 10 (left), and 25 cm downstream from the pipeline (right) 86

Figure 5-28. Time series of the maximum shear stress (Pa) directly underneath the pipeline (right); and time series of the scour slope (degrees) for the 75 cm/s simulations (left). 87

Figure 5-29. Time series of the maximum shear stress (Pa) directly underneath the pipeline (right); and time series of the scour slope (degrees) for the 50 cm/s simulations (left). 87

Figure 5-30. Time series of the maximum shear stress directly underneath the pipeline (right);
and time series of the scour slope (degrees) for the 35 cm/s simulations (left). 88
Figure 5-31. Schematic representation of the scour slope relative to the pipeline..... 89

ABSTRACT

Long unsupported pipelines subjected to strong bottom currents will experience vortex induced vibrations, which significantly increase pipeline fatigue. In this study, two important considerations for pipeline risk assessment methodologies are investigated: 1) the effects of bathymetric data resolution on the modeling of pipeline spans, and 2) bed erosions in the vicinity of pipeline touchdown locations. Investigations were carried out using the sophisticated computational fluid dynamics software ANSYS FLUENT. Numerical simulations on sediment beds created from bathymetric data with 1, 5, and 10-foot resolutions allowed for the comparison and evaluation of predicted bed shear stress patterns. It was determined that low resolution bathymetric data, combined with steep shoulder slopes, causes underestimations of bed shear stress and erosion rates. Numerical simulations using current magnitudes of 35, 50, and 75 cm/s were also preformed to emulate natural erosion processes at a pipeline touchdown location. The 75 cm/s current magnitude created the largest morphology changes, causing the sediment bed to drop as much as 23 cm. The six-day simulations showed that both the maximum bed shear stress and scour slope approach a uniform steady state value. This observation was used to develop a methodology to predict scour propagation along the longitudinal axis of pipeline spans.

SeaQ, JV. (SeaQ), a joint venture between Sea Engineering, Inc. and AQ, LLC., formed a Joint Industry Project (JIP) called Risk Assessment for Pipelines In Deepwater (RAPID). The JIP included support from the Bureau of Ocean Energy Management, Regulation, and Enforcement (BOEMRE) to enhance and extend SeaQ's pipeline risk assessment methodology. The goal was to determine whether or not future risks increase significantly relative to baseline conditions for deepwater pipelines in areas with an uneven seabed. Secondary objectives of the RAPID JIP were:

- Improvement of the predictive capability and reliability of the modeling framework, which includes incorporation of site-specific data and model validation.
- Use the improved and validated modeling framework to evaluate bed scour in the vicinity of a pipeline over a wide range of conditions.

SECTION 1 INTRODUCTION

1.1 PIPELINE RISK AND THE ROLE OF DEEP-SEA FURROWS

Offshore pipelines are used extensively to transport hydrocarbons from oceanic reserves to storage units. The first marine pipeline was built in the late nineteenth century (Guo, 2005). Since then, the petroleum industry has proven that pipelines offer the most economical means of large scale transportation of crude oil, natural gas, and their products (Guo, 2005). Petroleum is crucial to many industries, and because of this, the prominence of offshore pipelines will continue to flourish. Currently, 11,954 miles of marine pipelines are being built or planned (Beaubouef, 2010). The vital role of these pipelines is undeniable; however, the consequences of pipeline failure are severe both economically and environmentally. It is therefore critical to develop reliable and cost effective methods for evaluating pipeline risk and route selection.

Two potential causes for pipeline failure are regional scale hydrodynamic forces and vortex induced vibrations (VIV). Hydrodynamic forces are of most concern to pipelines with multiple unsupported spans. In conjunction with strong episodic events, these pipelines may experience lateral instability and movement. Although the effects of hydrodynamic forces warrant attention, vortex induced vibrations are perhaps of greatest concern. Due to boundary layer separation, flow around a pipeline can result in the oscillatory shedding of sheet vortices (Blevins, 2001). Each time a vortex is shed it alters the pressure distribution around the pipeline, creating a time-varying force at the frequency of the shedding. Under resonance conditions the pipe will begin to vibrate, leading to accelerated pipeline fatigue and possibly failure.

Natural seabed undulations can inherently create dangerous conditions for pipelines by causing unsupported spans. Recently deep-sea sedimentary channels, known as furrow fields, have been identified as a potentially significant factor in pipeline route selection. Furrows are found in cohesive sediments and are longitudinal bed forms that tend to be aligned parallel to bottom

currents. They have been observed in both deep-sea and lake regions such as the Bahama Outer ridge, the English Channel, and Lake Superior (Flood, 1983). Furrows that are potentially hazardous to pipelines have also been identified in the vicinity of the Sigsbee Escarpment in the Gulf of Mexico (GOM), specifically the Atlantis region. Although the width of many of these furrows is smaller than that needed to cause the onset of VIV, horizontal erosion along the pipelines longitudinal axis may create spans that exceed this critical length. In order to accurately predict pipeline risks in furrow fields, risk assessment models must incorporate site-specific data and accurate erosion models to account for this horizontal propagation.

In 2006, SeaQ developed a risk assessment procedure for pipelines in the GOM. The methodology was geared towards identifying hazardous zones on a regional scale. However, due to limited research on horizontal scour propagation rates, the accuracy of the procedure is limited when attempting to analyze spans on an individual basis. The most thorough research on propagation rates has been conducted with non-cohesive sediments, and may not be applicable to the GOM (Cheng, 2009, Sumer,2002).

Additionally, the quality of bathymetric data required to conduct accurate pipeline risk assessments is also of interest. The costs associated with data collections are directly related to the resolution of the bathymetric survey. If data collected from single-beam surveys are sufficient enough to conduct pipeline risk assessments, investigators can substantially save on cost by avoiding multi-beam techniques.

1.2 STUDY OBJECTIVES

The main focus of this study was to enhance the predictive capabilities and reliability of the current pipeline risk assessment procedure used for regions with an uneven seabed. The study had two primary objectives:

- Evaluate the effects of bathymetric data resolution on the modeling process of pipeline spans and the assessment of pipeline risk in furrowed regions

- Improve the understanding of the bed erosion in the vicinity of pipeline spans in order to improve risk of modeling

In order to achieve these objectives, modeling was carried out using sophisticated computational fluids dynamics (CFD) software called ANSYS FLUENT. Detailed information on the effects of bathymetric data resolution and span hydrodynamics was collected through numerical modeling. The data was then integrated with recent findings from Cheng et al. (2006) to predict erosion rates in the Atlantis region on an individual span bases. Although this study uses site specific data collected in the GOM, the methodology and results can be generalized and applied to any region with large-scale seabed undulations to estimate horizontal scour propagation rates.

1.3 REPORT STRUCTURE

The main body of the report contains the following sections:

- *Section 2:* a methodology to evaluate pipeline risk in a furrow field is reviewed along with current findings on horizontal propagation rates.
- *Section 3:* descriptions of the mathematical models used to evaluate span hydrodynamics are given. The physical setup for the CFD simulations is also discussed.
- *Section 4:* an analysis of the effects of bathymetric data resolution on the pipeline risk assessment procedure is presented.
- *Section 5:* a model for predicting horizontal propagation rates at span shoulders is developed, and predicted horizontal propagation rates are presented.
- *Section 6:* conclusions are formulated from the various analyses conducted during this study. Recommendations to refine the present analysis and reduce uncertainty in future work are provided.

SECTION 2 LITERATURE REVIEW

A thorough understanding of the most current pipeline risk assessment model will assist readers in comprehending the relevance of this study. It is therefore pertinent to review the Assessment of Pipeline Risk in Furrow Fields Located in the Gulf of Mexico (SeaQ, 2006). A brief summary of Cheng et al. research on scour propagation rates will also be given (2009). The assumptions made in this study to calculate horizontal propagation rates are justified by Cheng et al. findings (2009).

2.1 ASSESSMENT OF PIPELINE RISK IN FURROW FIELDS

The objective of Assessment of Pipeline Risk in Furrow Fields Located in the Gulf of Mexico was to ascertain the regional risk of pipeline failure based on existing furrow geometries (widths and depths). The study incorporated multi-beam bathymetry data, near-bottom currents, and surface sediment properties to produce a regional scale estimate of pipeline risk. The flow chart in Figure 2- 1 shows an outline of the general procedure. A brief description of each step follows:

Current Analysis: Current meter data in the Atlantis region was separated into bins based on current magnitude. The bins were then used to determine the frequency and duration of a specific current magnitude interval.

Hydrodynamic Modeling: STORM/CFD 2000 was used to predicted bed shear stress patterns for four idealized furrows with varying width to depth ratios. It was determined that increases in the width:depth ratio of furrows caused an increase in bed shear stress.

Relationship Between Erosion Rate and Furrow Geometry: Data from box cores taken near the Atlantis region were analyzed to determine erosion rate based on bed shear stress. Because hydrodynamic modeling showed a linear relationship between current magnitude and near-bed velocity, SeaQ was able to develop an empirical formula for bed erosion based on current magnitude and furrow geometry.

Maximum Allowable Pipeline Span: The maximum allowable pipeline span (length causing the onset of VIV) was calculated based on a methodology developed by the Bureau of Ocean Energy Management, Regulation, and Enforcement (1997). Based on the physical properties of the pipelines in the Atlantis region, and the current data, a maximum allowable free-span length of 38 m was calculated.

Determining Increases in Pipeline Spans: Bathymetry data was analyzed to create a spatial map of the average width:depth ratios over the Atlantis region. Increases in pipeline span lengths (ΔL) were then computed regionally by combining the determined spatial distribution of span geometries and current magnitudes with the developed empirical relationship for bed erosion. When calculating horizontal erosion, a 1:1 ratio between vertical and horizontal scour propagation was assumed because limited data was available on shoulder scour dynamics.

Determine Risk of Spanned Pipelines: A pipeline risk factor was defined as:

$$R_{pipe} = \frac{L + 2\Delta L}{L_c}$$

where L is the initial free-span length of the pipeline (i.e. furrow width), ΔL is the free-span length increase (factor of two account for both shoulders), and L_c is the maximum allowable pipeline span length (38 m for the Atlantis region). A pipeline risk factor of one or greater indicates that the free-span length is equivalent to or larger than the critical free-span length. Pipeline fatigue due to VIV may occur. Risk factors were predicted over the entire Atlantis region for a two and ten year time period (Figure 2-2 and Figure 2-3).

2.2 THREE-DIMENSIONAL SCOUR BELOW OFFSHORE PIPELINS IN STEADY CURRENTS

Cheng et al. experimentally investigated three-dimensional scour below offshore pipelines subject to steady currents. The major emphasis was on the analysis of scour propagation velocity along the pipeline after the initiation process. Most studies on local scour below pipeline prior to Cheng et al. were based on two-dimensional flume tests, where the local scour profile in the plane perpendicular to the pipeline axis was measured (Brors, 1999, Li, 1999,

Liang, 2004). However, in reality the scour process is three-dimensional. The main objective of Cheng et al. research was to develop a method to predict the longitudinal scour rates below pipelines.

Physical experiments were conducted in a water flume 4 m wide, 2.5 m deep and 50 m long. A sand pit was constructed in the middle of the flume (4 m long and 4 m wide). Tests were conducted using a smooth plastic pipe with a diameter of 50 mm, and a depth averaged velocity between 0.36 and 0.54 m/s. Local scour depths directly below the pipeline were measured using conductivity probes. The experimental setup is shown in Figure 2-4. Diagram of the experimental setup used by Cheng et al. Cheng et al. reported the following conclusions:

- Pipeline scour propagates horizontally at either a constant rate, or two constant rates, depending on pipeline embedment depth, the incoming flow velocity, and the incident angle of the incoming flow
- Scour propagation rates increase with increases flow rate, and decrease with decreasing flow rate
- The scour slope at the shoulder region remains fairly constant throughout each test, and the angle of repose of sand is a good estimate for the scour slope (it should be noted that the research was conducted using non cohesive sediments)
- An empirical formula for horizontal propagation rates was developed by assuming that lateral movement is purely induced by scour pit deepening. The formula can be written as:

$$V_h = K \left(25 \frac{\sqrt{g(s-1) d_{50}^3}}{D \tan \beta} \theta^{\frac{5}{3}} \left(1 - \frac{e}{D} \right) \right)$$

where V_h is the horizontal scour propagation rate, g is the acceleration of gravity, d_{50} is the average particle diameter of the sediment, D is the pipeline diameter, β is the average shoulder slope, θ shields parameter, e is the embedment depth of the pipeline, and K is an adjustment factor to account for additional scour mechanisms

SECTION 3

COMPUTATIONAL FLUID DYNAMICS

The two main techniques employed to investigate pipeline scour are experimental testing and numerical modeling. With the resources and time available for this study, computer modeling offered the capability to examine multiple span geometries and current speeds. It also allowed for easy visualization of flow patterns around pipelines, which may offer insight into scour mechanisms. This section outlines the modeling process used for simulations in ANSYS FLUENT, including mathematical modeling details.

3.1 GENERAL OVERVIEW OF THE MODELING PROCESS

All engineering simulations start with geometry creation. A physical representation of the desired study region must be created. To accomplish this, the ANSYS software package comes with a built-in computer aided design program, called ANSYS Design Modeler. Design Modeler provides powerful tools for construction of geometry from the ground up. Using familiar solid modeling operations, a complex model can be produced. 2-D sketches can be extruded into 3-D solids and then modified with Boolean operations.

Once the geometry has been created, it must be meshed in order to carry out a CFD simulation. This step is performed within ANSYS Meshing. ANSYS Meshing contains a compilation of algorithms that give users the ability to create unstructured tetrahedral, hexahedral, and hybrid meshes. The combination of automated surface meshing, boundary layer technology (including automatic proximity handling) and an advancing front tetrahedral mesh algorithm ensures high-quality meshing for fluid flow analysis.

CFD calculations are performed within ANSYS FLUENT. ANSYS FLUENT provides comprehensive modeling capabilities for a wide spectrum of incompressible and compressible fluid flow problems (6). It combines a broad range of mathematical model with the ability to analyze complex geometries. For all flows, ANSYS FLUENT simultaneously solves conservation equations for mass and momentum. When dealing with turbulence flows, additional equations are solved.

Ultimately, this leads to predictions of flow properties such as velocity, pressure, and shear stresses. The basic procedure for a simulation can be summarized as:

1. Create model geometry and mesh
2. Setup the solver and physical models
3. Compute and monitor the solution

3.2 DESCRIPTION OF MATHEMATICAL MODELS

The current magnitudes and physical characteristics of pipeline spans in the GOM create turbulent conditions. A pipeline of diameter 0.41 m and current speeds of 35 and 100 cm/s (i.e. the range explored in this study) lead to a Reynolds Number (Re) of 96,000 and 270,000, respectively (calculations are based on a kinematic viscosity of 0.015 cm²/s). For flow around pipelines the transition from laminar to turbulent flow occurs at a Re of roughly 50,000. Turbulent conditions in the vicinity of pipeline spans are characterized by fluctuating velocity fields. These fluctuations can be of small scale and high frequency, and are therefore too computationally expensive to simulate directly. In order to reduce computational demands, simulations were run using an ensemble-averaged version of the governing Navier-Stokes equations. To form a solvable set of equations, a turbulence model was needed to determine unknown quantities in terms of known quantities.

In ensemble averaging, the instantaneous Navier-Stokes equations are decomposed into mean and fluctuating components. For the velocity components:

$$u_i = \bar{u}_i + u_i'$$

where \bar{u}_i and u_i' are the mean and fluctuating velocity components ($i = 1, 2, 3$ for three-dimensionality). Likewise, for the pressure and other scalar quantities:

$$\phi_i = \bar{\phi}_i + \phi_i'$$

where ϕ denotes a scalar such as pressure or energy. After substitution and manipulations of the above expressions into the governing equations, the Reynolds Averaged Navier-Stokes Equations (RANS) are obtained (assuming incompressible flow):

$$\frac{\partial}{\partial x_i} (\rho \bar{u}_i) = 0; \text{ (mass conservation)}$$

$$\frac{\partial}{\partial x_j} (\rho \bar{u}_i \bar{u}_j) = -\frac{\partial \bar{p} \delta_{ij}}{\partial x_i} + \frac{\partial}{\partial x_j} \left[\mu \left(\frac{\partial \bar{u}_i}{\partial x_j} + \frac{\partial \bar{u}_j}{\partial x_i} \right) \right] + \frac{\partial}{\partial x_j} (-\rho \overline{u'_i u'_j}); \text{ (momentum conservation)}$$

where p is the pressure, δ_{ij} is the Dirac delta function, and μ is the absolute viscosity. The RANS equations have the same general form as the instantaneous Navier-Stokes equations, with the velocity and pressure variables now represented by the ensemble averaged values. The Reynolds stress terms ($-\rho \overline{u'_i u'_j}$) also appear, which account for the combined effects of all turbulence scales. For this study, the Boussinesq hypothesis was employed in order to relate the Reynolds stress terms to mean velocity gradients:

$$-\rho \overline{u'_i u'_j} = \mu_t \left(\frac{\partial u_i}{\partial x_j} + \frac{\partial u_j}{\partial x_i} \right) - \frac{2}{3} \left(\rho k + \mu_t \frac{\delta u_k}{\delta x_k} \right) \delta_{ij}$$

where k is the turbulent kinetic energy, and μ_t is the turbulent viscosity. The advantage of the Boussinesq hypothesis is the relatively low computational cost associated with μ_t . It does however assume μ_t is an isotropic scalar quantity, which is not strictly true. With this in mind, flow near span regions does not show significant signs of turbulence anisotropy, which is characterized by highly swirling and stress-driven secondary flows (ANSYS FLUENT, 2009). For additional information on the Boussinesq hypothesis, the reader is asked to consult Hinze (1975).

Although numerous closure models exist for calculating k and μ_t , the shear-stress transport (SST) $k-\omega$ model was chosen for this study. Of the two-equation closure models available, the SST $k-\omega$ model best predicts flow patterns near walls (Menter, 1994). Recognizing the close

proximity of the seabed and pipeline to the flow region of interest, this was an important consideration. Also, past modeling efforts have shown the SST k - ω model closely approximates flow patterns characterized by adverse pressure gradients and separating flow, both of which were present in our simulations (Menter, 2003). It should be mentioned the SST k - ω model does over estimate turbulence production in regions with large normal strain, like stagnation points and regions with strong acceleration. This tendency, however, is much less pronounced than with the other two-equation closure models.

The additional transport equations allotted by the SST k - ω model are:

$$\frac{\partial}{\partial x_i} (\rho k \bar{u}_i) = \frac{\partial}{\partial x_j} \left(\Gamma_k \frac{\partial k}{\partial x_j} \right) + \widetilde{G}_k - Y_k$$

$$\frac{\partial}{\partial x_i} (\rho \omega \bar{u}_i) = \frac{\partial}{\partial x_j} \left(\Gamma_\omega \frac{\partial \omega}{\partial x_j} \right) + \widetilde{G}_\omega - Y_\omega + D_\omega$$

In these equations, ω is the specific dissipation rate, \widetilde{G}_k represents the generation of k due to mean velocity gradients, \widetilde{G}_ω represents the generation of ω , Γ_k and Γ_ω represent the effective diffusivities of k and ω , and Y_k and Y_ω represent the dissipation of k and ω due to turbulence, and D_ω represents the cross-diffusion term (for further details on all variables the reader is guided to 4.5.1 of ANSYS FLUENT Theory Guide, 2009). Finally, the turbulent viscosity is solved by relating it to the effective diffusivities through:

$$\Gamma_k = \mu + \frac{\mu_t}{\sigma_k}$$

$$\Gamma_\omega = \mu + \frac{\mu_t}{\sigma_\omega}$$

where σ_k and σ_ω are the turbulent Prandtl numbers for k and ω .

3.3 MODEL GEOMETRY AND BOUNDARY CONDITIONS FOR CONSTRUCTED SPANS

Span profiles extracted from bathymetric data in the area of the Atlantis oil and gas pipelines were imported into Design Modeler to construct seabed spans; serving as the lower bounds for CFD analyses (See Section 4.1 METHODS OF INVESTIGATION FOR DATA RESOLUTION ANALYSIS for further details about profile extraction). The 2-D seabed profiles were extruded outward to create 3D surfaces. Bed elevations were assumed constant in the extrusion direction for the initial bed form. To simplify simulations and reduce computational demands, only the first 15 m of span profiles were modeled in each simulation. With the exception of imported bathymetry profiles, all dimensions were held constant between simulations.

The upstream face, or velocity inlet, was positioned 3.4 m upstream from the pipeline axis. Similarly, the downstream face, or pressure outlet, was placed 6.9 m downstream. Preliminary simulations were performed to ensure both the upstream and downstream faces were positioned far enough away from the pipeline to avoid reverse flow conditions. The highest imported profile elevation point was taken as the level bed height and extended 10 m away from the span. The pipeline (diameter of 0.40 m) was positioned perpendicular to the upstream and downstream faces. This elevated placement allowed for easily reproducible meshes by avoiding high aspect ratios and skewness in cells near the pipeline-bed interface. The top of the control volume was defined as being 3 m above level bed. Figure 3- 1. Diagram of the physical setup used for CFD models. The velocity inlet is the face 3.4 m upstream from the pipeline, and the pressure outlet is the face 6.9 m downstream from the pipeline. shows a schematic diagram of the setup.

Velocity profiles for both the data resolution and horizontal scour propagation studies were computed by running CFD simulations on spans identical to the ones analyzed, but without pipelines. For these initial runs, current magnitudes were perpendicular to the velocity inlet. The exiting velocity profiles were saved and later prescribed as the inlet conditions for actual study simulations. A no slip boundary condition was assigned to the seabed and pipeline for all simulations.

After completing the geometries, spans were brought into ANSYS Meshing for grid generation. A meshing algorithm was created and applied universally to all geometries. The algorithm was designed to achieve two goals:

- Produced nearly identical meshes in the region near the pipeline for all seabed geometries
- Adequately resolve velocity gradients

By keeping the mesh consistent between simulations, deviations in bed shear due to grid differences were avoided. The algorithm applied a tetrahedral mesh around the pipeline, extending 1.6 m upstream, 2 m downstream, and 1 m above the pipeline. Elements within the tetrahedral zone were assigned an edge length of 0.1 m. A hexahedral mesh was applied to the remainder of the control volume, with cell edge lengths of 0.1 m in the stream wise direction and 0.4 m in the cross stream direction.

SECTION 4

TASK 1: INVESTIGATING THE EFFECTS OF BATHYMETRIC DATA RESOLUTION

The effects of bathymetric data resolution were explored to determine the relative importance of collecting high-resolution data on pipeline span risk. The objective was to ascertain if high-resolution data is necessary to accurately gauge risk of potential failure of identified pipeline spans. Bed shear stress patterns and bed height deviations (difference between constructed beds elevations to the measured bed elevations) computed using bathymetric data with varying resolutions were examined.

4.1 METHODS OF INVESTIGATION FOR DATA RESOLUTION ANALYSIS

Pipeline spans were initially identified through visual observation of geo-referenced video recordings along the Atlantis oil and gas pipelines. The locations where the spans begin and end (pipeline span shoulder locations) were used to extract seafloor elevation data within the span from existing multi-beam datasets.

The original 1-foot resolution (1 ft. x 1 ft. cell spacing) multiband dataset collected along a length of the pipeline was utilized for this task. Because it is common practice in industry, bathymetric data resolutions are reported in feet (all other measurements are in the metric system). A bathymetric profile was extracted from the bed directly beneath the pipeline axis. Due to the high-frequency nature of the extracted profile, a 10 ft. running average filter was applied to smooth the seafloor fluctuations. This dataset was used as the basis for the bathymetry beneath the length of pipeline.

The smoothed 1-foot resolution dataset was also decimated twice (keeping every 5th and 10th points) to create a total of three datasets for comparison. Previously identified span starting and ending coordinates (Northings and Eastings) were used to extract the individual span bathymetry profiles from each of the three datasets (smoothed 1'x1', 5' x 5' and 10' x 10'). A total of 79 spans were identified and extracted from each resolution dataset.

Spans were characterized according to their width:depth (W:D) ratios, a method employed during previous pipeline span analysis efforts (SeaQ, 2006); however, it is recognized that W:D ratios should not be the only method of characterization because they do not fully describe the span characteristics. Two individual spans can have the same W:D ratio and have markedly different scour tendencies (e.g. if one span is half as deep, but twice as wide as the second). Research has shown the distance between the pipeline and the seabed is of high importance to erosion processes (Cheng, 2009). Therefore, spans were also characterized by their shoulder slopes, the angle formed between the pipeline and down-sloping span shoulder. To simplify this analysis, pipelines were assumed to be oriented horizontally, though it is acknowledged that seafloor pipelines are typically not often oriented in this manner.

Because angles between elevation points vary along the pipeline, angles were computed in several manners to gauge variability in computational methods:

- 1) Angle between the first two span profile elevation points at each span shoulder.
- 2) Mean angle of the first 5 angles computed at each span shoulder (assumed to be the average seafloor angle of the first 5 ft adjacent to the pipeline touchdown location).
- 3) Mean angle of the first 10 angles computed at each span shoulder (assumed to be average seafloor angle of the first 10 ft adjacent to the pipeline touchdown location).

Shoulder slope angles were computed using the slopes between the first 2 data points nearest the span shoulders, the first 5 points nearest the shoulders and the first 10 points nearest the shoulders. A mean value of individual point-point slopes were taken as representative values for the first 5 and first 10 point calculations. The slopes were computed for all three bathymetric profiles (1 ft, 5 ft and 10 ft resolutions).

Tables 3-1 through 3-3 identify the statistical summary of the shoulder slope angles computed as described above. The minimum and maximum slopes identify outliers that are bound to

exist; however, mean angles for all bathymetric resolution datasets computed were typically less than 3 degrees. Histograms of the shoulder slope angles were plotted for each of the datasets analyzed, which support this observation. Those corresponding to the 1 ft resolution dataset are shown in Figure 4-1 through Figure 4-3.

Method	Min Angle	Max Angle	Mean Angle	Median Angle	STD Angle
2-pt Angle	0.009	5.372	1.378	0.962	1.227
Avg of 5 pts.	0.127	9.573	1.955	1.591	1.535
Avg of 10 pts.	0.176	15.091	2.503	1.992	2.165

Table 4-1. Summary statistics of slope angles computed on 1 ft resolution bathymetric profile.

Method	Min Angle	Max Angle	Mean Angle	Median Angle	STD Angle
2-pt Angle	0.016	21.188	2.776	2.094	2.631
Avg of 5 pts.	0.256	9.397	2.04	1.731	1.601
Avg of 10 pts.	0.358	5.189	1.643	1.365	1.044

Table 4-2. Summary statistics of slope angles computed on 5 ft resolution bathymetric profile.

Method	Min Angle	Max Angle	Mean Angle	Median Angle	STD Angle
2-pt Angle	0.091	19.245	2.563	1.894	2.549
Avg of 5 pts.	0.132	4.875	1.434	1.161	0.992
Avg of 10 pts.	0.132	5.236	1.397	1.262	0.873

Table 4-2. Summary statistics of slope angles computed on 10 ft resolution bathymetric profile.

Once the statistical distribution of the span angles was known, three shoulders were selected to investigate the effects bathymetric resolution. The shoulder angles selected covered the natural range seen in the Atlantis region, being 0.4, 0.9, and 5.4 degrees as defined by analysis (2-pt shoulder angle from the 1-foot resolution data). For discussion purposes, the analyzed spans will be referred to as Span 1 (0.4 degree shoulder slope), Span 2 (0.9 degree shoulder slope), and Span 3 (5.4 degree shoulder slope).

Three constructs were created per span, one from each bathymetric data resolution. CFD simulations were performed on each construct using a far field current speed of 75 cm/s. Although this magnitude is on the upper range of those measured in the Atlantis region, it was chosen in order to illustrate shear stress patterns that may not be as obvious in simulations made using lower current speeds.

4.2 BATHYMETRIC RESOLUTION EFFECTS ON BED PROFILES

Bed profiles taken directly below the pipeline from CFD simulations were plotted along with the 1-foot resolution bathymetric data (Figure 4-4 through Figure 4-6). To focus on span details, the level bed region was not plotted. The 1-foot resolution bathymetric data was taken as the best representation of the span morphology and will be referred to as the seabed. It is important to remember the pipeline was positioned 10 cm above the highest elevation point. For clarity, profiles were adjusted to begin at the same height. This adjustment makes the distance between the pipeline and the profiles more apparent. Three trends are seen in Figures 1 thru 3:

- The 1-foot resolution constructs closely resemble the seabed
- Lower bathymetry resolution creates larger deviations between the constructed bed and the seabed
- Steeper span shoulders cause larger deviations between the constructed bed and the seabed.

The shape of the seabed for all three spans is accurately represented by the beds constructed from 1-foot resolution bathymetry data. The maximum difference between the seabed and the 1-foot (English) constructs occurred for Span 3, but is only 0.37 cm. It can be inferred by this small deviation the geometry creation process for the seabeds is reliable. If accurate bathymetry data are brought into the model, the constructed bed will closely resemble the span.

As the bathymetric resolution decreases, the difference between the constructed bed and the seabed increases. The construct from the 10 ft resolution data is farther away from the seabed for all three spans. Bed profiles created from low-resolution data have a greater tendency to miss inherent seabed undulations. As the sampling interval increases, the probability of capturing local extreme elevations is reduced. This effect was seen for Span 1, where the 1 ft resolution construct follows the curvature of the seabed, yet the 5 and 10 ft constructs are nearly linear. The bathymetric data shows the shoulder slope often starts out shallow, and then breaks to a steeper slope within the first 1.5 m (Figure 4-6). The lower-resolution constructs continuously missed this initial slope, causing their profiles to drop below the seabed in the vicinity of the touchdown location (i.e. a horizontal distance of 0 m).

Steep shoulder slopes tend to cause significant deviation between the constructs and the seabed. This deviation is an outcome of two factors. As already mentioned, low-resolution bathymetry data has an inherent tendency to miss the initial shoulder slope. If the angle after the break is steep, the beginning geometry of the span will be misrepresented. For Span 3, the beds created from the 5 and 10-ft resolution bathymetric data dropped more than 27 cm below the seabed over the first 2 m of the span. Secondly, low-resolution data may falsely identify the beginning location of a span as being several feet (as much as one resolution interval) from its actual position. If this offset is in the direction of the span, and the span shoulder angle is steep, the highest elevation point recorded can be greatly underestimated. The lowered span start height will create an apparent span that is shallower than its true bathymetry. For geometries that level after the shoulder, like Span 3, a lowered span start height will result in a constructed bed that is closer to the pipeline for the entire midsection (Figure 4-6).

Distances between the constructed beds and the seabed were quantified by computing the average bed deviations for each profile (Figure 4-7). This calculation was made by first determining the distance between the constructs and the seabed every 5 cm. The values were then averaged over the first 2 m of the span. For Span 1, the average bed difference was less than 1 cm for all bathymetric data resolutions. Constructs for Span 3 showed the largest

deviations. The beds created from 5 and 10-foot resolution bathymetric data had an average bed difference of 21 and 23 cm, respectfully for Span 3.

Figure 4-7 also shows that as the shoulder angle increases, the variability of the average bed differences increases. This suggests the ability to properly construct spans is dependent on the shoulder slope. Constructs of steeper spans will have larger uncertainty. To quantify the variability, standard deviations (σ) were computed for each span. The standard deviation of the mean bed differences for Spans 1, 2, and 3 was 0.2, 0.7, and 12.6 cm.

4.3 BATHYMETRIC RESOLUTION EFFECTS ON BED SHEAR

Bed shear stress was calculated within ANSYS FLUENT using a stand wall treatment model. The effects of slope angles and bathymetric data resolution on shear stress patterns were examined on both a global and local scale.

- Global Scale: The entire 3D bed of the reconstructs
- Local: A 2D bed profile

For the local analysis, bed profiles and shear stresses were extracted from CFD simulations directly underneath the pipeline center. In the current section, general shear stress trends that relate to the effects of shoulder slope and bathymetric data resolution are addressed. Hydrodynamic patterns and their effects on bed shear stress are examined in Section 5.

Figure 4-8 through Figure 4-10 show the global shear stress patterns for Spans 1, 2, and 3. Each figure contains three sub windows, one for each bathymetric data resolution. The top frame corresponds to 1-foot resolution construct, the bottom left frame corresponds to the 5-foot resolution construct, and the bottom right frame corresponds to the 10-foot resolution construct. The net flow direction for all simulations was perpendicular to the longitudinal axis of the span (i.e. positive z direction). The pipeline was colored gray in all images to elucidate its position.

Predicted shear stresses were largest directly underneath the pipeline shoulder. Of the three shoulder slopes analyzed, Span 1 had the highest bed shear stress (a maximum of about 1.6 Pa for all three data resolutions) (Figure 4-8). This was due to its shallow shoulder slope. A shallow shoulder slope causes close proximity between the seabed and the pipeline near the touchdown location. Conversely, the bed shear stress distribution for Span 3 rapidly declines when moving into the span (Figure 4-10).

The reported observations on the effects of bathymetric data resolution on the bed construction process can be extended to the current discussion. The lower the bathymetric data resolution, the more the constructed spans deviate from the seabed. As mentioned, this deviation normally causes the constructed beds to drop away from the pipeline more than the actual seabed. Computed global shear stresses are lower in the vicinity of the touchdown location for constructs created from the 5 and 10-foot bathymetric data. As will be discussed, erosion rate is proportional to bed shear stress (Section 5.2). Using 5 and 10-foot resolution bathymetric data therefore has the potential of underestimating erosion rates.

Profiles taken from directly beneath the pipeline for the 1, 5, and 10-foot resolution constructs are shown for all three spans in Figure 4-11 through Figure 4-13. Many of the same patterns identified by analyzing global shear stress patterns are seen in the 2D profiles. Shear stress is highest for Span one, and drops the quickest for Span 3. The advantage of looking at the 2D profiles is the ability to see the effects of subtle bed changes on shear stress. This is illustrated by the drop in shear stress computed within the undulating bed for Span 1 at roughly 5m from the touchdown location (Figure 4-13).

Bed misrepresentation caused by lower resolution data lead to underestimated bed shear stress predictions. Although this pattern is seen for all three spans, the significant bed deviations for Span 3 caused the largest differences in computed bed shear stresses between data resolutions (Figure 4-13). These differences occur both in the vicinity of the touchdown location and in the level region inside the span.

The maximum shear stresses calculated for each simulation are plotted in Figure 4-14. With the exception of Span 1, beds created from lower resolution data continuously predicted lower maximum shear stress. As seen with the mean bed deviations, the variance in the maximum shear stress calculations increases with increasing shoulder slope (σ values of 0.01, 0.05 and 0.12 for Spans 1, 2, and 3). The uncertainty associated with low resolution data will be largest for steep spans.

SECTION 5

TASK 2: SPAN HYDRODYNAMICS AND BED EROSION

5.1 SPAN HYDRODYNAMICS

Boundary flows near walls (e.g. a seabed) have been studied in detail and are well understood. Anytime a foreign body (e.g. a pipeline) is introduced into the marine environment near the seabed, complex flow interactions result that requires a strong conceptual and quantitative understanding. The purpose of this section is to describe the general features of the flow patterns around a pipeline on the seabed, at the span shoulder, and under the span.

A pipeline in normal turbulent free stream flow, very far from a seabed, will cause a flow separation around the pipeline and a vortex sheet to form in the downstream wake of the pipeline. The regular periodic forces associated with the vortices causes Vortex Induced Vibration (VIV) which, as discussed previously, is the primary fatigue risk due to the spans investigated herein. As the distance between the pipeline and the seabed decreases, the vortex shedding will cease. Vortex shedding is non-existent when the pipeline touches the seabed (Bearman, 1978). When the flow along the seabed encounters the pipeline it causes the near-bed boundary layer to separate and grow. Figure 5-1. Schematic of flow characteristics around a pipeline on the seabed. a) Flow streamlines over the pipeline showing flow separation and downstream recirculation. b) Pressure distribution around the pipeline. shows the flow approaching a pipeline on the seabed from the left. As the flow hits the pipeline shown in Figure 5-1a, it detached from the bed at (M) and forms a recirculation zone at (P). The pressure distribution (Figure 5-1b) has a low pressure zone on the top of the pipe that causes a net lifting force on the pipe. A high pressure is exerted on the bottom front of the pipe in response to the flow stagnation in this zone.

The flow response varies as the pipe is separated from the bed in the shoulder region and lateral pressure instabilities develop. A three dimensional flow distribution is created as spiral vortices form in the shoulder region in the wake of the pipeline (Sumer, 2002). The interaction of the pipeline on the seabed and the flow in these areas induces increased shear

stresses on the seabed which can result in sediment mobilization. In addition, the constriction of flow at the shoulder and underneath the spanning pipeline further from the shoulder will modify and accelerate flows such that the shear stresses can increase and result in sediment mobilization.

The FLUENT model of the pipeline span over a typical furrow can be used to further investigate the characteristics of the flow in the vicinity of the pipeline on the seabed, the shoulder of contact, and the span over the furrow. Figure 5-2 shows a calculated velocity vector cross section where the pipeline is resting on the sediment bed and shear stress on the sediment bed through the region. The vectors show the incoming flow forced up and over the pipeline and then a detachment and form a recirculation zone behind the pipeline, consistent with that depicted in Figure 5-1. Figure 5-3 shows a cross section of velocity contours around the pipeline in the shoulder region. The view shows the stagnation of the velocities (blue) near the interface of the pipeline and the bed in the shoulder region. Additionally the flow acceleration over the top of the pipeline is evident. The acceleration of the flow is responsible for the low pressure area shown in Figure 5-4 of the model simulations and conceptualized in Figure 5-1. These results are qualitatively consistent with the experimental flow visualization conducted by Bearman and Zdrakovich (1978).

As mentioned previously, the imbalance in pressure in the shoulder region where there is a transition from a pipeline in contact with the sediment bed to a span creates a spiral vortex. Figure 5-5 shows a cross section of velocity vectors immediately in the wake of the pipeline. The shoulder region is in the middle of the figure with the bed contact region to the left of the figure. The vectors show significant lateral and vertical velocities in the wake. These velocities represent the formation of the spiral vortices described in Sumer and Fredsoe (2002).

Overall, the primary interest of this study is in the resulting interaction of these hydrodynamic patterns with the sediment bed through the exerted shear stresses. Figure 5-6 and Figure 5-7 show a combination of views of velocity vectors along the sediment bed and the resulting sediment bed shear stresses. The shoulder region, where the gap between the pipeline and the

sediment bed is the narrowest, causes the largest acceleration in flow and subsequently produces the largest shear stresses. The maximum shear stresses of approximately 1.3 Pa are clearly seen at the shoulder interface. The flow also accelerates underneath the pipeline where the flow is constricted, yet to a lesser extent than the shoulder. The wake region behind the length of pipeline in contact with the bed experiences generally reduced shear stress due to the disruption of the boundary layer. Although, an angled region of elevated shear stress is evident due to the spiral vortices forms in the shoulder region propagating laterally in the wake. Overall, the model produces patterns of hydrodynamic behavior expected from previous researchers and provides an effective tool for evaluating sediment bed response to these complex flow situations.

5.2 METHODS OF INVESTIGATION FOR 6-DAY BED EROSION

The next task was to investigate pipeline erosion. The shoulder slope of Span 2 (0.9 degrees) made it a good representation of the common geometries seen in the Atlantis region. For CFD simulations, the initial bed was created using 1-foot resolution bathymetric data as described in Section 3. Current data was studied to determine the appropriate current magnitudes for the CFD simulations.

Near-bottom currents were measured in proximity to the Atlantis oil pipeline for nearly two complete years (1999-2001). The currents from the sensor nearest the seafloor (1989 m) at the measurement location were selected for further analysis. Current magnitudes were separated into 10 cm/s bins and a histogram of annual frequencies was produced. The values in the table below are the number of *annual* hours that a current magnitude in a bin was measured. The 3rd current meter at location i2 (water depth of 1989 m relative to MSL) was used for this analysis.

BinStart_cm/s	BinEnd_cm/s	Annual Occurrence #Hours	%Annual Occurrence
0	10	2263	25.530
10	20	3941	44.461
20	30	1908	21.525
30	40	567	6.397
40	50	125	1.410
50	60	34	0.384
60	70	15.5	0.175
70	80	7.5	0.085
80	90	2.5	0.028
90	100	0.5	0.006

Table 5-3. Annual No. of occurrences of current magnitudes measured at location I2, at a depth of 1989m.

Three current speeds were selected to investigate hydrodynamic effects on sediment bed mobilization; 35 cm/s, 50 cm/s, and 75 cm/s. The relatively high lower limit was chosen for this analysis because preliminary simulation using a current speed of 25 cm/s showed a maximum bed shear stress of 0.17 Pa (Figure 5-8). Considering the cohesive nature of the sediments in the Atlantis region, this small shear stress is not likely to produce significant bed movement (SeaQ, 2006). Even sand, which is highly erodible, has a critical shear stress (minimum bed shear required to initiate bed movement) of roughly 0.2 Pa.

CFD simulations were individually performed for all three current speeds to compute shear stresses on the initial sediment bed. Spatial coordinates and shear stresses were then extracted along 2D transects of the models, taken at regular distances from the velocity inlet. The erosion rate at each extracted coordinate was calculated through an experimentally and field tested empirical relationship between erosion rate and bed shear stress:

$$E = A\tau^n$$

where E is erosion rate (cm/s), τ is bed shear stress (N/m²), and A and n are site-specific parameters that depend on the chemical and physical morphology of the sediments. Although

knowledge is limited on the sediment properties in the Atlantis region, the most extensive core studies suggest an A and n value of roughly 0.00005 and 2.1 (SeaQ, 2006).

Bed displacement (d), or erosion, was calculated by assuming the mobilization of sediment was constant over a specified time interval (Δt). This time interval was chosen independently for each current magnitude so that the maximum bed movement within the interval was between 3 and 8 cm (Δt for 35 cm/s, 50 cm/s, and 75 cm/s were 6, 2, and 1 days respectively). The lower limit was set to minimize geometry creation errors, while the upper limit prevented inherent problems associated with assuming a constant erosion rate (i.e. cap Δt). It is recognized a dynamic relationship between the sediment bed and near bed velocity gradients exist and will create unsteady erosion rates. However, as long as the bed movement is small, the effects are minimal. The bed displacement at each extracted coordinate was then calculated as:

$$d = E\Delta t$$

Profiles were adjusted by assuming the displacement was purely vertically as scour first developed. With an initial shoulder slope of 0.9 degrees, the horizontal propagation rate is expected to be negligible. The adjusted profiles were then brought back into Design Modeler, and a new seabed was constructed. The adjusted sediment bed was then taken through the same steps as those for the initial bed form. This process was repeated for each current magnitude until 6 days had lapsed (current speed was assumed constant for all simulation).

5.3 SIX-DAY BED EROSION RESULTS AND DISCUSSION

5.3.1 Global Trends: Computed shear stresses were plotted in ANSYS FLUENT on the three-dimensional sediment bed for each simulation (Figure 5-9 through Figure 5-12). Figure 5-9 pertains to the 75 cm/s case, where the sub windows are: top left is the initial bed form, top right is the bed form after day 1, bottom left is the bed form after day 2, and the bottom right is the bed form after day 3. Figure 5-10 also displays the results from the 75 cm/s case, but for later days: top left is the bed form after day 3 (same as bottom right for Figure 5-9), top right is

the bed form after day 4, bottom left is the bed form after day 5, and bottom right is the bed form after day 6. Similarly, Figure 5-11 shows the bed shear stress for the 50 cm/s case: top left is the initial bed form, top right is the bed form after day 2, bottom left is the bed form after day 4, and the bottom right is the bed form after day 6. Figure 5-12 displays the results from the 35 cm/s simulations, where the initial bed form is on the left, and the bed after day 6 is on the right.

Simulations for all three current magnitudes show a reduction in shear stress as the sediment bed drops away from the pipeline. The larger the distance between the pipeline and the seabed, the less the near-bed velocity and boundary layer gradients are affected by the presence of the pipeline. Because these gradients are proportional to shear stress, the bed shear stress drops. After six days of 75 cm/s current speeds, the shear stress underneath the pipeline reduces by more than 0.3 Pa (Figure 5-9 Figure 5-10). The morphology of the sediment bed in 35 and 50 cm/s simulations change less than that for the 75 cm/s case. As a result, the reduction in shear stress is also less (changes after six days of 35 and 50 cm/s current speeds is roughly 0.03 and 0.1 Pa).

As the morphology of the sediment bed changes in the 50 and 75 cm/s simulations, the angled region of elevated shear stress within the wake zone widens. The bed profiles directly downstream from the pipeline show significant erosion near the end of the span shoulder (Figure 5-14. Time series of bed profiles for the 75 cm/s simulations. Profiles were taken at 25, 50, 100, and 200 cm downstream from the pipeline axis., bottom sub windows). The eroded shoulder essentially creates an effective channel for flow from within the span to the wake zone, enhancing the lateral propagation of spiral vortices in the wake of the pipeline.

5.3.2 Local Trends: Bed height profiles were extracted along transects 10 and 25 cm upstream, directly below, and 25, 50, 100, and 200 cm downstream from the pipeline axis. Time series of the bed profiles for all three current speeds are plotted in Figure 5-13 through Figure 5-18. As with the bathymetric data resolution analysis, the touchdown location is directly underneath the pipeline at the top of the span shoulder (i.e. 0 m into the span).

The time varying seabed profiles showed the most change with high current magnitudes. The mean bed drop was computed by averaging the difference between the initial seabed and the adjusted seabed every 5 cm over the first 2 m of the span shoulder. Mean and maximum bed drops are plotted in Figure 5-19 through Figure 5-21 for all simulations. Increases in current magnitude caused increases in bed shear, leading to higher erosion rates. The maximum bed drop for the 75 cm/s simulation was 23 cm, respectfully (Figure 5-19). This change bed morphology is more than 10 times that seen for the 35 cm/s case, where the maximum bed drop was roughly 2 cm (Figure 5-21). Time series of the mean and maximum bed drop for the 50 and 75 cm/s simulations show an initial decrease in the rate of bed change with time, supporting observations reported by Cheng et al (2009). Data were curve fitted to better show this rate decrease. The slope of the red curve in Figure 5-19 through Figure 5-21 represents the vertical scour rate directly below the pipeline. The average vertical scour rate for the 75 cm/s simulation begins at roughly 5 cm/day and drops to 2 cm/day, respectfully.

Bed erosion diminishes with distance from the pipelines longitudinal axis. After 6 days of 35 and 50 cm/s current speeds, changes in bed morphology 200 cm from the pipelines axis are minimal (

Figure 5-16 and Figure 5-18). The small changes seen for the 35 cm/s case were likely caused by geometry creation errors due to the extrusion process in Design Modeler. Simulations run with a current speed of 75 cm/s do show erosion at further transects, but the general trend of decreasing erosion with increasing distance from the pipeline is still present (Figure 5-14).

Cross-stream flow resulting from the presence of the pipeline shifts the region of highest shear into the span on the downstream side of the pipeline (Figure 1-4). The further away from the pipeline axis, the deeper the maximum shear stress is shifted. As a result, bed erosion is reduced at the top of the shoulder on the downstream side of the pipeline (Figure 5-14,

Figure 5-16, and Figure 5-18).

Figure 5-22 through Figure 5-27 show scatter plots of shear stress along profiles extracted 10 cm upstream, directly below, and 10 and 25 cm downstream from the pipeline axis. As expected, the sediment bed drops the most in areas of high shear. The sensitivity of the analysis is illustrated in Figure 5-23, where computed bed shear stresses fluctuate along the initial seabed. Because erosion rate is dependent on bed shear stress, the adjusted bed profile for ‘after day 1’ contains undulations. By shorting the time interval used for calculating bed erosion, this effect would be minimized. However, even with the current time step, the sediment bed quickly smoothes with time due to the nonlinear relationship between shear stress and erosion rate.

After 6 days, shear stress distributions underneath the pipeline for all current magnitudes appear to be approaching a uniform or steady state value. If the same shear stress is applied across shoulder, the shape of the scour slope will not change. Experimental results by Cheng et al. support this observation (2009). Time series of the maximum shear stress and the scour slope are plotted in Figure 5-28 through Figure 5-30. The scour slope was computed as the angle between the pipeline axis and the line connecting the top of the span to the elevation point 40 cm into the span. Data in each time series was empirically fit to extrapolate steady state shear stress and scour slopes values:

$$S_{max} = a(b - e^{-ct})$$

$$\beta = a'(b' - e^{-c't})$$

where S_{max} is the maximum shear stress on the sediment bed, β is the scour slope angle, t is the time after scour initiation (i.e. pipeline placement), and a, b, c, a', b', c' are empirical constants (Table 5-2). Steady state shear stresses and scour slopes were computed by taking the limit of S_{max} and β as t goes to infinity. Table 5-2 contains calculated steady state values and empirical constants. The limited number of simulations for the 35 cm/s case made it impossible to curve fit. The mean shear stress and scour slope computed after day 6 were taken as the steady state values.

Current Magnitude (cm/s)	a	b	c	a'	b'	c'	S _{max} (Pa)	β (Degrees)
35	-	-	-	-	-	-	0.23	3.1
50	-0.118	-3.99	0.56	10.3	1.11	0.287	0.47082	11.433
75	-0.58	-1.04	0.14	28.58	1.041	0.224	0.60112	29.75178

Table 5-2. Steady state values and empirical constants resulting from 35, 50, and 75 cm/s current speeds. Due to limited data, curve fitting was not possible for the 35 cm/s case. Steady state values were taken as those calculated after the sixth day.

5.3.3 Calculating Horizontal Propagation Rates: A conceptual model was developed to calculate propagation rates along the longitudinal axis of pipeline spans. The model is based on the following assumptions:

- The shear stress distribution within a shoulder scour will eventually reach steady state
- The scour slope will remain constant once the steady state shear stress is reached
- The time required to reach the steady state shear stress is much less than the time period in which bed erosion is being calculated over.

The numerical results from this study, and the experimental finding by Cheng et al., support the first two assumptions. The third assumption is justifiable when assessing long-term pipeline risk. After only 6 days, the maximum shear stress for all current speeds was within 34% of the predicted steady state values. Figure 5-31 shows a schematic representation of the relative position of the pipeline and scour slope. If the angle of the scour slope is held constant, line AB will move in the normal direction at rate E_s (E_s is the erosion rate caused by the steady state shear stress). Breaking the movement into vector components, the steady state horizontal propagation rate can be calculated as:

$$V_h = E_s \sin \beta$$

where V_h is the horizontal propagation rate, and beta is the steady state scour slope. By combining the equation for E and V_h , and plugging in the appropriate values from Table 5-2, horizontal propagation rates were calculated for each current speed. Because extreme episodic events may control scour morphology, the horizontal propagation rates for the 35 and 50 cm/s

cases were calculated two ways: 1) using the equilibrium scour slope predicted by the current speed of interest; 2) using the equilibrium scour slope predicted for 75 cm/s current. Calculated horizontal propagation rates are presented in Table 5-3.

Current Magnitude (cm/s)	V_h (cm/day) calculated using steady state scour slope from:	
	Current Speed of Interest	Current speed of 75 cm/s
35	0.10	0.15
50	0.17	0.44
75	0.73	0.73

Table 5-3: Steady state horizontal propagation rates.

SECTION 6 CONCLUSIONS AND RECOMMENDATIONS

As discussed in Section 1, this study had two primary objectives: 1) evaluate the effects of bathymetric data resolution on the modeling process of pipeline spans and the assessment of pipeline risk in furrowed regions; and 2) develop a model to investigate bed erosion in the vicinity of pipeline touchdown locations. By achieving the first objective, the required bathymetric data resolution for further investigations of pipeline spans can now be assessed on a site specific basis. The second objective of this study lead to a predictive model for vertical and horizontal scour propagation rates that can be used to analyze scour rates along pipelines on an individual span base.

Low-resolution bathymetric data has a tendency to underestimate bed shear stress. This underestimation is the result of an inaccurate representation of the seabed. As bathymetric resolution decreases, the difference between the constructed bed and the seabed increases. Large sampling intervals can inherently miss local maximums, thereby leading to constructs that do not contain seabed undulations that may be important to modeling processes. The bathymetric data analyzed in this study showed spans often contain shoulder slopes that start off mild, and then break to a steeper slope. Again, the larger the sampling interval, the less likely the initial shoulder slope will be captured. The largest underestimation of shear stresses occurred in two regions: 1) in close proximity to the touchdown location; and 2) in the middle of the span.

This study showed the angle of the shoulder slope is an important characteristic in determining shear stress distribution beneath pipeline spans. A shallow shoulder slope will causes a small gap between the seabed and the pipeline over a large length of the pipeline. As a result, shear stresses on the sediment bed beneath the pipeline are high. The shoulder slope angle also dictates the degree of uncertainty in computed shear stresses. The dispersion in predicted maximum shear stresses for Span 3 (shoulder slope of 5.4 degrees) was much larger than that for Span 1 (shoulder slope of 0.4 degrees). It can be inferred from these results that investigators studying pipeline risk should evaluate the proper degree of data resolution on a

case by case base. The decision should be based on two factors: 1) the objective of the study; and 2) the physical characteristic of the spans in the region of interest. If detailed hydrodynamic modeling is required to address study objectives, high resolution bathymetric data is required to capture detailed shear stress patterns. On the other hand, if the study is aimed towards indentifying regional characteristics of seabed undulations, low resolution bathymetric data is sufficient at gathering width to depth ratios and general span locations. If pre-existing bathymetric data is available, regions known to have steep shoulder slopes should be approach with caution.

The use of CFD has proved to be valuable for investigating pipeline erosion. Many previously reported hydrodynamic patterns around pipelines were identified in this study, but state-of-the-art CFD has also allowed for the quantitative analysis of these patterns. This included evaluation of accelerated flow in the vicinity of the pipeline touchdown location, recirculation zones, stagnation zones, and spiral vortices. Bed erosion was the greatest in the vicinity of the touchdown location for high current speeds. These conditions create large velocity gradients that accelerate bed mobilization. As scour developed around the pipeline, bed shear stress distributions dropped. As expected, the large change in seabed morphology for the 75 cm/s case caused the largest reduction in shear stress. This was depicted on both a global and local scale.

The study also showed shear stress distributions within scour pits tend toward a uniform or steady state value. Once the shear stress becomes uniform, the shape of the scour slope will not change. This observation was used to create a conceptual model to calculate horizontal propagation rates through predicted steady state shear stresses and scour slopes. Although the methodology was applied to one average specific span found in the Atlantis region, it can be generalized for any span in any location if the proper data is available.

6.1 DESIGN CONSIDERATIONS

The section below describes design considerations and recommendations that are derived from recent analysis projects (JIP and SeaQ evaluations) as well as published guidelines (e.g. from the BOEMRE and DNV). Scour around pipeline touchdown locations (e.g. span shoulders) may lead to an increase in potential for VIV occurrence and pipeline fatigue as a consequence of increasing span length and depth. The following considerations are recommended for pre- and post-pipeline placement to reduce or avoid pipeline fatigue:

6.1.1 Recommendations Preceding Pipeline Placement: The suggestions in this section will help identify areas of high potential for VIV and pipeline fatigue prior to pipeline placement and routing.

Bathymetric Survey(s)

- High resolution multi-beam bathymetric survey(s) preceding pipeline placement can identify potential areas where pipeline spans may immediately occur due to seabed undulations. When possible, this data should be collected.
- High resolution bathymetry yields information about slope angles of seabed undulations and furrows. Estimated bed shear stresses and scour rates at pipeline span shoulders are proportional to the gap, which is the distance between the pipeline and the seabed. The gap beneath the pipeline is sometimes estimated as the average of the central third of the pipeline span, and is dependent on the angle of the sediment bed beneath the pipeline. Therefore, accurate predictions of slope angles will result in more accurate shear stress and scour predictions, hence increasing the reliability of pipeline risk assessment.

Current Measurements

- Prior to pipeline placement and routing, near-bed current measurements in close proximity to potential pipeline routes should be collected to determine dominant flow direction and magnitude range.

- Current measurements should be made in the *outer zone* (i.e. relatively far from the seabed, where turbulent fluctuations are minimal) 1-2 bedform heights above the crest of the local bedforms (as defined by DNV, 2006).
- If data from only one nearby current meter is available, a data distribution (e.g. Weibull distribution) can be created and propagated to other nearby locations to describe current magnitudes and directions (DNV, 2006). Future studies should incorporate this method of evaluating and applying current meter data in risk analysis.

Sediment Characteristics

- In-situ sediment characteristics of the near-surface sediments in close proximity to existing pipelines or potential pipeline routes should be collected to yield site-specific information regarding sediment erosion potential. SEDFlume technology is one method of collecting the necessary data. SEDFlume has been designed to measure site-specific sediment erosion potential of undisturbed near-surface sediments (less than 2 meters); use of this technology or a similar approach should be performed near anticipated pipeline routes.
- According to the DNV (2006), soil data down to a depth equal to $\frac{1}{2}$ to 1 times the pipe diameter is most important to consider in this context; however, site-specific characteristics should always be considered and may dictate the importance of alternative (i.e. deeper) sample depths.

Route Selection

- Pipeline route locations should be selected to avoid or minimize regions with high current flows and large span lengths, if possible.
- If a pipeline must cross a high current flow region (i.e. potential scour or VIV region), erosion-reducing mitigations should be considered (e.g. concrete mats and geotechnical fabric or similar actions) [BOEMRE, 1997].

- Pipeline deflection and bending material characteristics should be evaluated to determine the maximum span length that can be crossed without causing the onset of VIV, overstressing, or structural failure (critical fatigue).

Pipeline Lay

- The pipeline angle relative to the dominant flow direction is important for cross-flow and in-line VIV analysis and shoulder scour assessments. In order to minimize the effects of cross and inline flow on pipeline fatigue, the horizontal lay orientation should be at an angle 30-60 degrees oblique to the dominant flow direction. This will reduce potential cross and inline VIV; however, the angle between the pipeline and longitudinal axis of the furrow (or undulation) may be offset from the orthogonal position, lengthening the unsupported distance of the pipeline. The maximum pipeline span length needs to be considered concurrently.
- Pipelines oriented perpendicularly to flow direction are most susceptible to potential cross-flow VIV because the highest cross-flow velocities are realized in this scenario. Conversely, pipelines oriented parallel to the flow direction are least susceptible to cross-flow VIV, but most susceptible to in-line VIV. This consideration should not be forgotten when deciding pipeline route selection.
- If a pipeline crosses a span oblique to the dominant flow direction, shear stresses and erosion rates at the shoulder spans are reduced. This phenomenon further validates the importance of avoiding pipeline placement orthogonal to dominate flow direction.

Pipeline Risk of Failure

- Near-bed current measurements, combined with 3-dimensional CFD software and empirical modeling (as done in this study), should be used to predict shear stresses and scour rates if a pipeline span risk is determined to be significant. The predicted scour rates should be incorporated into the risk assessment analysis for the span.
- The potential vertical and horizontal (along pipeline axis) scour distances over the anticipated pipeline lifecycle duration should be assessed. If the as-laid pipeline span

plus the scoured horizontal distance creates a span that is vulnerable to critical fatigue, the span should be avoided.

6.1.2 Recommendations Following Pipeline Placement: In the following bullets, recommendations for pipeline monitoring subsequent to placement are discussed. These suggestions may help identify areas that require immediate modifications to avoid VIV and pipeline critical fatigue, or may identify areas that should be monitored with future inspections. In addition, investigative surveys following pipeline placement yield baseline conditions against which future investigations can be compared to.

Bathymetric Survey(s)

- A high resolution bathymetric survey following pipeline placement will identify as-built (as-laid) pipeline spans, whether due to seafloor fluctuations, or a result of pipeline system operation and the resulting axial tension. Also, valuable information regarding pipeline embedment in the seabed sediment will be obtained.
- The survey resolution should be related to the actual roughness of the seabed, or elevation oscillation frequency of the seabed (DNV, 2006). Relatively flat terrain does not require high resolution surveys; however, the existence of furrow fields or variability in seabed elevation may necessitate high resolution bathymetry data. As shown, for detailed investigations of shear stresses and erosion rates for steep shoulder slopes, high resolution data is required.
- High-resolution bathymetric surveys should be conducted at least every 5 years to inspect scour progression around existing pipeline spans that were identified in the as-built survey. This will not only provide a means for monitoring risk, it will also allow the confirmation of predicted erosion rates and extrapolated pipeline risk factors.
- Periodic surveys will indicate if new spans have formed since the previous inspection, or if the existing pipeline span geometries are evolving over time. They will also indicate if further monitoring is necessary, or if mitigation measures should be considered to reduce risk.

Free Span Evaluation for VIV and structural failure.

- Identified as-laid pipeline spans should be analyzed further for VIV and structural risk (deflection limit and fatigue) potential based on the measured current speeds, soil characteristics, span geometry and anticipated scour. Potential vibration modes of pipelines are important in determining fatigue risk. The vibration period dictates the potential for pipeline failure (e.g. single mode or multi-mode VIV, DNV [2006]).
- Span lengths and depths should be evaluated to determine if pipeline deflection may cause a touchdown point within a span. Pipeline touchdowns within a span will change the hydrodynamic patterns and create a new scour scenario. The scenario warrants further investigation.
- It should be determine if identified free spans are *scour-induced* and may change with time, or due to natural *seabed undulations*. Spans caused by natural undulations may be time invariant due to the nature of the sediment bed; the span length will not increase. However, even if a span geometry is unchanging, the pipeline may still be vulnerable to VIV risk. This possibility should be investigated.

Pipeline, Seafloor and Environmental Characteristics

- Physical and mechanical properties of the *pipeline materials* affect both the static and dynamic response of the pipeline free span, and need to be investigated (BOEMRE, 1997). Properties of the *pipeline contents* must also be considered. The density of the contents affects both the bending moment imposed on the free span (static response), and the natural frequency of the free-spanning pipeline (dynamic response) (BOEMRE, 1997).
- Environmental properties (e.g. seawater density, current velocity, seawater viscosity and Strouhal Number) near the free span, which have been described in the JIP report, should be characterized to the extent possible.
- The pipeline support and geometric configuration of the free span in terms of the gap between the pipeline and seafloor, the free-span fixity constant, the pipe tension and the ramping ratio should be considered (BOEMRE, 1997):

- The gap beneath the pipeline will affect the velocity of the current flow around the pipeline. It also limits to the amount of allowable pipeline deflection.
 - The gap can be an indicator of high risk for shallow and steep sloped spans because VIV is a function of the gap.
- The fixity constant describes the type of pipeline span shoulder support. Pipeline span end conditions are neither simply supported nor fixed. Therefore, this constant considers pipeline embedment at the shoulders as well as soil characteristics such as soil stiffness.
 - The degree of pipeline embedment or suspension will cause the pipeline to react differently under applied flow forces, acting to reduce, impede or enhance scour potential. A pipeline-soil interaction analysis will yield insight into the potential for pipeline settlement.
- As pipeline tension increases, the maximum allowable free span increases correspondingly. This is difficult to estimate however, and is often assigned a conservative value.
- Damping of vibrations is directly related to the pipeline material and contents, the support conditions at the span shoulder, and the seawater properties.
- The pipelines vertical orientation relative to the seafloor can vary. Depending upon the adjacent sea bed and overall pipeline lay characteristics, pipelines may have a concave or convex deflection. Concaved deflection occurs if the span length is large and the pipeline is unsupported along the length. Conversely, pipelines may deflect upward if there are seafloor obstruction, or as a result of axial tension. If pipeline strength and material characteristics are known, deflection calculations should be made to check against acceptable limits.

Increase Site-Specific Data and Measurements

- According to the DNV, our present data inventory of free spans is considered *not well defined* (2006). To be *well defined* or *very well defined*, by the definition in the most recent DNV, span characteristics such as span length, gap ratio and effective axial forces

must be known along with site-specific soil and environmental conditions. In the present study, current measurements and soil characteristics from a distant location were assumed to exist, which may not be accurate. If possible, more accurate site data should be obtained.

- Structural analysis of the pipeline and pipeline spans may yield beneficial information about pipeline-soil interactions and static loads. If pipeline deflection and bending characteristics are known, more accurate span scour and pipeline vibration calculations can be made. These calculations will improve the reliability of risk assessments.

Empirical Modeling as Another Approach

- To validate CFD based risk assessments, empirical models (e.g. Response Models) should be used to provide steady state VIV amplitude response as a function of basic hydrodynamic and structural parameters. Cross-flow and in-line vibrations are considered separately in these models and are detailed in DNV (2006).
- Empirical models can be applied to existing identified spans to analyze risk.

6.2 FUTURE RESEARCH TOPICS

The information gathered during this study is useful for predicting bathymetric data quality requirements, and scour propagation rates along the horizontal axis of pipeline spans. However, improvements can be made to the methodologies used in this study to reduce uncertainty in the results, and increase the predictive reliability. Recommendations for additional research are separated into three broad categories: 1) methodology improvements for analyzing bathymetric data resolution effects; 2) methodology improvements for investigating seabed erosion; and 3) analysis, and incorporation of site specific data into the analysis. Brief descriptions of possible future studies in each category are presented below for consideration by the Bureau of Ocean Energy Management, Regulation, and Enforcement.

Methodology Improvements for Analyzing Bathymetric Data Resolution Effects

- Analyze additional shoulder slopes to develop a relationship that would allow for quantitative predictions of the uncertainty in shear stress calculation for any shoulder slope angle
- Evaluate the effects of bathymetric data resolution on a long-time-scale study of bed erosion
- Validate the conclusions drawn from this study with varying resolution bathymetric data from a specific site

Methodology Improvements for Investigating Seabed Erosion

- Conduct additional simulations to evaluate the effects of the angle between the pipeline and level bed (i.e. non horizontal pipelines)
- Conduct a parameterization study to investigate changes in erosion patterns resulting from varying sediment properties (i.e. A and n)
- Further evaluate the horizontal scour propagation rates prior to steady state conditions
- Develop a technique that would allow automated dynamic meshing and run it over longer time periods to validate steady state shear stresses and scour slopes
- Incorporate pipeline sagging into erosion simulations to account for hydrodynamic effects that may result from angle changes between the pipeline and the shoulder
- Incorporate time varying boundary conditions to better simulate environmental conditions
- Perform additional simulations to determine approach angle (angle between the current direction and the pipeline) effects on shoulder scour

Analysis and Incorporation of Site Specific Data Into the Analysis

- Use site-specific data to calibrate and validate the hydrodynamic and bed scour models (e.g. current meter data collected from within large seabed undulations)
- Use site-specific data to quantify the variability and uncertainty in bed properties (e.g. erosion rates)

- Conduct a series of bathymetric surveys for a specific region over a period of time to validate horizontal propagation rates along pipelines

SECTION 7 REFERENCES

- Guo, B., Song, S., Chacko, J., and Ghalambor, A., 2005. Offshore Pipelines. Jordan Hill: Gulf Professional Publishing
- Beaubouef, B., 2010. Offshore Pipeline and Construction Review. Pipeline and Gas Technology Online <http://www.pipelineandgastechology.com/Construction/ForecastsReviews/item59035.php>
- Blevins, R., 2001. Flow-Induced Vibration, Second Ed. Florida: Krieger Publishing Company
- Flood, R.D., 1983. Classification of sedimentary furrows and a model for furrow initiation and evolution. *GSA Bulletin* 94:630-639
- Cheng, L., Yeow, K., Zhang, Z., and Teng, B., 2009. Three-Dimensional Scour Below Offshore Pipelines in Steady Currents. *Coastal Engr.*, (56)577-590
- Sumer, B.M., Fredsoe, J., 2002. The Mechanics of Scour in the Marine Environment. Singapore: World Scientific Publishing Co.
- SeaQ, 2006. Assessment of Pipeline Risk in Furrow Fields Located in the Gulf of Mexico. SeaQ. BP Study 2006.
- Bureau of Ocean Energy Management, Regulation, and Enforcement, 1997. *Analysis and Assessment of Unsupported Subsea Pipeline Spans*. United States Department of the Interior Bureau of Ocean Energy Management, Regulation, and Enforcement. Prepared by Project Consulting Services, Inc. PCS Job Number 97058.
- Brors, B., 1999. Numerical Modeling of Flow and Scour at Pipelines. *ASCE J. Hydr. Engr.*,125(5):511–523.
- Li, F., Cheng, L.,1999. A Numerical Model for Local Scour Under Offshore Pipelines. *ASCE J. Hydr. Engr.*,125(4):400–406.
- Liang, D.F., Cheng, L., 2004. Numerical Modelling of Scour Below a Pipeline in Currents. Part II: Scour Simulation. *Coastal Engr.*52(1):43–62.
- ANSYS Inc., 2009. ANSYS FLUENT 12.0 Theory Guide. New Hamshire: ANSYS Inc.
- ANSYS Inc., 2009. ANSYS FLUENT 12.0 Users Guide. New Hamshire: ANSYS Inc.

Hinze, J.O., 1975. *Turbulence*. New York: McGraw-Hill Publishing Co.

Menter, F.R., 1994. Two-equations Eddy-Viscosity Turbulence Models for Engineering Applications. *AIAA J.* 32(8):1598-1605

Menter, F.R., Kuntz, M., and Langtry, R., 2003. Ten Years of Experience with the SST Turbulence Model. *Turbulence, Heat and Mass Transfer 4*. Begell House Inc. 625-632

Bearman, M., and Zdravkovich, M., 1978. Flow Around a Circular Cylinder Near a Plane Boundary. *J. Fluid Mech.* 89(1):33-47

DNV, Det Norske Veritas, 2006. *Recommended Practice DNV-RP-F105*. Free Spanning Pipelines. 46 pgs.

BOEMRE, Bureau of Ocean Energy Management, Regulation, and Enforcement, 1997. *Analysis and Assessment of Unsupported Subsea Pipeline Spans*. Prepared by Project Consulting Services, Inc. 86 pgs.

Figures:

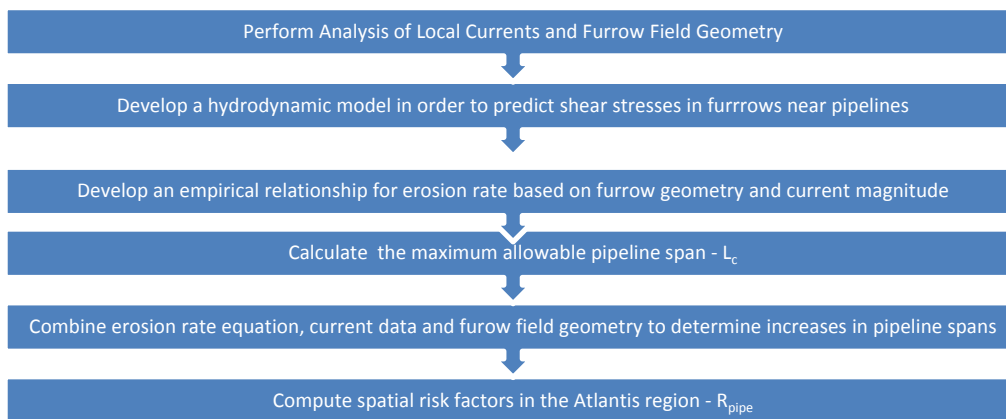


Figure 2- 1. Flow chart of the procedure developed by SeaQ to assess pipeline risk in furrow fields.

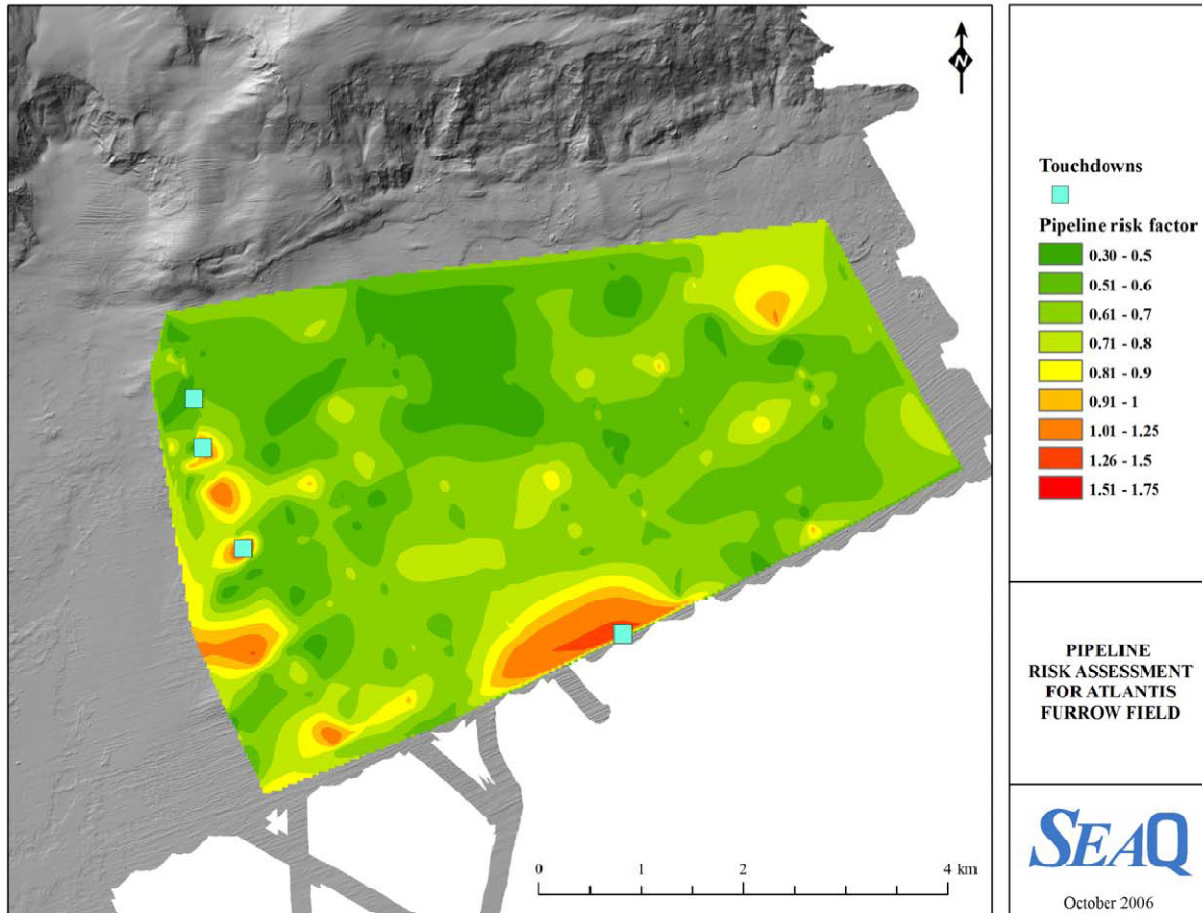


Figure 2-2. Spatial distribution of pipeline risk factors in the Atlantis region at the end of a two year period.

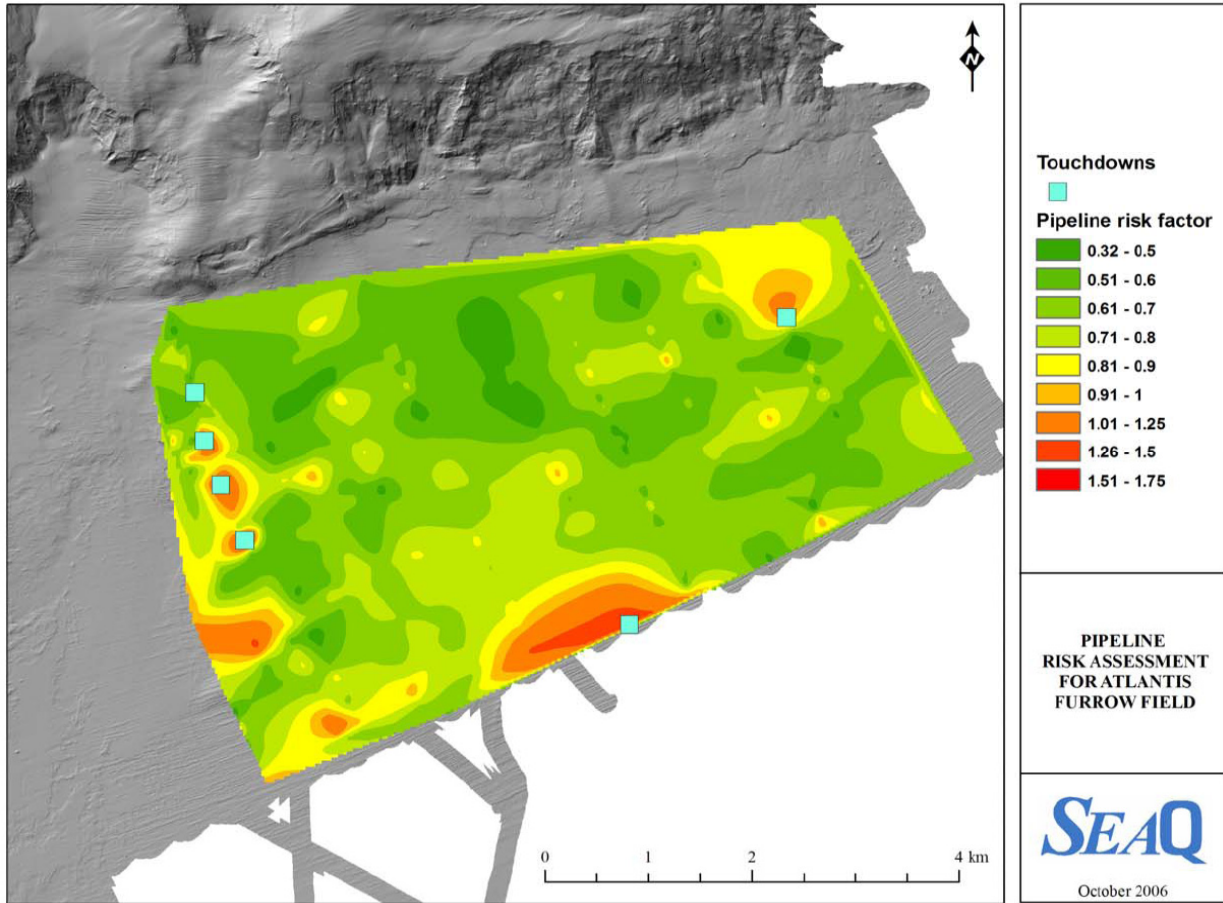


Figure 2-3. Spatial distribution of pipeline risk factors in the Atlantis region at the end of a ten year period.

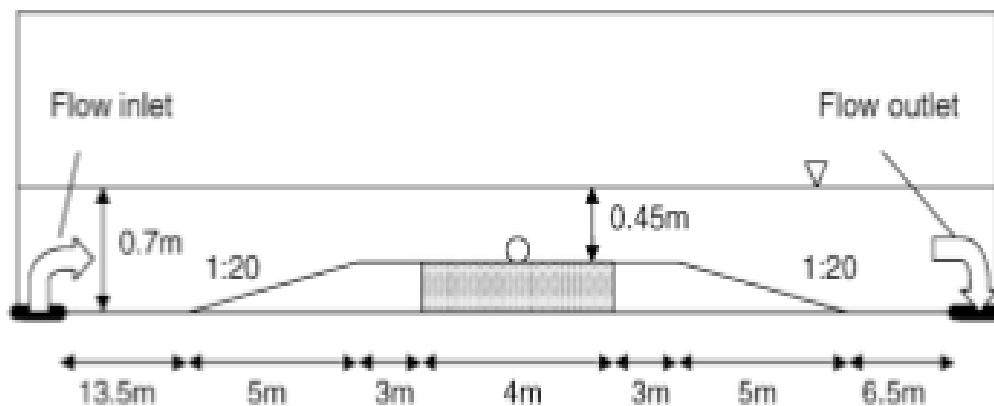


Figure 2-4. Diagram of the experimental setup used by Cheng et al.

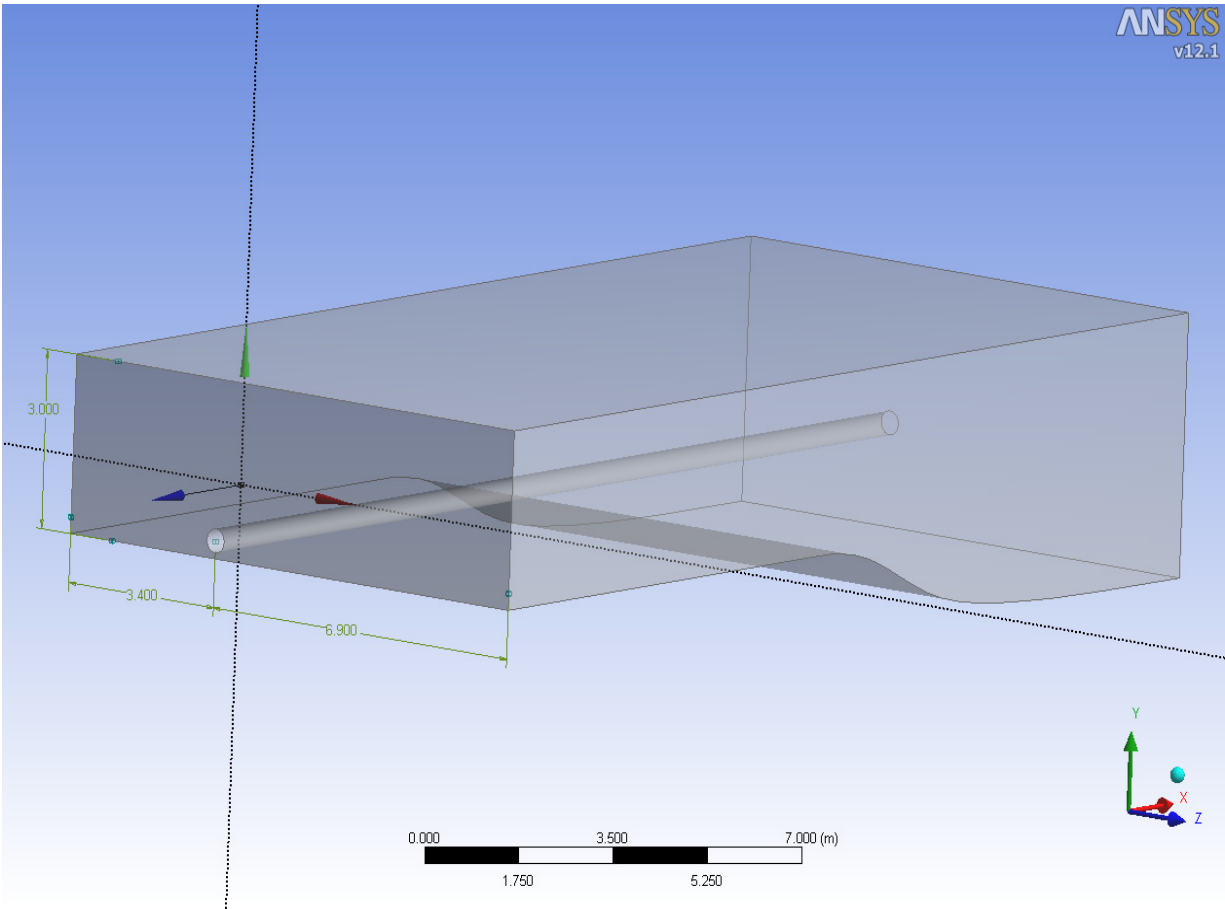


Figure 3- 1. Diagram of the physical setup used for CFD models. The velocity inlet is the face 3.4 m upstream from the pipeline, and the pressure outlet is the face 6.9 m downstream from the pipeline.

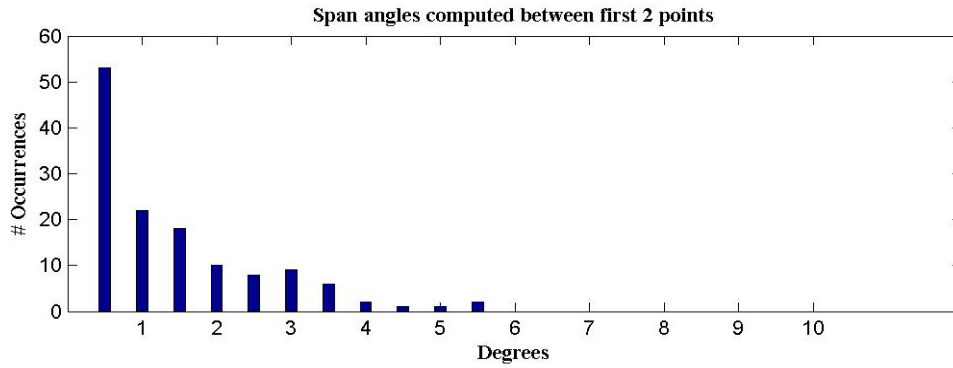


Figure 4-1. Histogram of shoulder slopes for 1 ft bathymetric resolution. Angles computed between first two points at each shoulder.

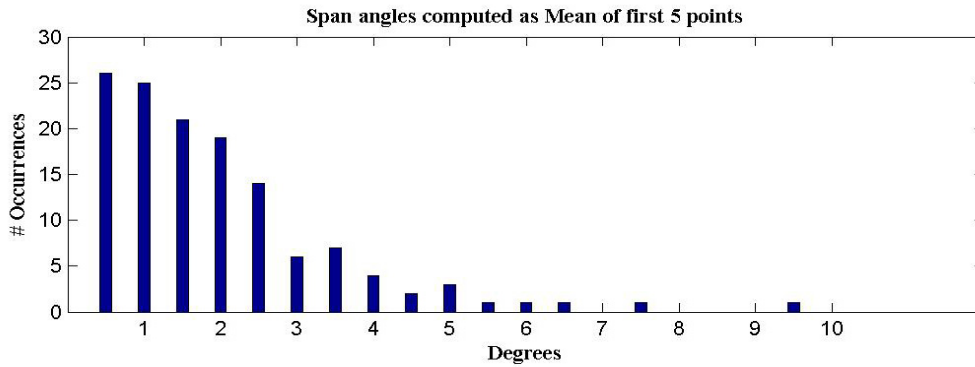


Figure 4-2. Histogram of shoulder slopes for 1 ft bathymetric resolution. Angles computed as average of 5 points at each shoulder.

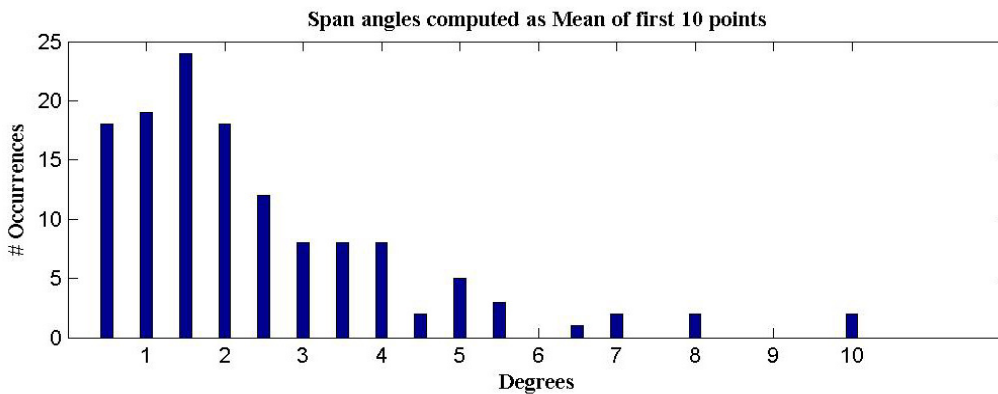


Figure 4-3. Histogram of shoulder slopes for 1 ft bathymetric resolution. Angles computed as average of 10 points at each shoulder.

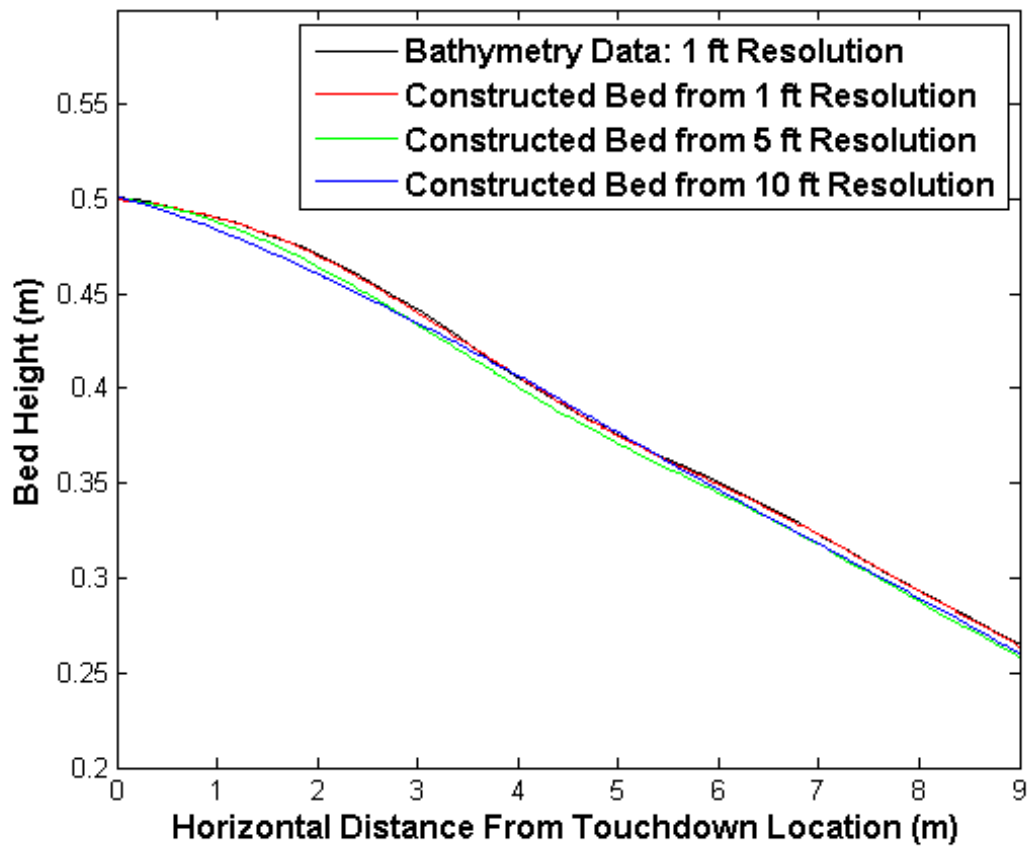


Figure 4-4. Comparison of constructed bed profiles to the seabed for Span 1 (0.4 degree shoulder slope).

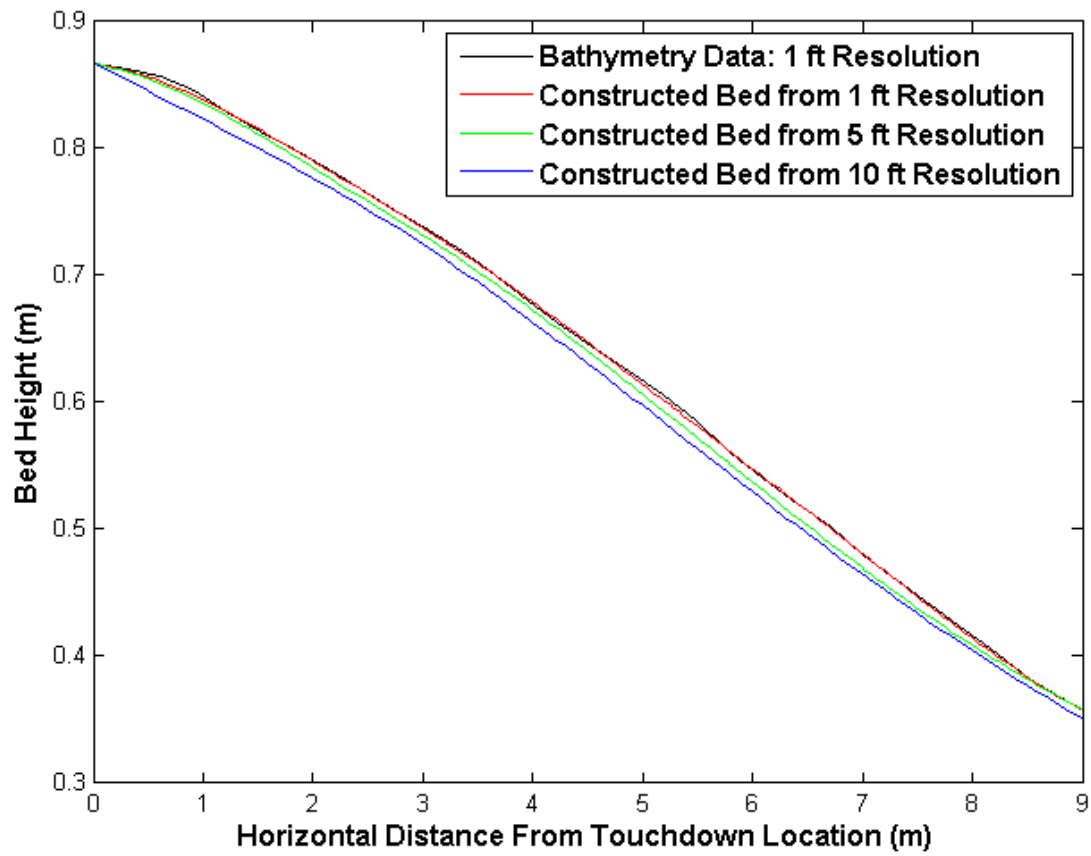


Figure 4-5. Comparison of constructed bed profiles to the seabed for Span 2 (0.9 degree shoulder slope).

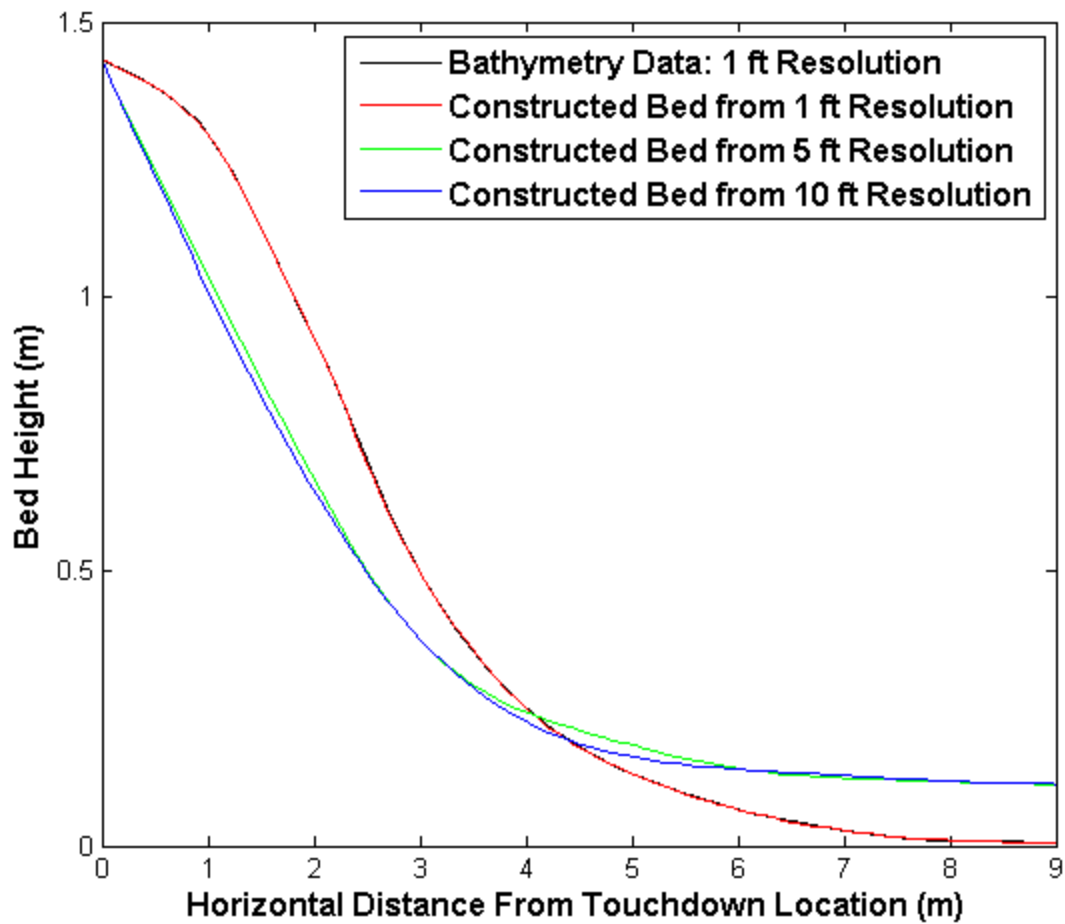


Figure 4-6. Comparison of constructed bed profiles to the seabed for Span 3 (5.4 degree shoulder slope).

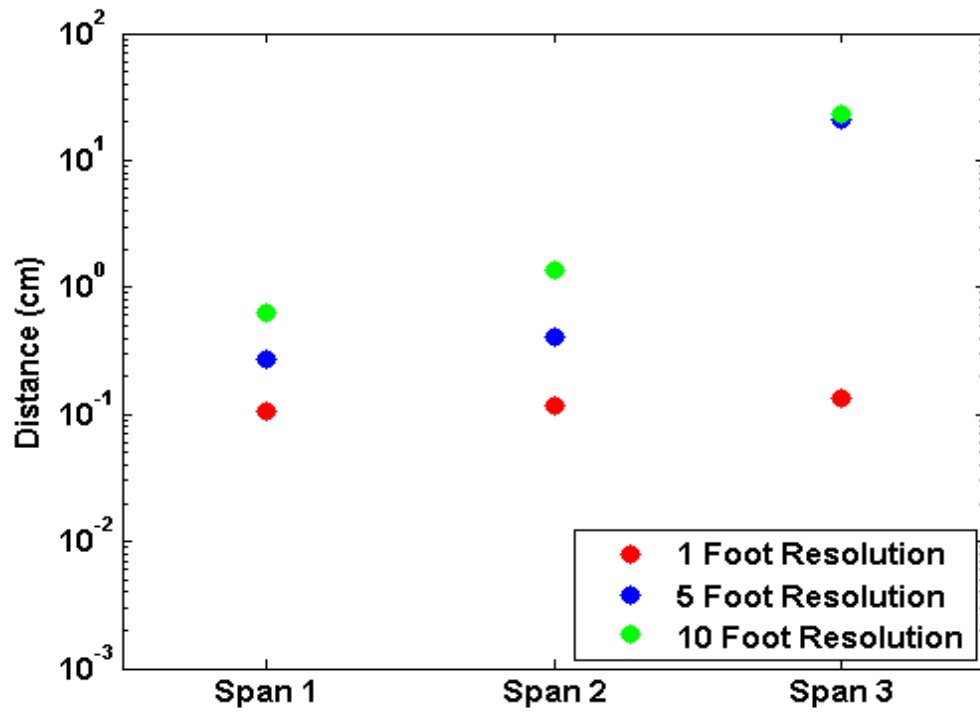


Figure 4-7. Average Difference (cm) between the constructed beds and the seabed over the first 2 feet of the span.

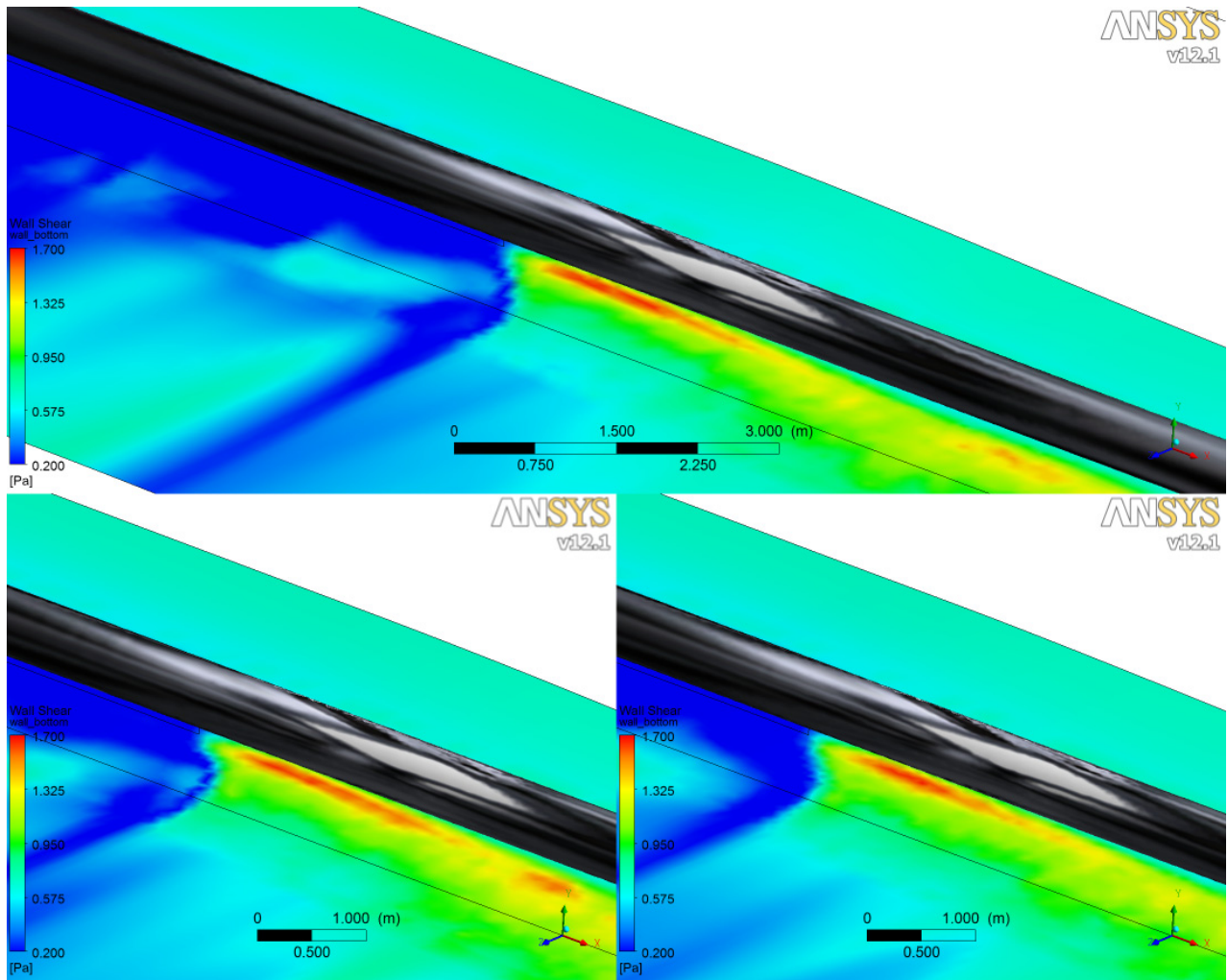


Figure 4-8. Global bed shear stress (Pa) patterns for Span 1. Constructs from varying data resolution are displayed in each sub window: top is the 1-foot resolution construct; bottom left is the 5-foot resolution construct; bottom right is the 10-resolution construct. The pipeline is colored gray to elucidate its position. Regions of high shear stress are represented by hot colors, while areas of low shear stress are depicted by cool colors.

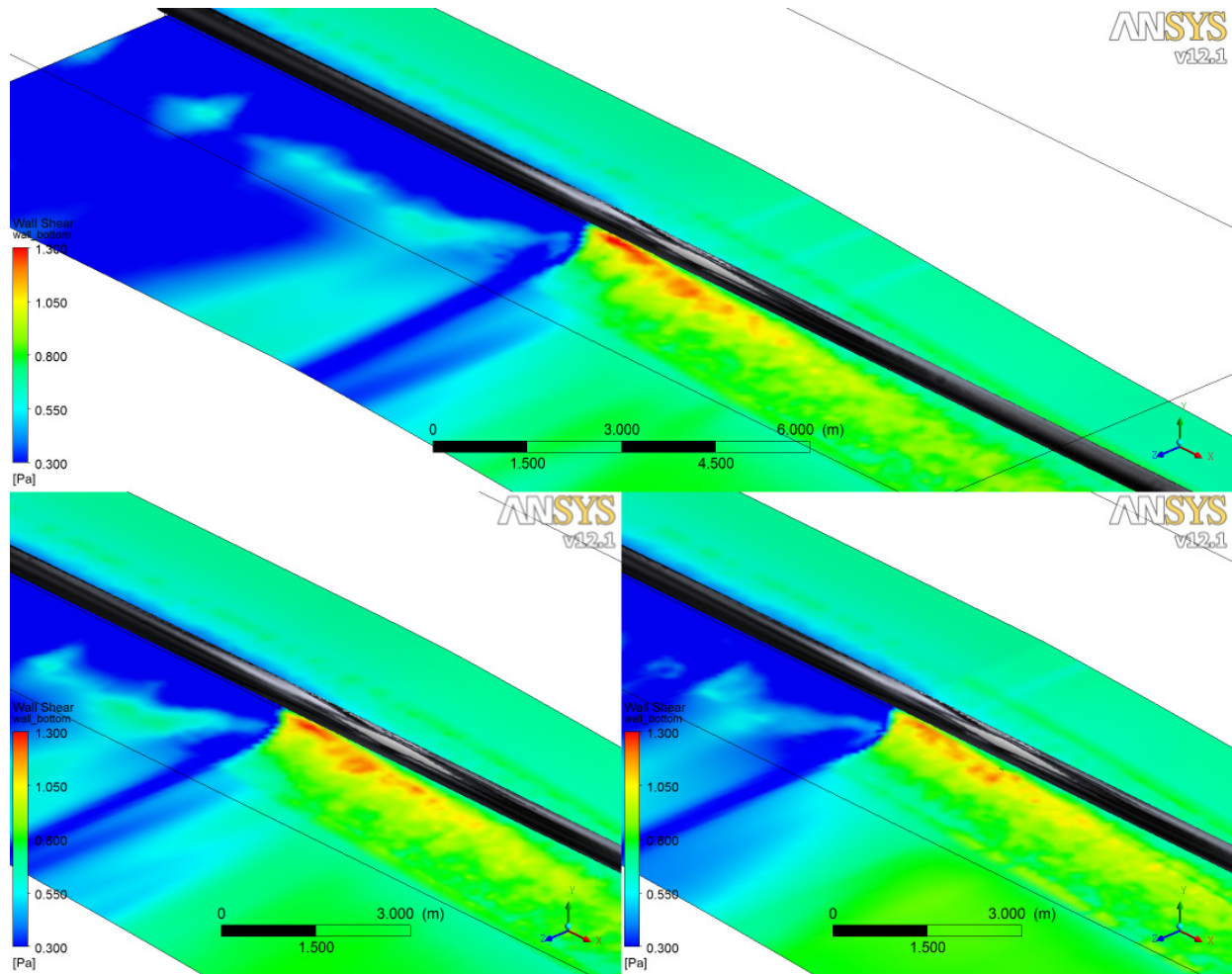


Figure 4-9. Global bed shear stress (Pa) patterns for Span 2. Constructs from varying data resolution are displayed in each sub window: top is the 1-foot resolution construct; bottom left is the 5-foot resolution construct; bottom right is the 10-resolution construct. The pipeline is colored gray to elucidate its position. Regions of high shear stress are represented by hot colors, while areas of low shear stress are depicted by cool colors.

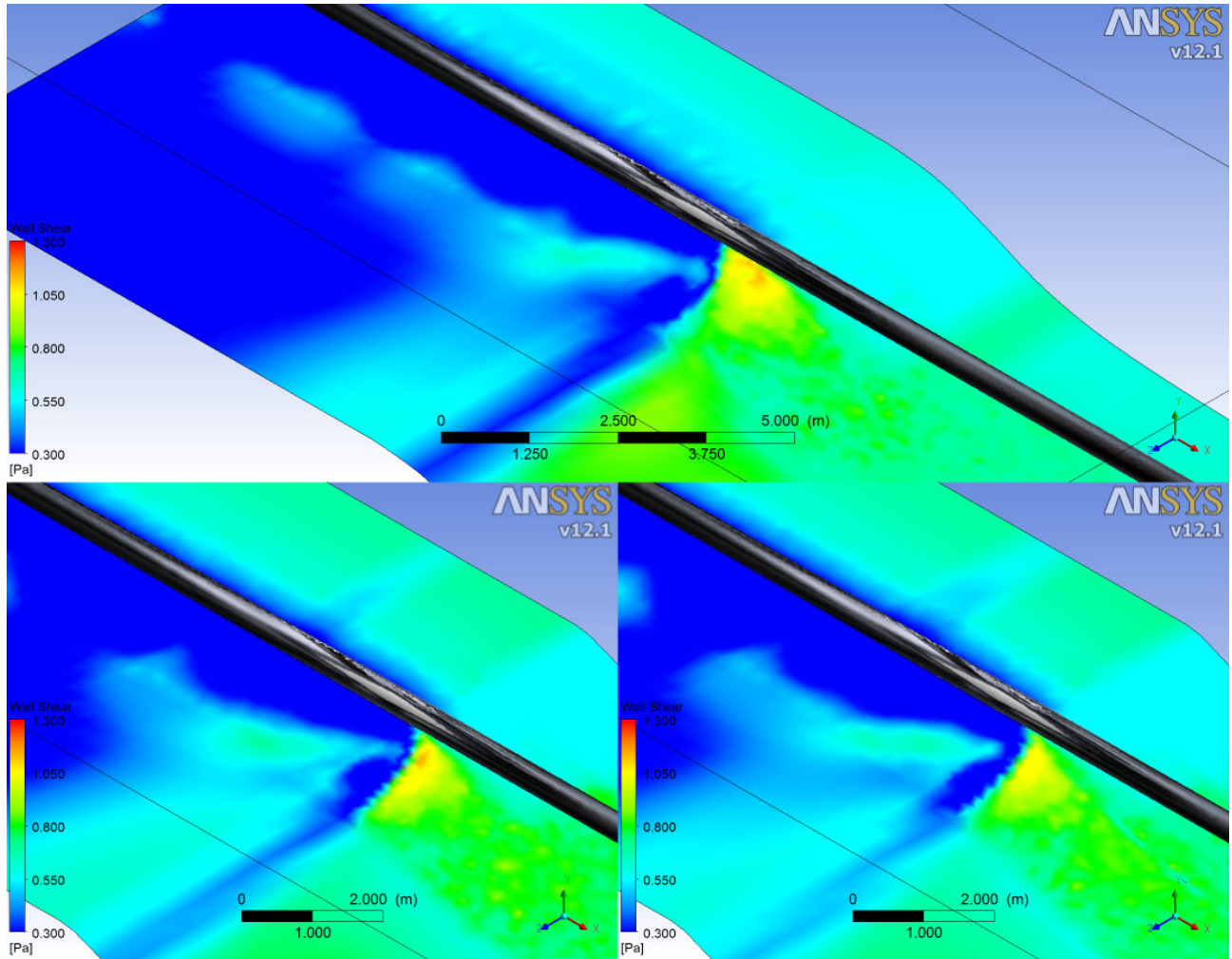


Figure 4-10. Global bed shear stress (Pa) patterns for Span 3. Constructs from varying data resolution are displayed in each sub window: top is the 1-foot resolution construct; bottom left is the 5-foot resolution construct; bottom right is the 10-resolution construct. The pipeline is colored gray to elucidate its position. Regions of high shear stress are represented by hot colors, while areas of low shear stress are depicted by cool colors.

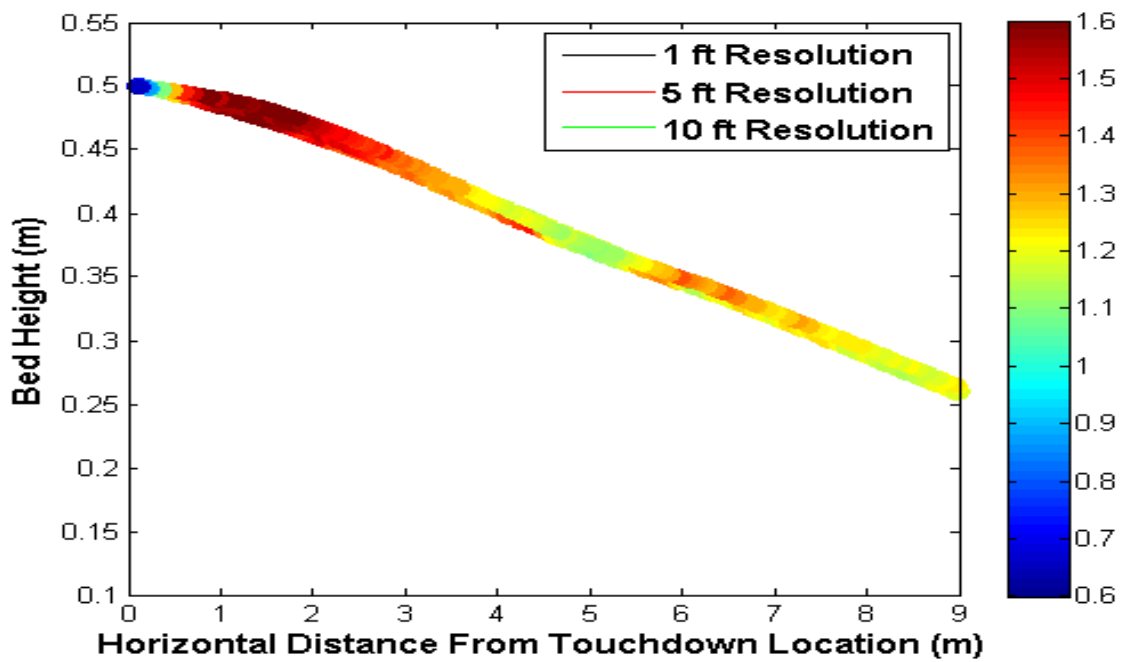


Figure 4-11. Bed shear stress (Pa) profiles for Span 1 directly under the pipe for 1, 5 and 10 foot data resolution constructs.

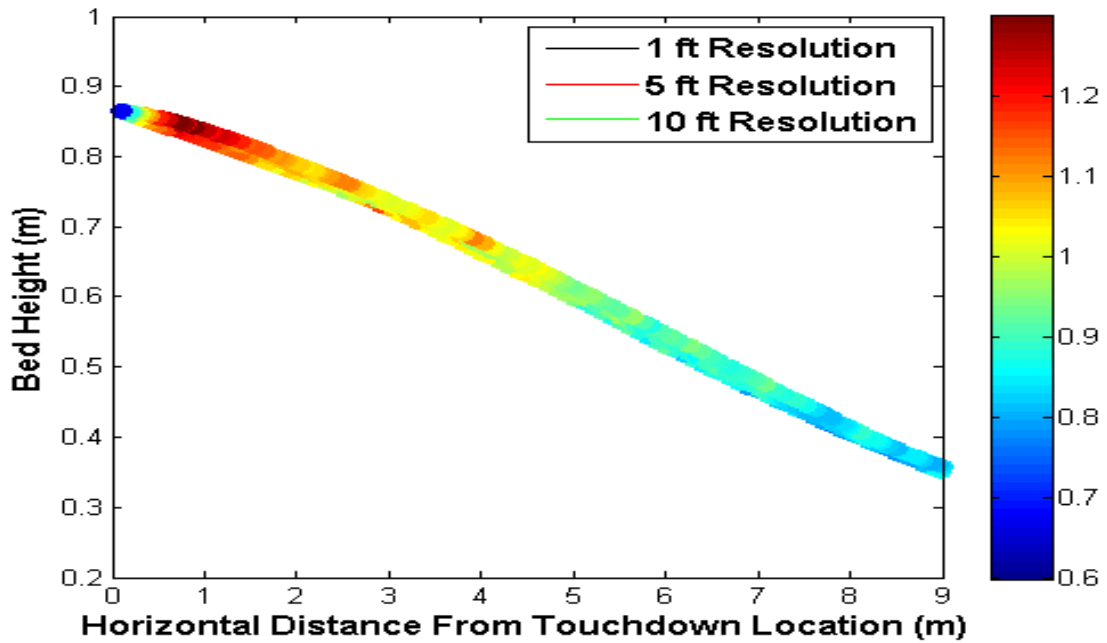


Figure 4-12. Bed shear stress (Pa) profiles for Span 2 directly under the pipe for 1, 5 and 10 foot data resolution constructs.

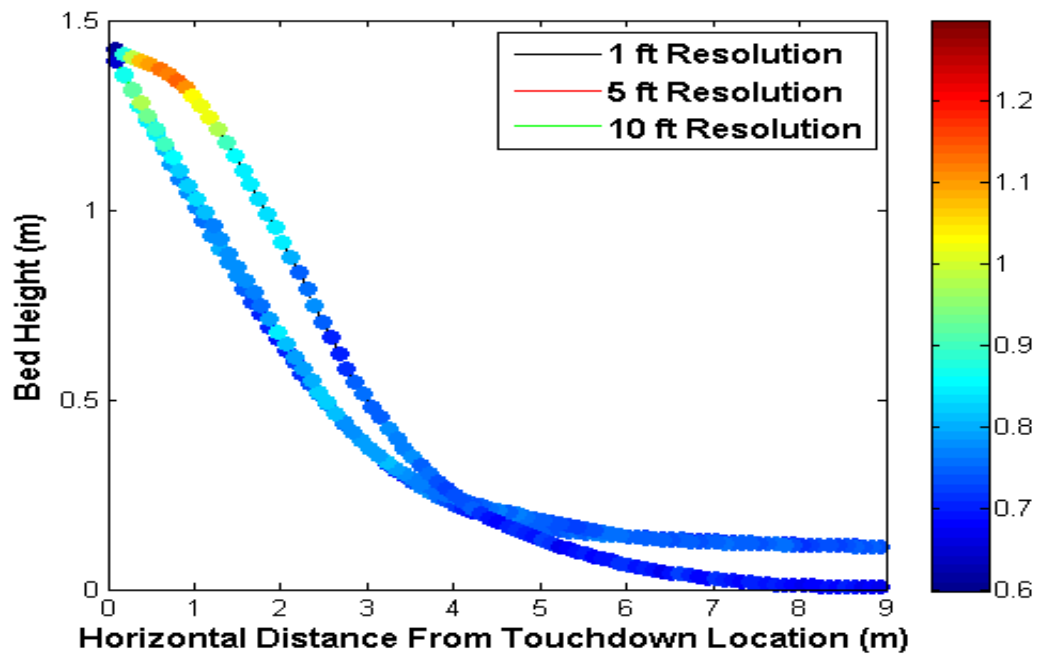


Figure 4-13. Bed shear stress (Pa) profiles for Span 3 directly under the pipe for 1, 5 and 10 foot data resolution constructs.

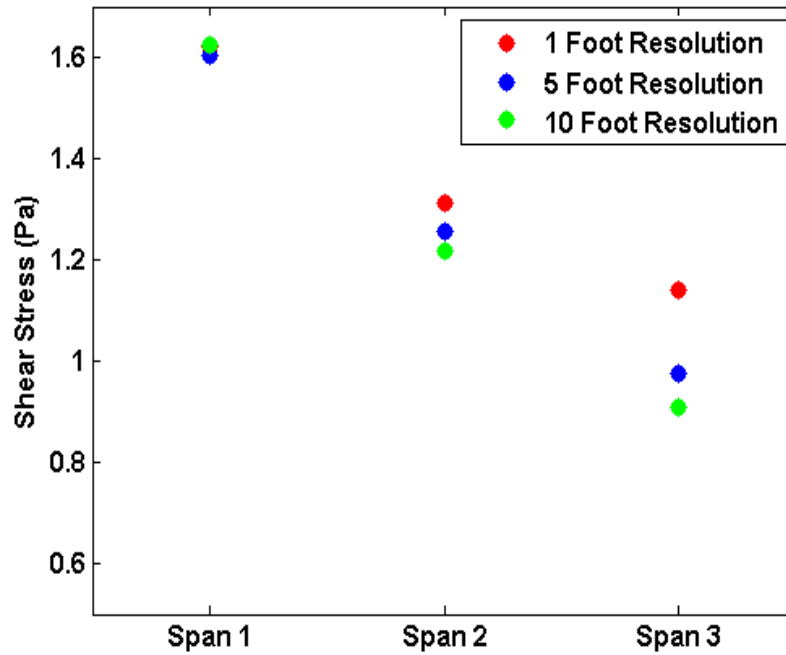


Figure 4-14. Maximum calculated shear stress (Pa) on the sediment bed for all constructs.

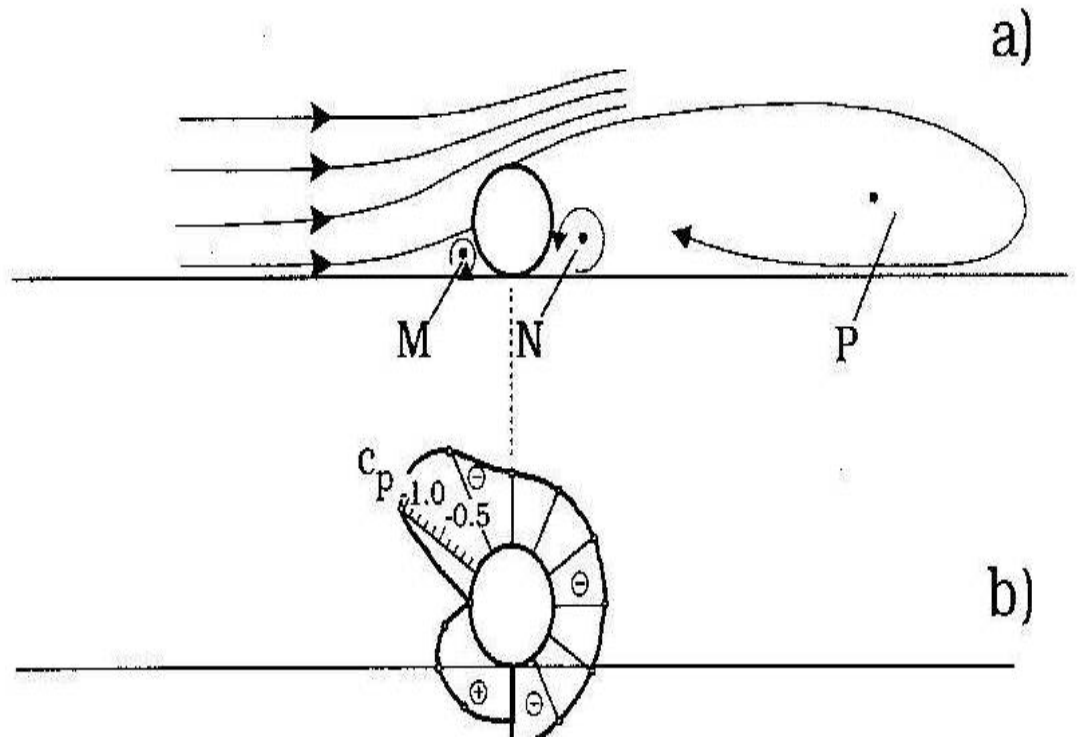


Figure 5-1. Schematic of flow characteristics around a pipeline on the seabed. a) Flow streamlines over the pipeline showing flow separation and downstream recirculation. b) Pressure distribution around the pipeline.

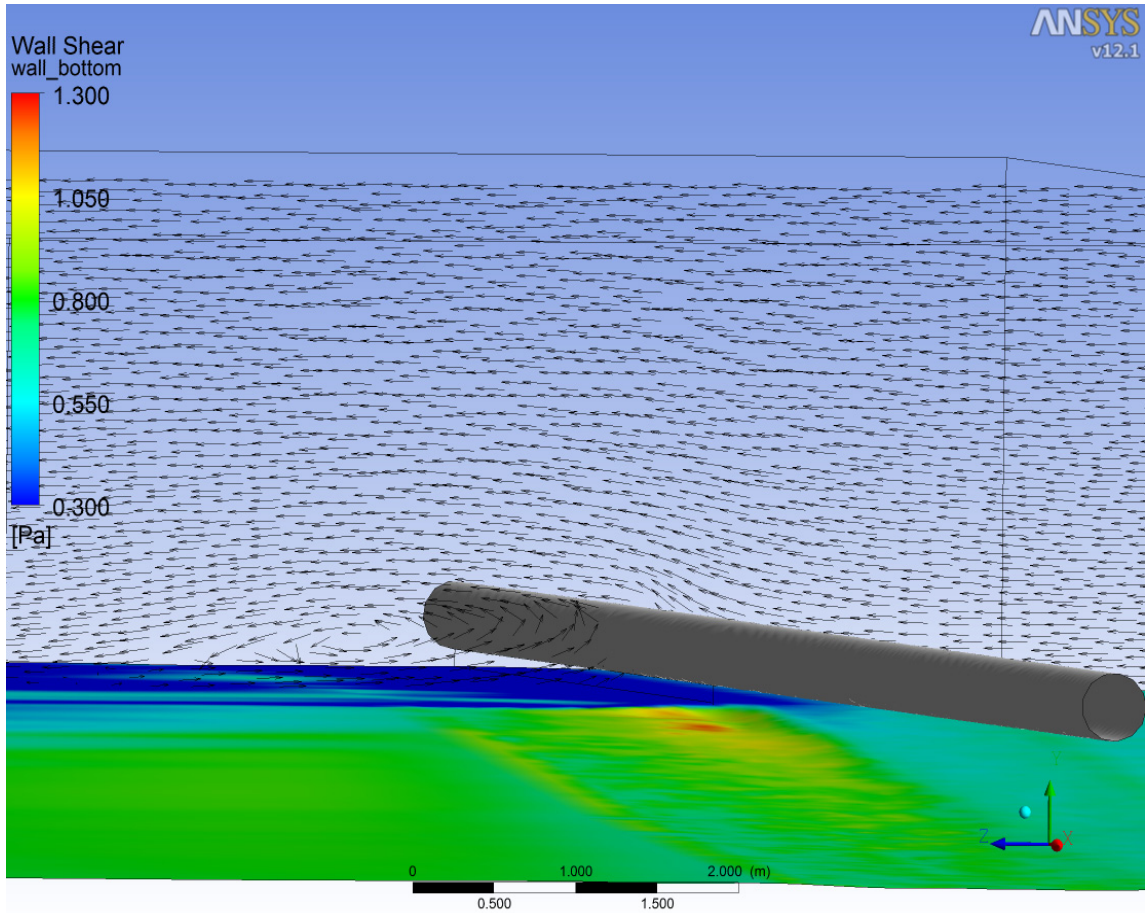


Figure 5-2. Figure 2. Velocity vectors and seabed shear stress contours (Pa) along an example pipeline span. The pipeline is in contact with the bed in the far side of the image and the near side is the span.

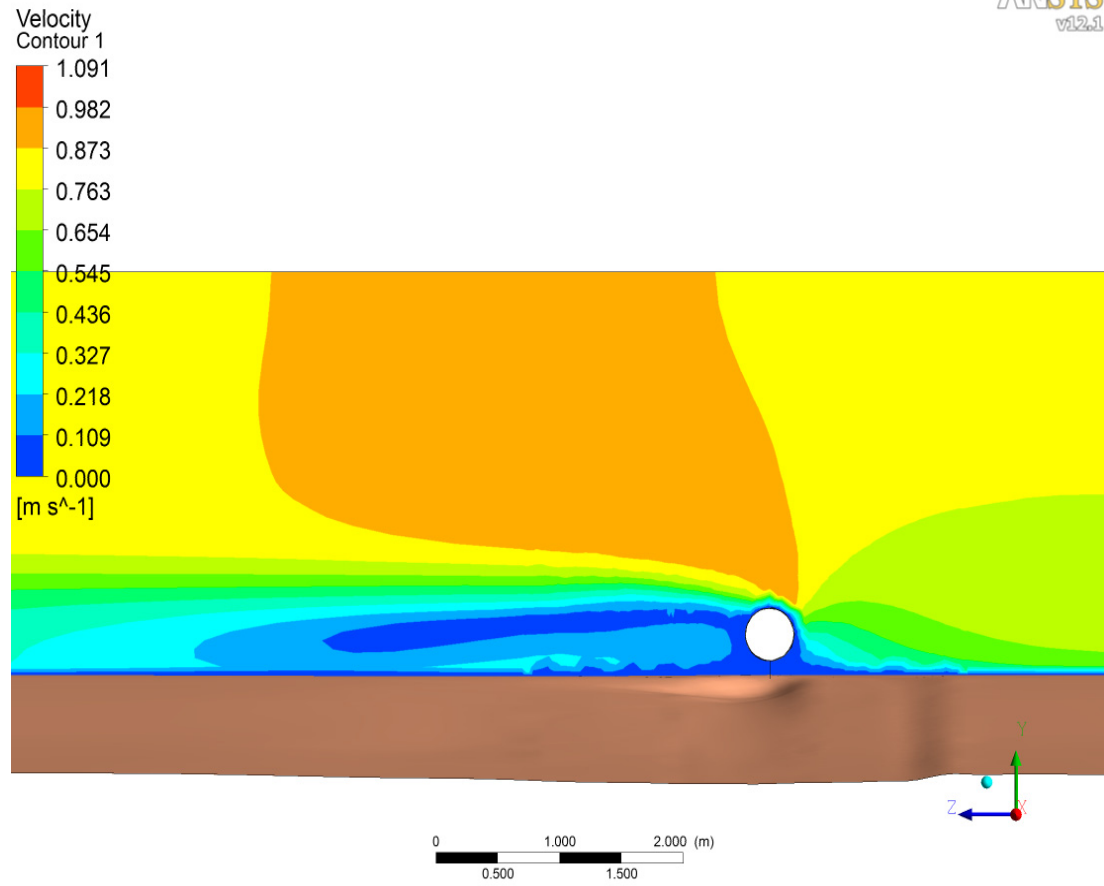


Figure 5-3. Velocity contour (m/s) cross section in the at the pipeline shoulder

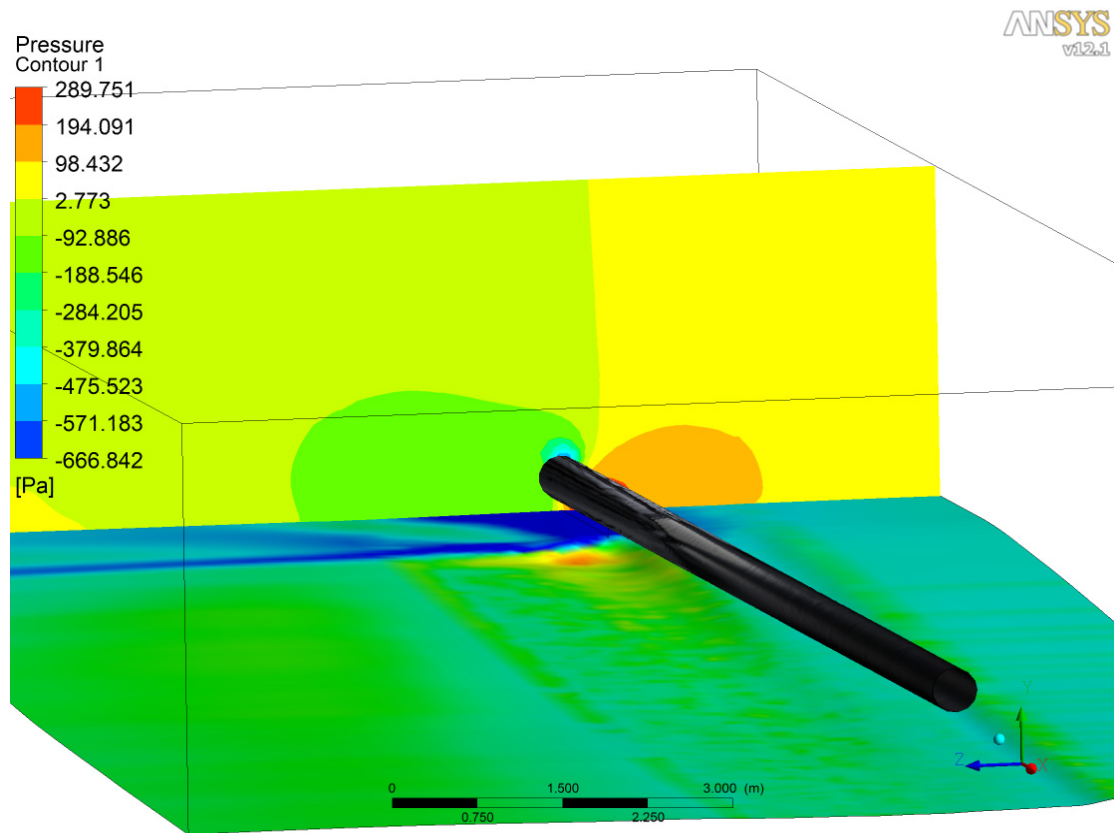


Figure 5-4. Pressure contour (Pa) cross section in the at the pipeline shoulder.

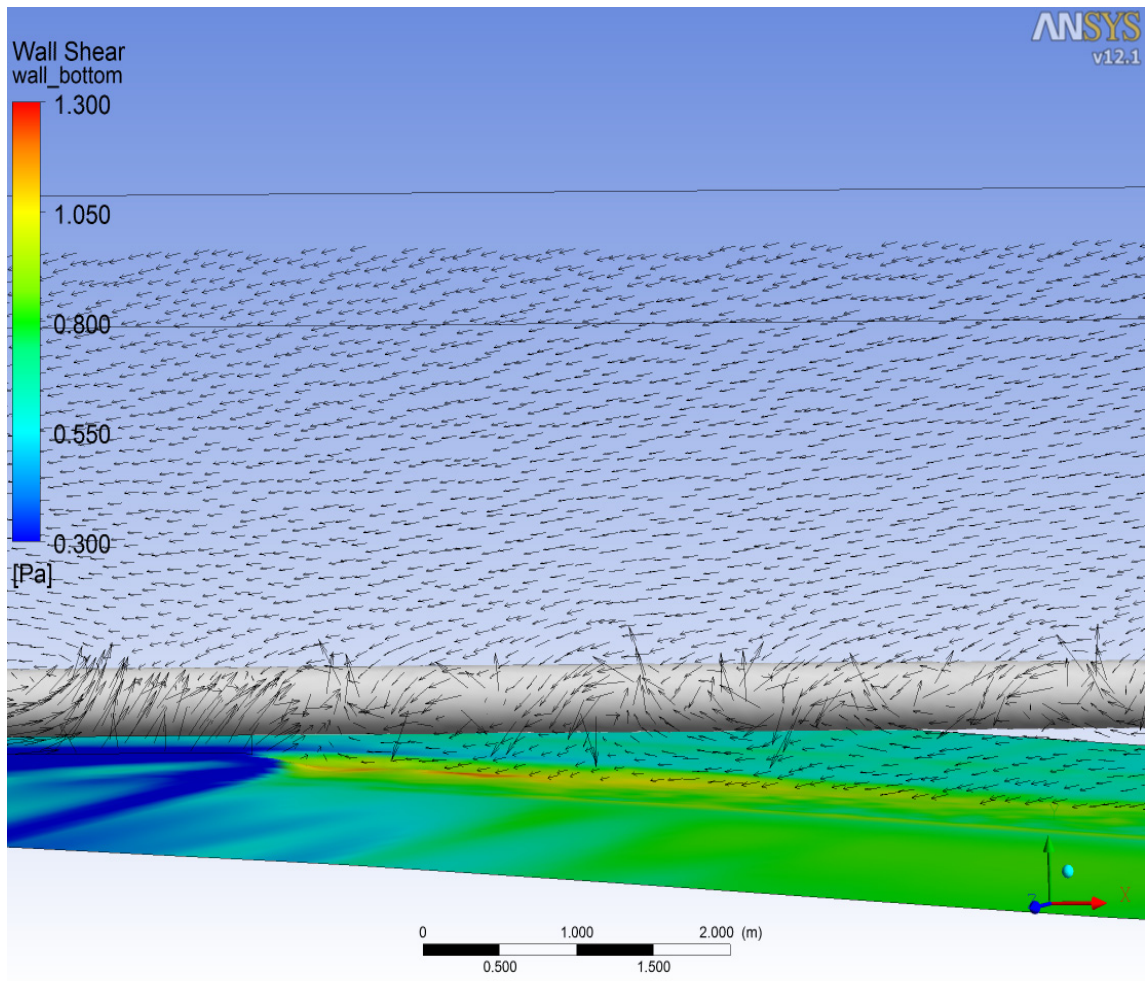


Figure 5-5. Velocity vectors (m/s) cross section and bed shear stress (Pa) in the wake of the pipeline shoulder.

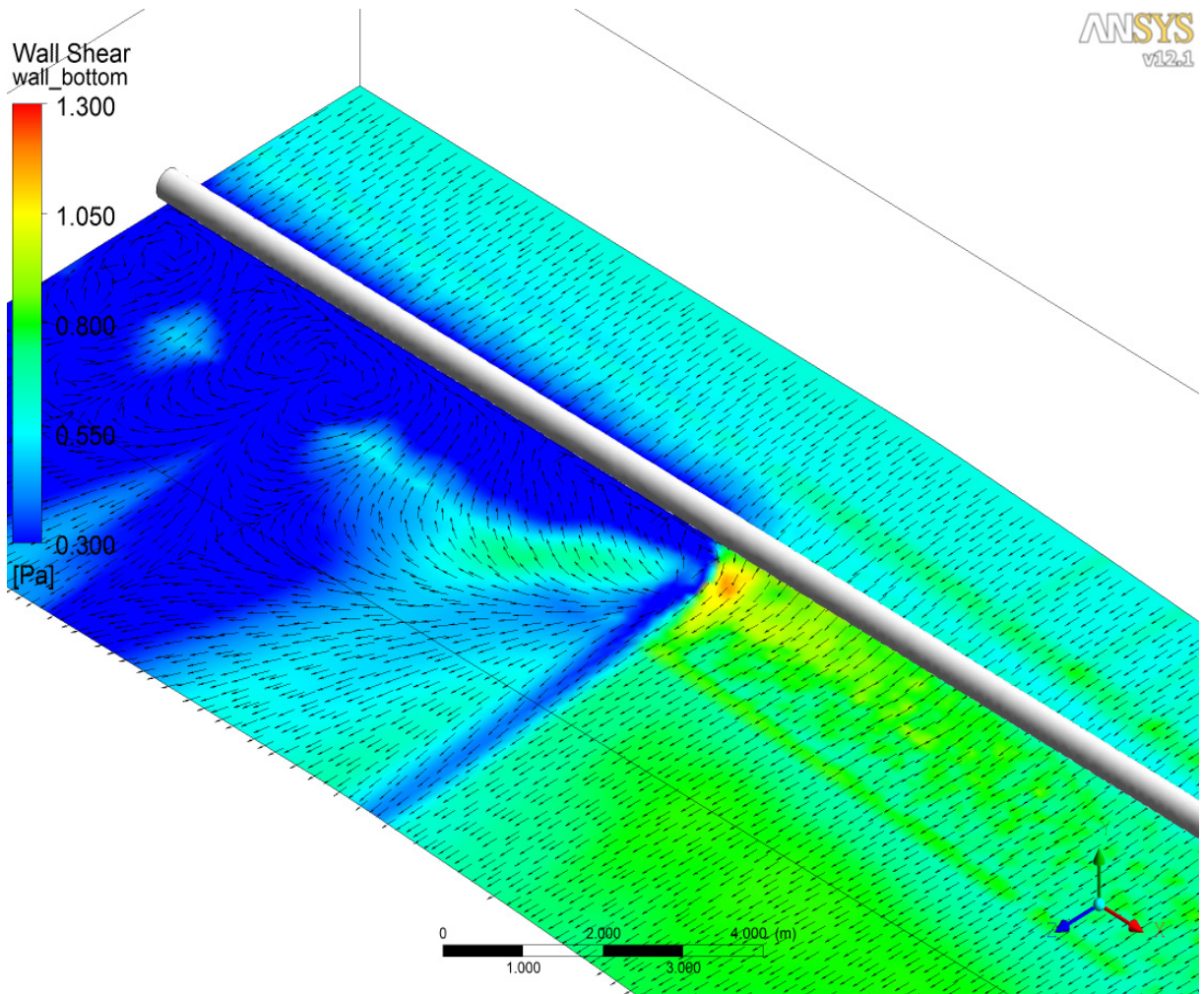


Figure 5-6. Velocity vectors (m/s) cross section and bed shear stress (Pa) over the pipeline shoulder region. Top half of the figure is where the pipeline is on the sediment bed, the middle is the shoulder region, and the lower half is the span region.

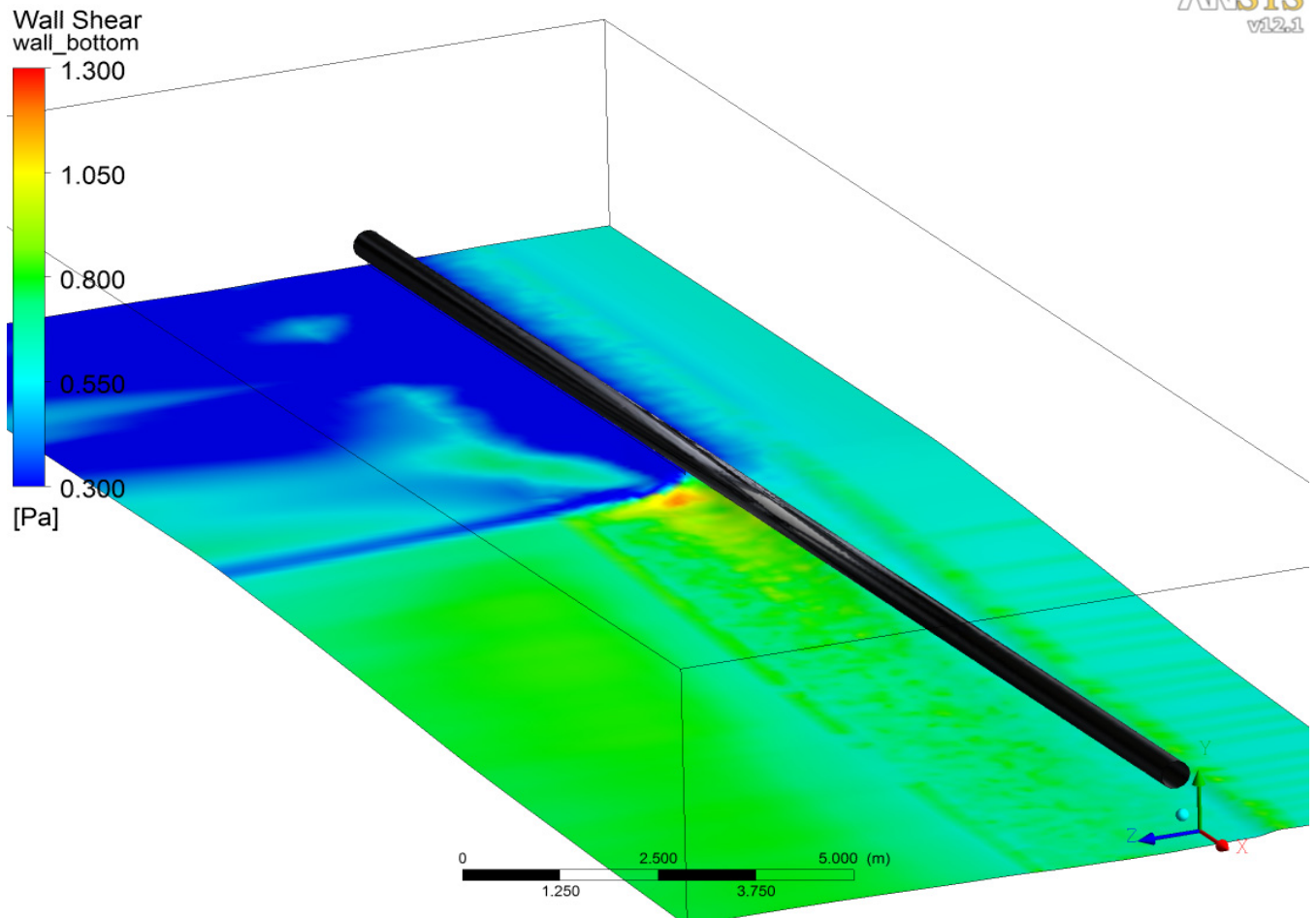


Figure 5-7. Bed shear stress (Pa) contours over the pipeline shoulder region. Top half of the figure is where the pipeline is on the sediment bed, the middle is the shoulder region, and the lower half is the span region.

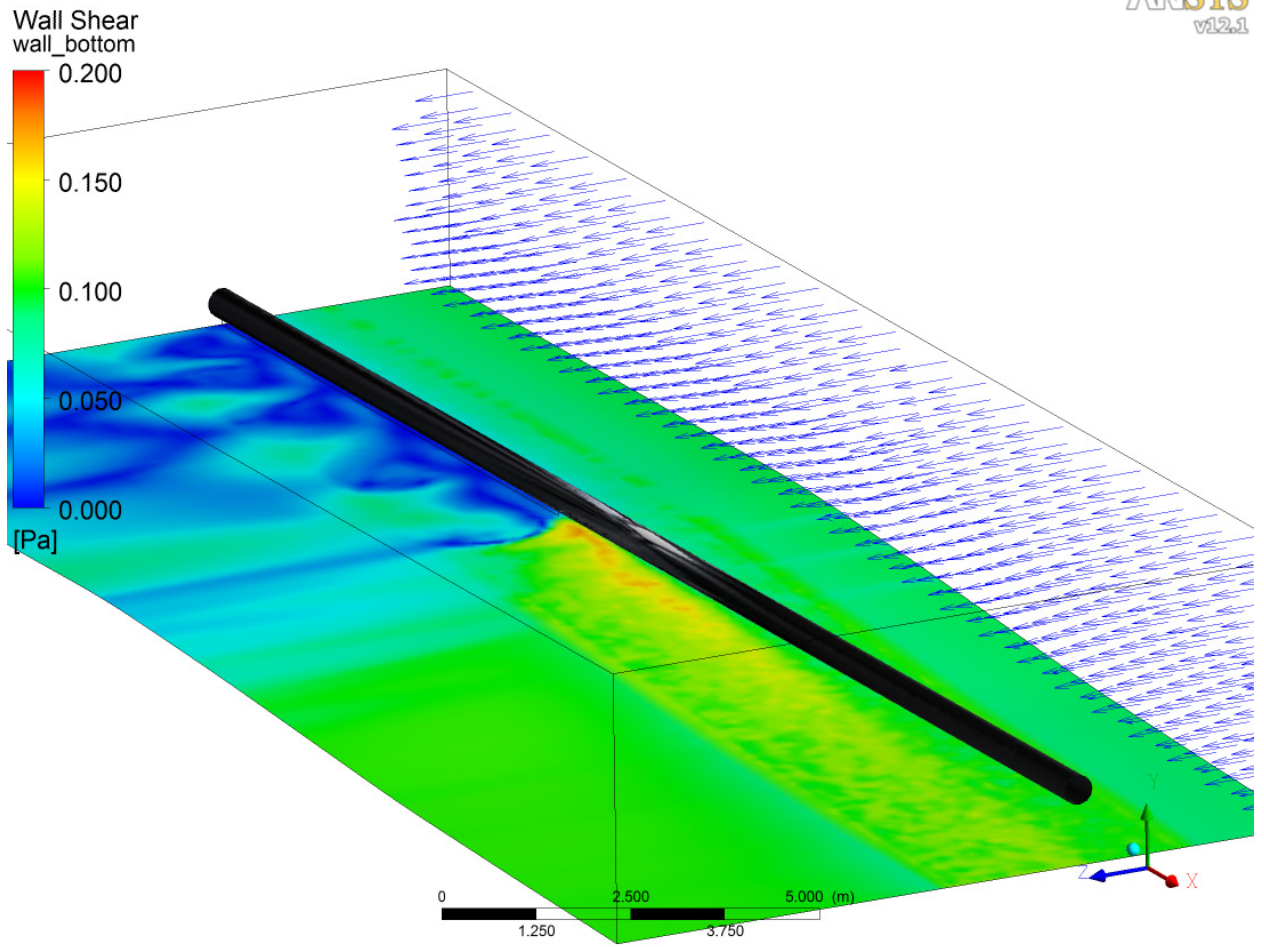


Figure 5-8. Global shear stress (Pa) pattern on Span 2 using a current speed of 25 cm/s. The bed shear stress was below the critical shear stress of sand (0.2 Pa) over the sediment bed.

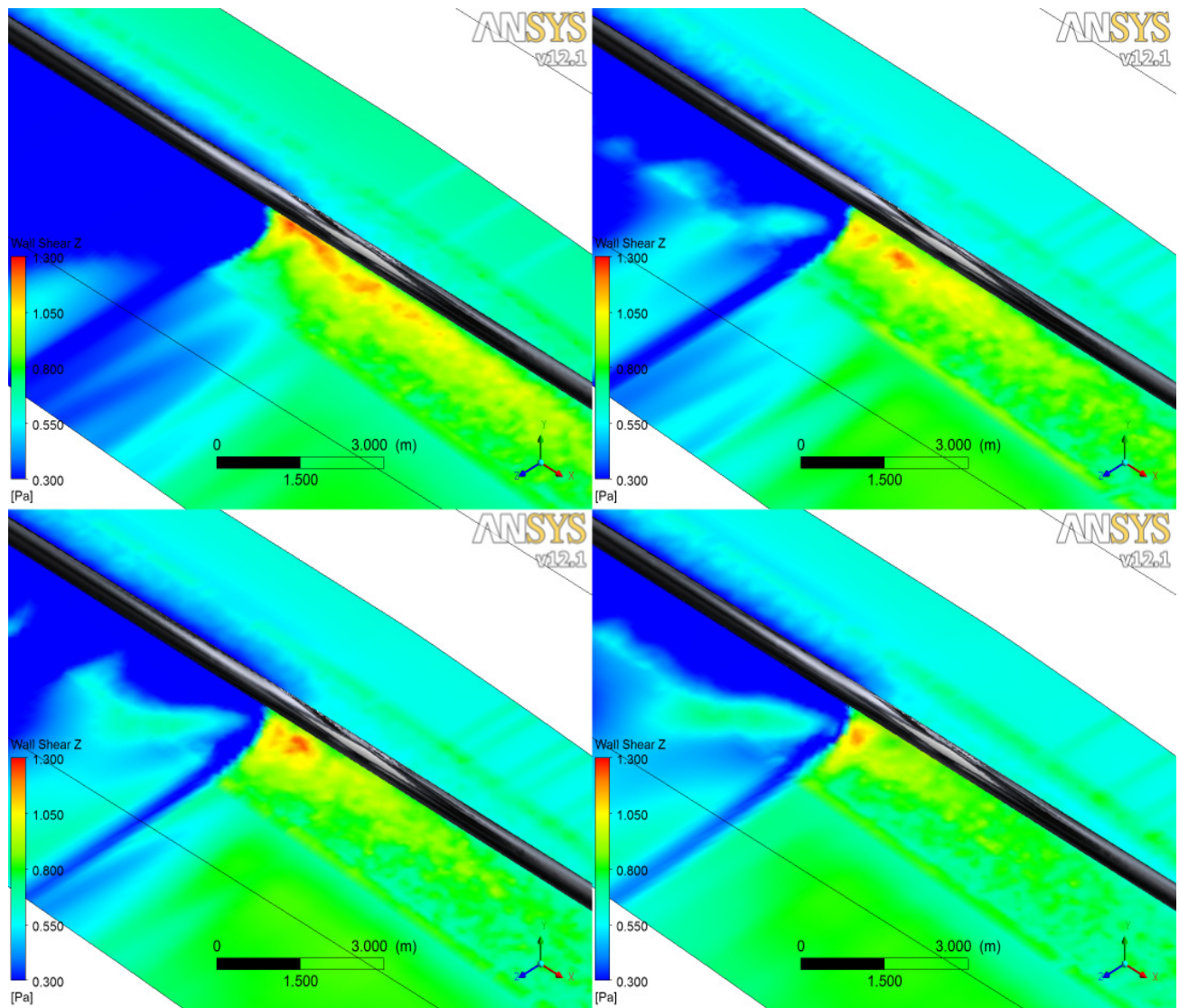


Figure 5-9. Global bed shear stress (Pa) on eroding bed for the initial bed form (top left), bed after 1 day (top right), bed after 2 days (bottom left), and bed after 3 days (bottom right) of 75 cm/s current speeds.

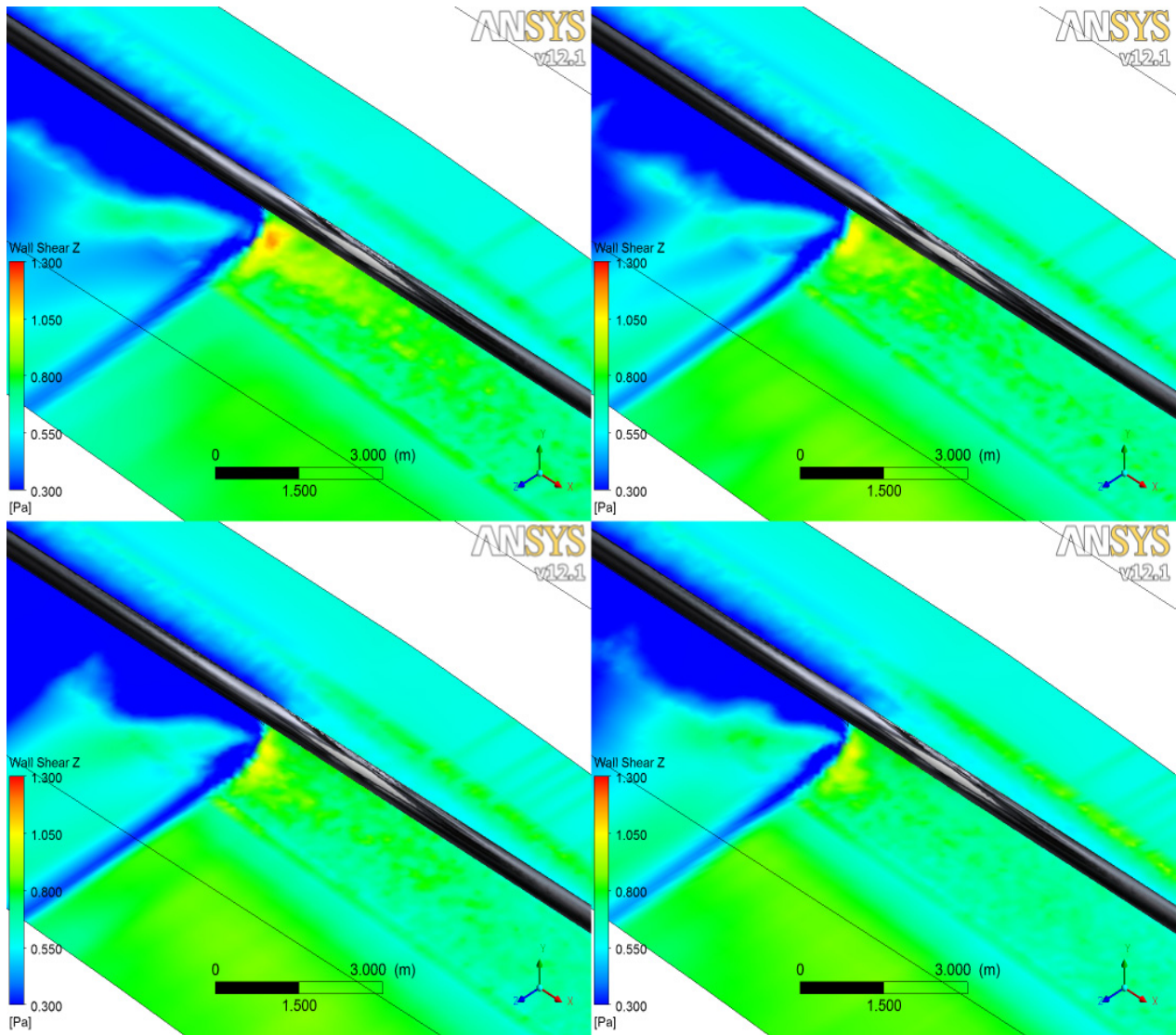


Figure 5-10. Global bed shear stress (Pa) on eroding bed after 3 days (top left), 4 days (top right), 5 days (bottom left), and 6 days (bottom right) of 75 cm/s current speeds.

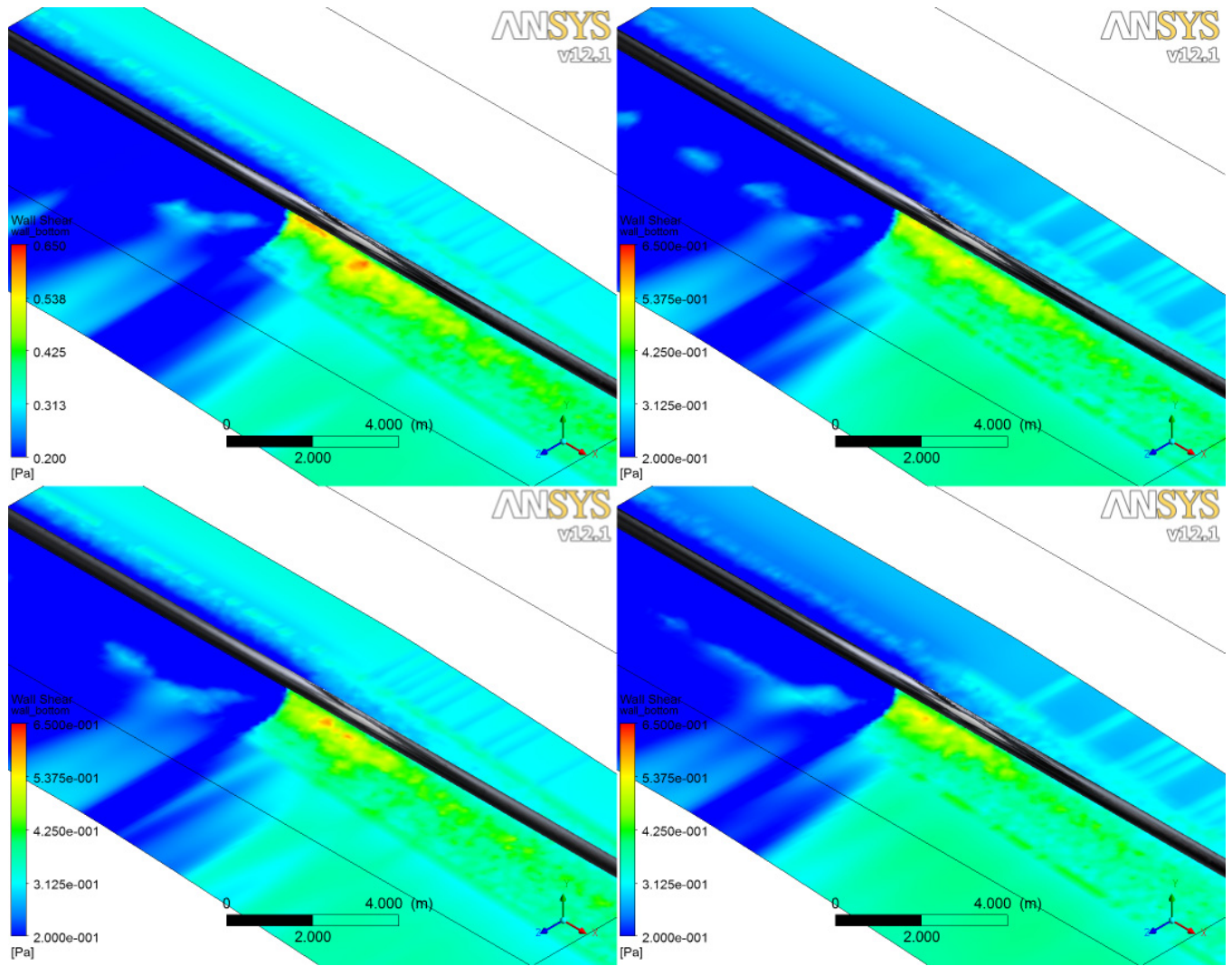


Figure 5-11. Global bed shear stress (Pa) on eroding bed for the initial bed form (top left), bed after 2 days (top right), bed after 4 days (bottom left), and bed after 6 days (bottom right) of 50 cm/s current speeds.

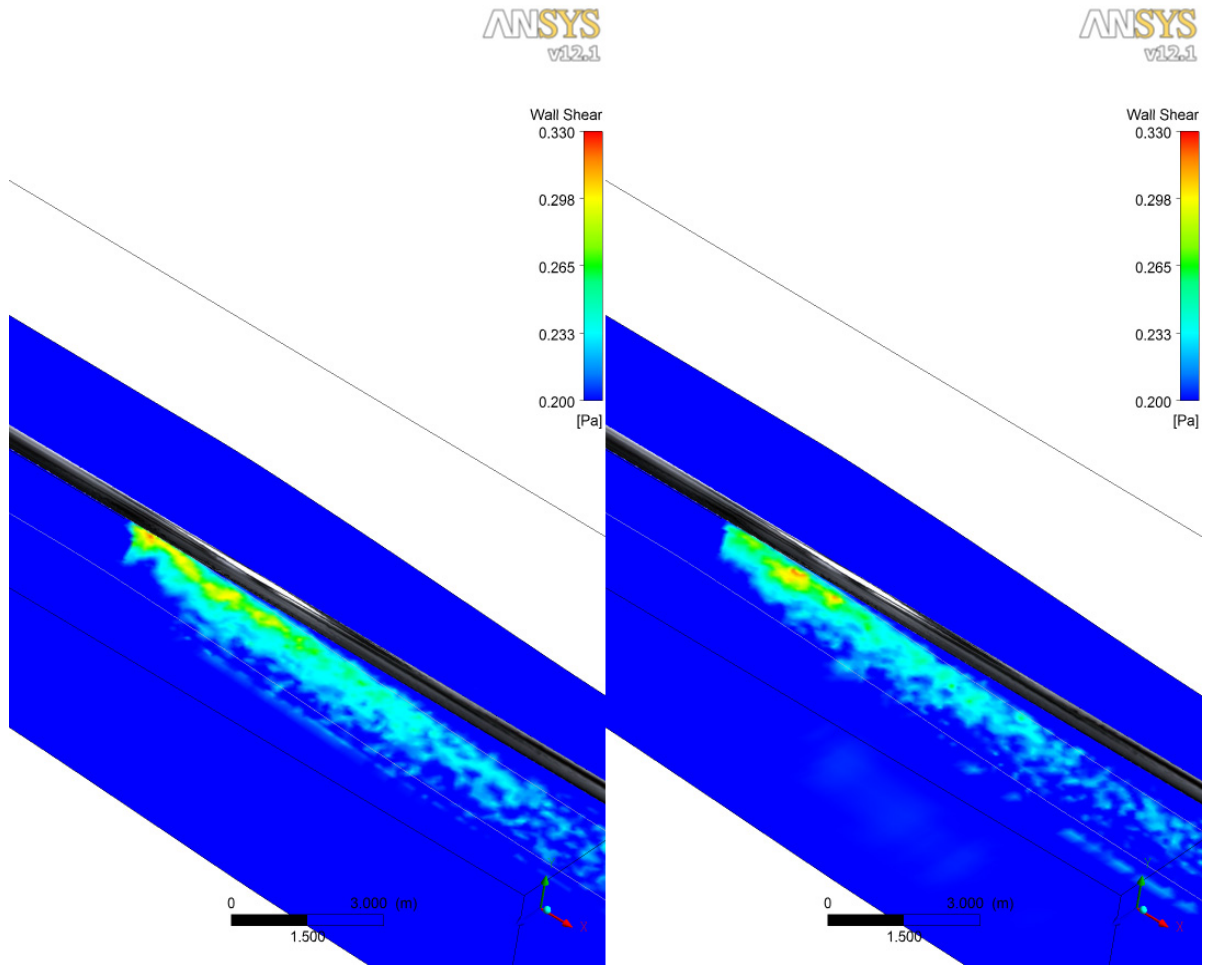


Figure 5-12. Global bed shear stress (Pa) on eroding bed for the initial bed form (right), and the bed after 6 days of 35 cm/s current speeds.

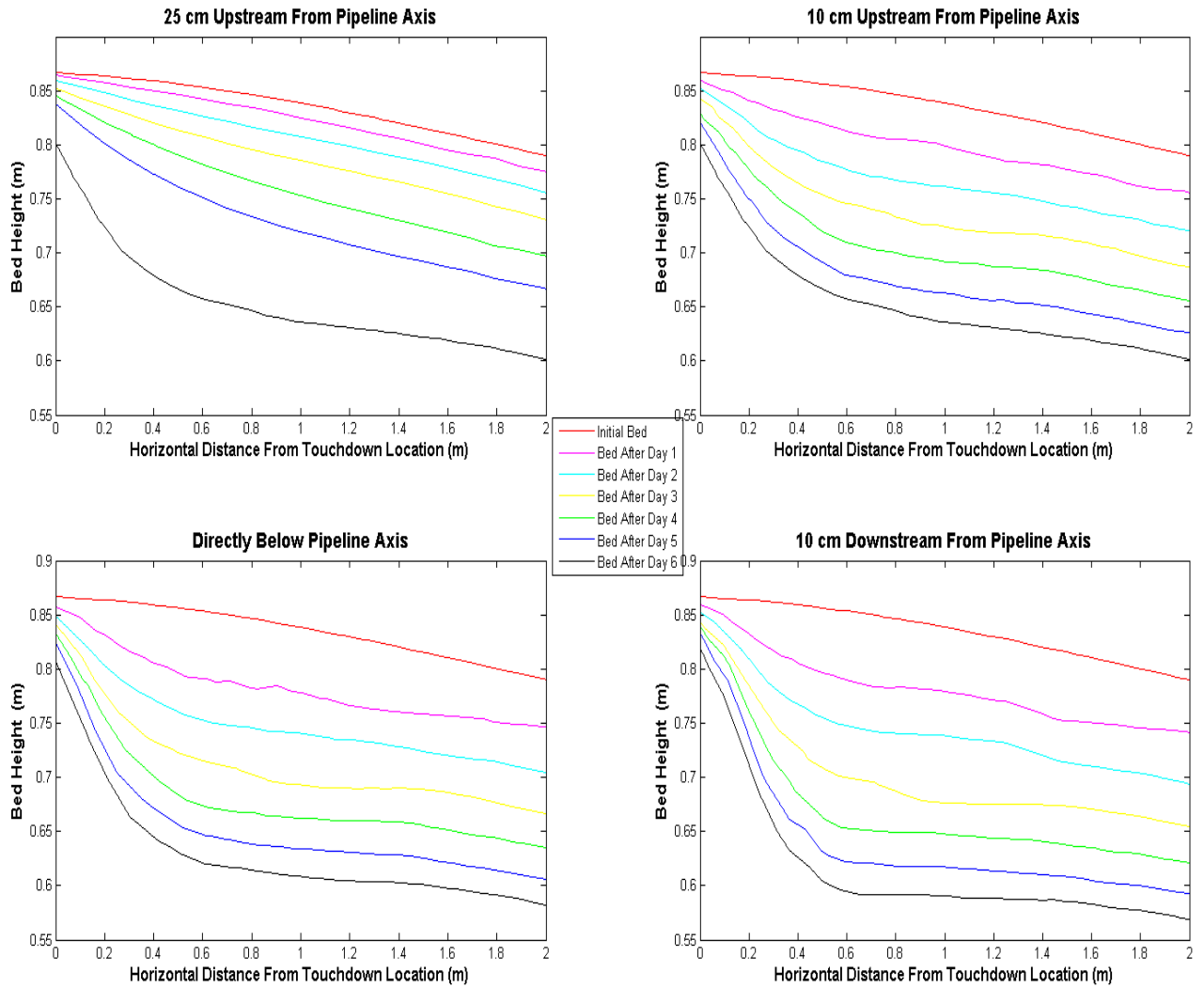


Figure 5-13. Time series of bed profiles for the 75 cm/s simulations. Profiles were taken at 10 and 25 cm upstream from the pipeline axis, directly below the pipeline axis, and 10 cm downstream from the pipeline axis.

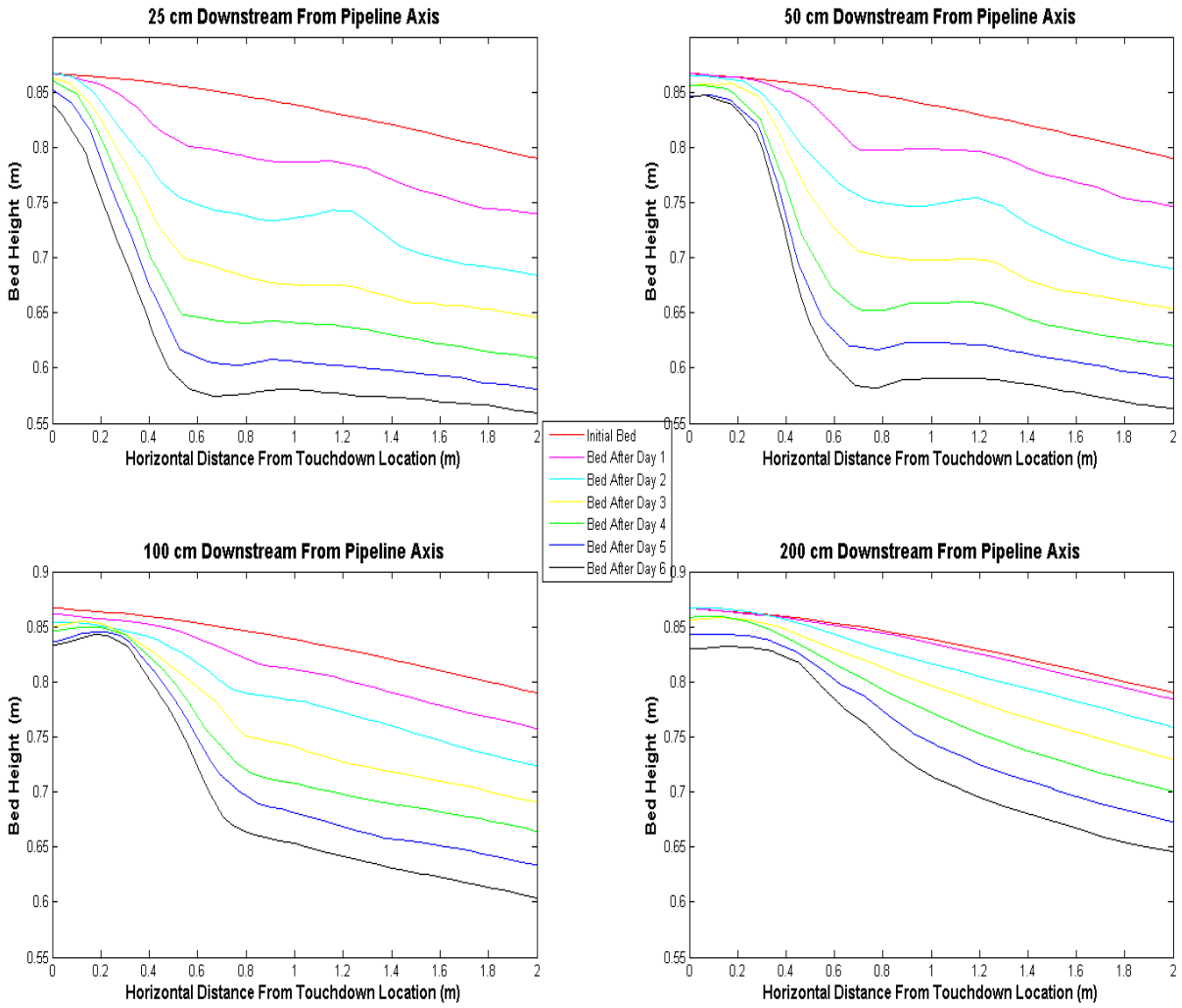


Figure 5-14. Time series of bed profiles for the 75 cm/s simulations. Profiles were taken at 25, 50, 100, and 200 cm downstream from the pipeline axis.

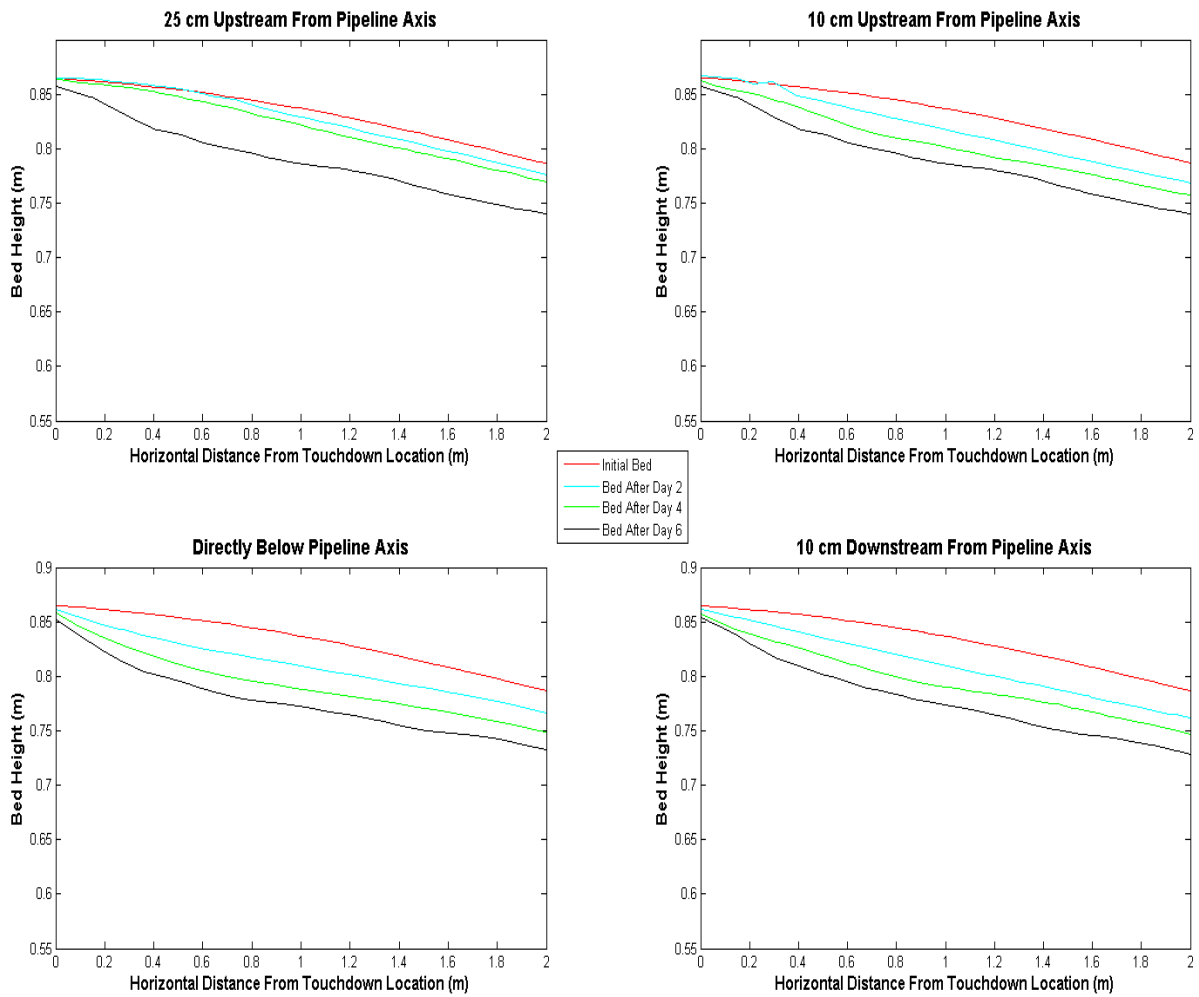


Figure 5-15. Time series of bed profiles for the 50 cm/s simulations. Profiles were taken at 10 and 25 cm upstream from the pipeline axis, directly below the pipeline axis, and 10 cm downstream from the pipeline axis.

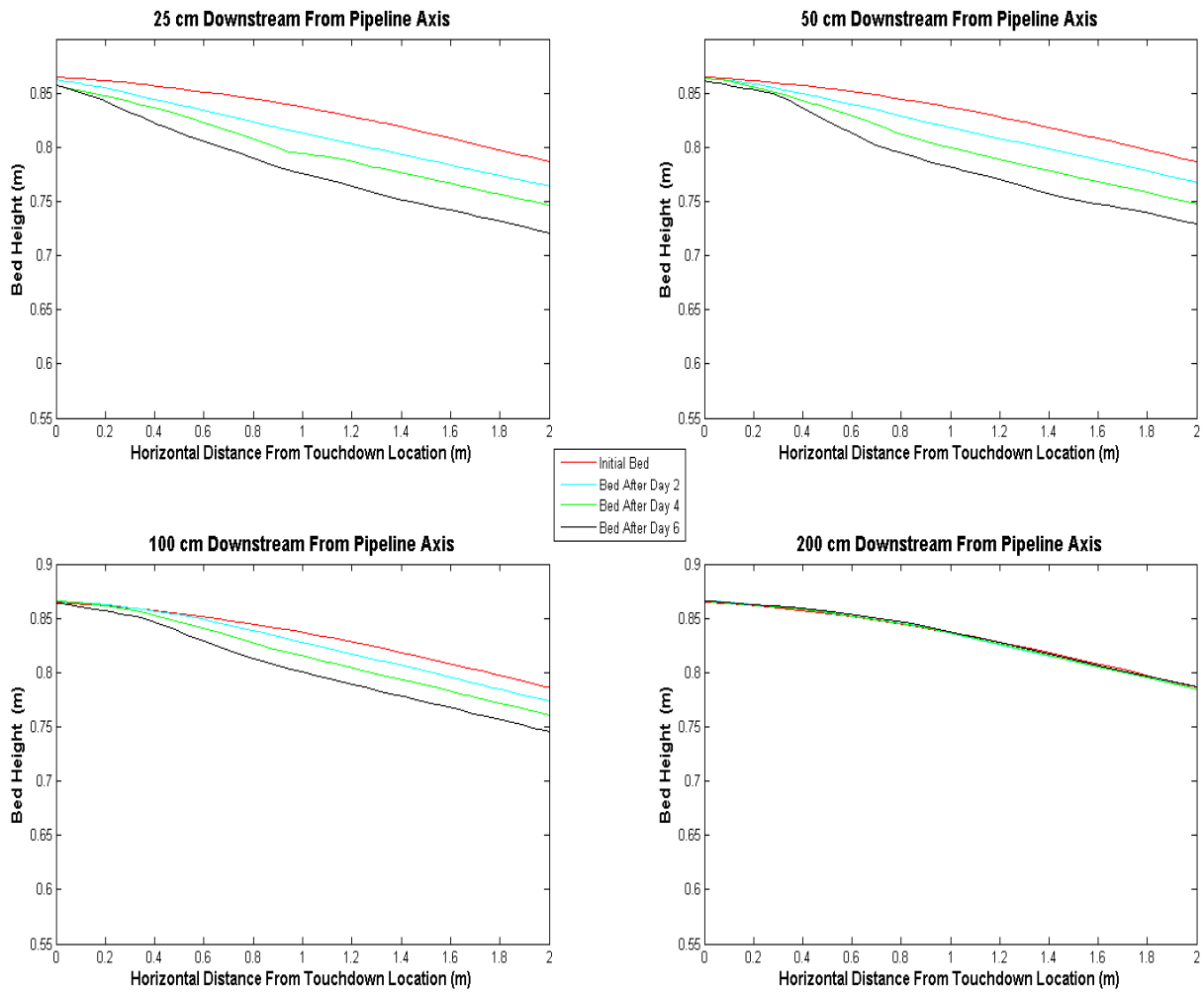


Figure 5-16. Time series of bed profiles for the 50 cm/s simulations. Profiles were taken at 25, 50, 100, and 200 cm downstream from the pipeline axis.

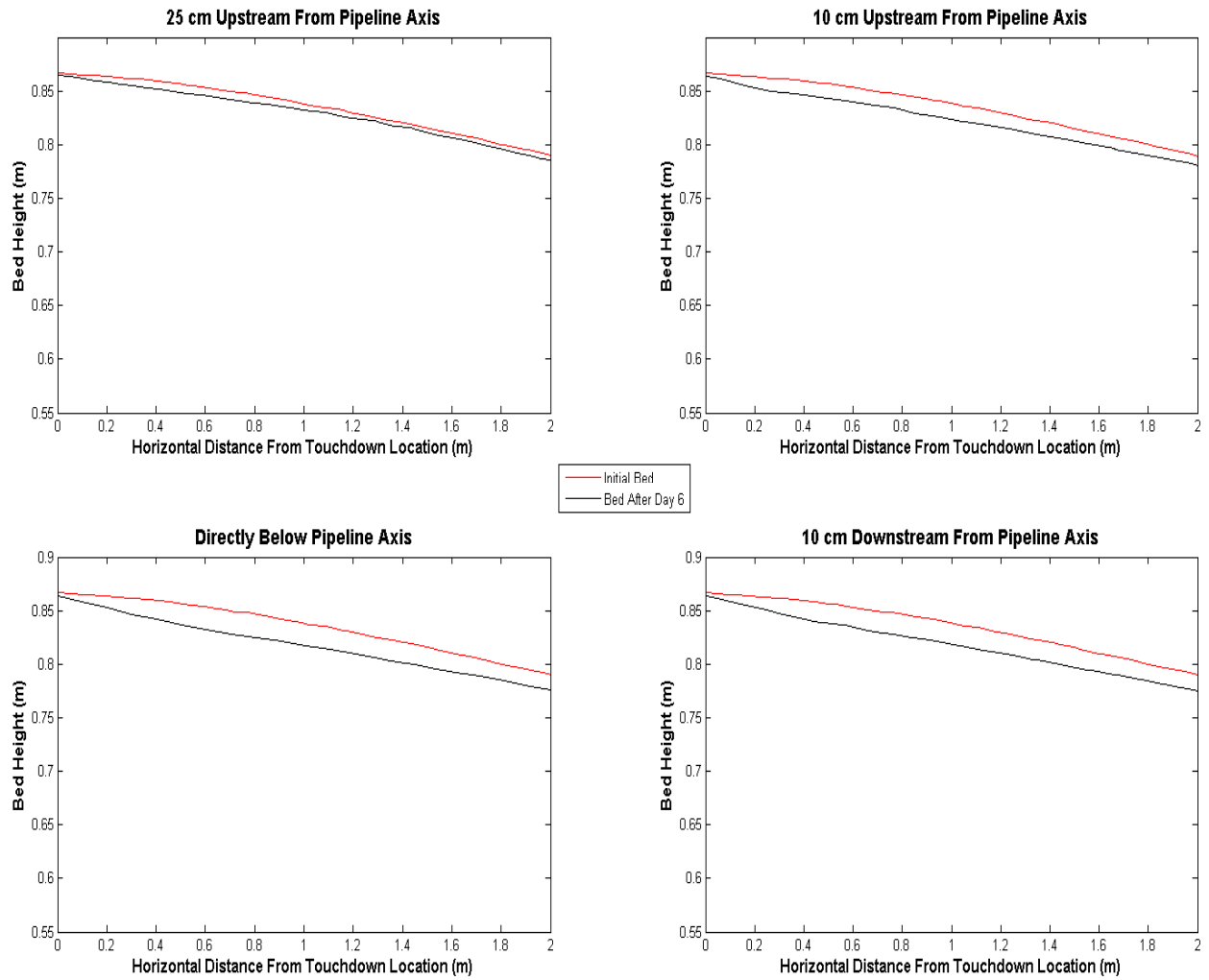


Figure 5-17. Time series of bed profiles for the 35 cm/s simulations. Profiles were taken at 10 and 25 cm upstream from the pipeline axis, directly below the pipeline axis, and 10 cm downstream from the pipeline axis.

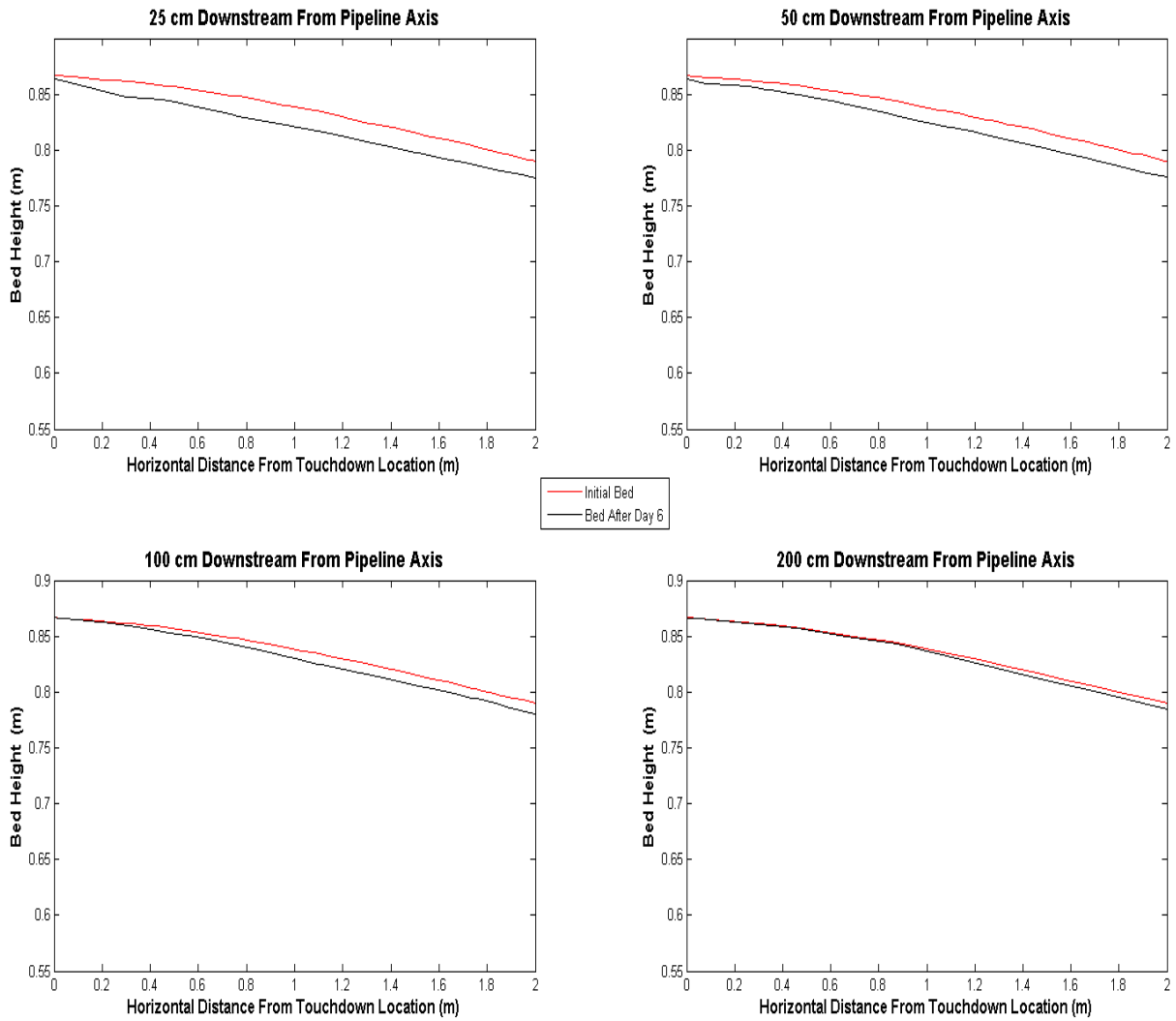


Figure 5-18. Time series of bed profiles for the 35 cm/s simulations. Profiles were taken at 25, 50, 100, and 200 cm downstream from the pipeline axis.

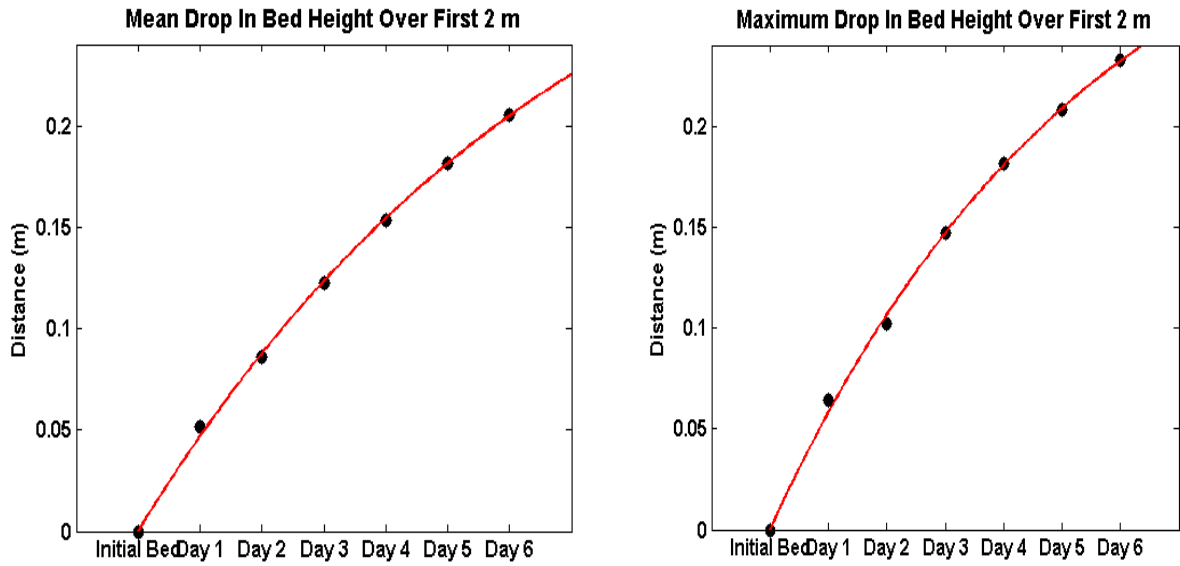


Figure 5-19. The mean (right) and maximum (left) drop in bed height (m) for the 75 cm/s simulations.

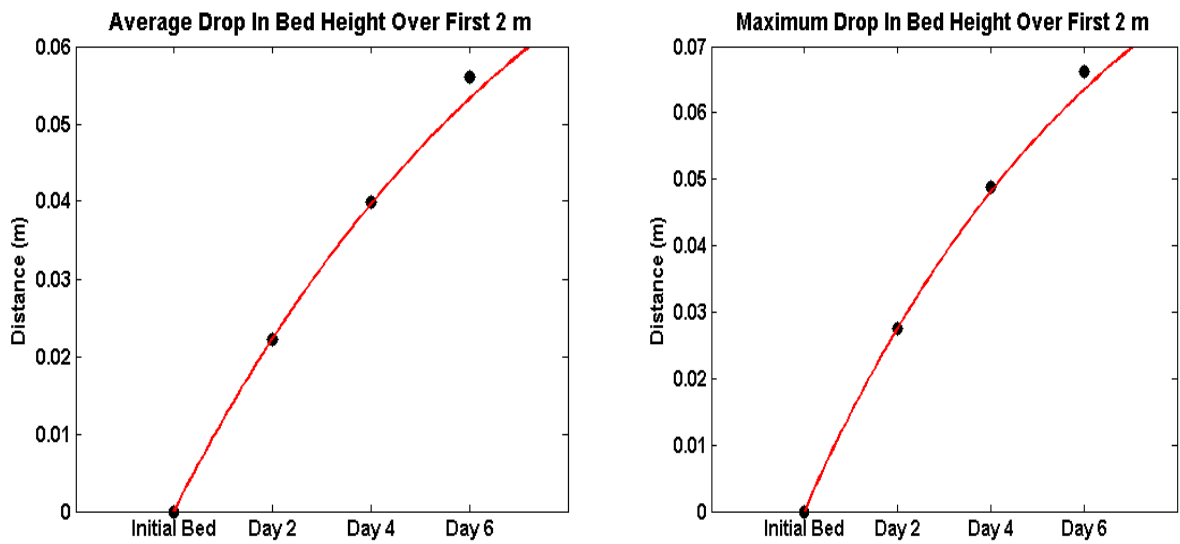


Figure 5-20. The mean (right) and maximum (left) drop in bed height (m) for the 50 cm/s simulations.

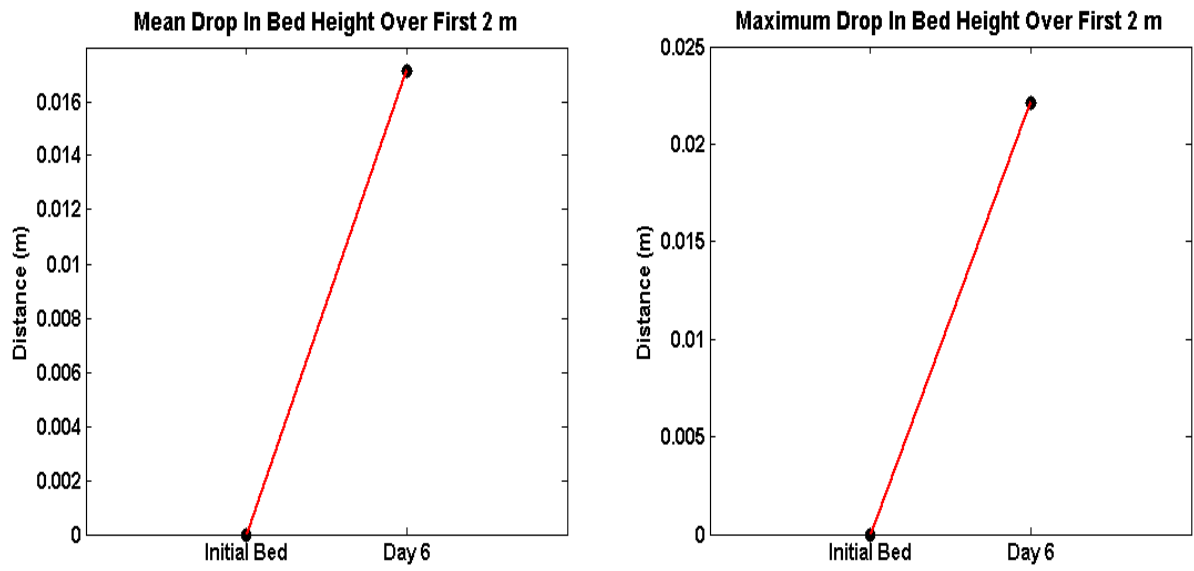


Figure 5-21. The mean (right) and maximum (left) drop in bed height (m) for the 35 cm/s simulations.

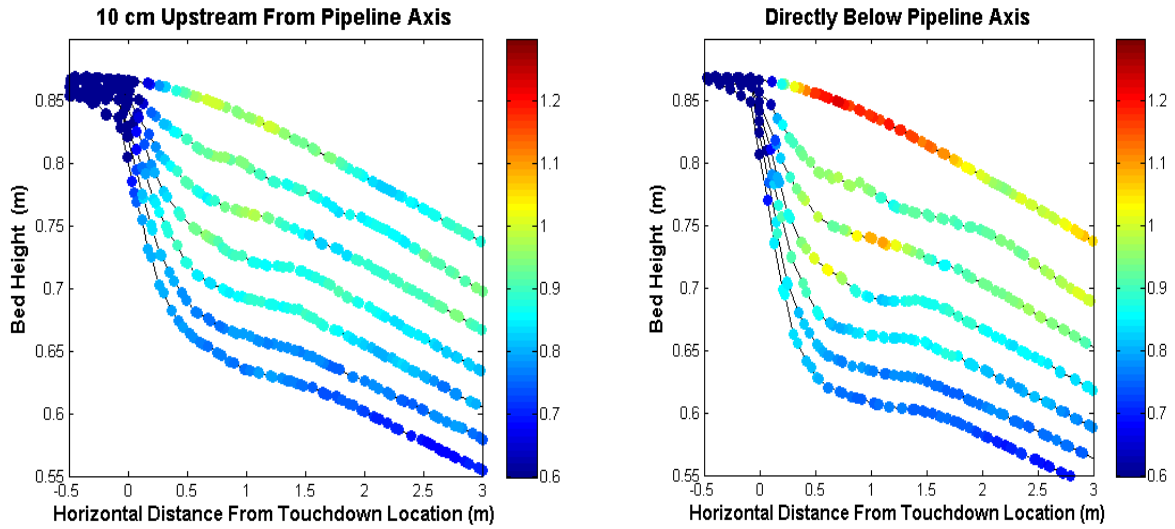


Figure 5-22. Time changing bed shear stress (Pa) profiles for the 75 cm/s simulations at 10 cm upstream from the pipeline axis (left), and directly below the pipeline axis (right).

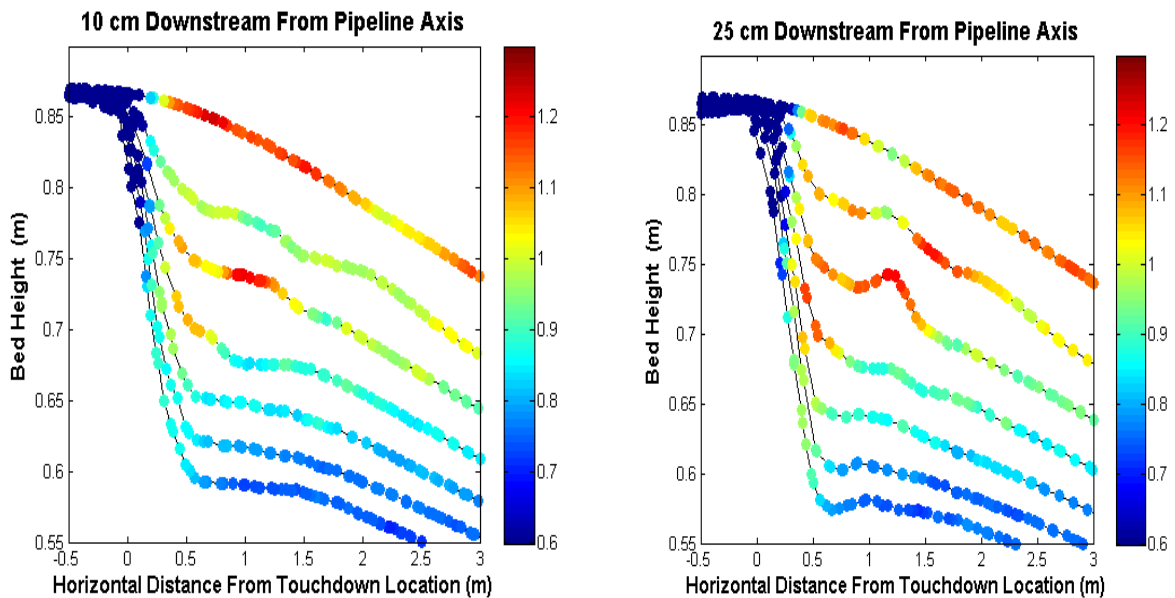


Figure 5-23. Time changing bed shear stress (Pa) profiles for the 75 cm/s simulations at 10 (left), and 25 cm downstream from the pipeline (right).

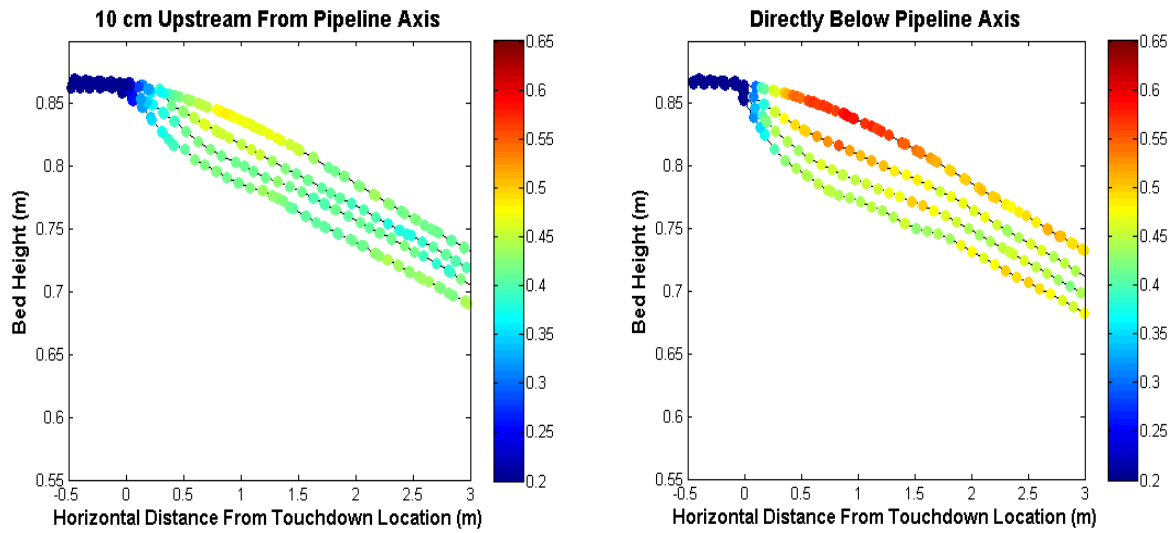


Figure 5-24. Time changing bed shear stress (Pa) profiles for the 50 cm/s simulations at 10 cm upstream from the pipeline axis (left), and directly below the pipeline axis (right).

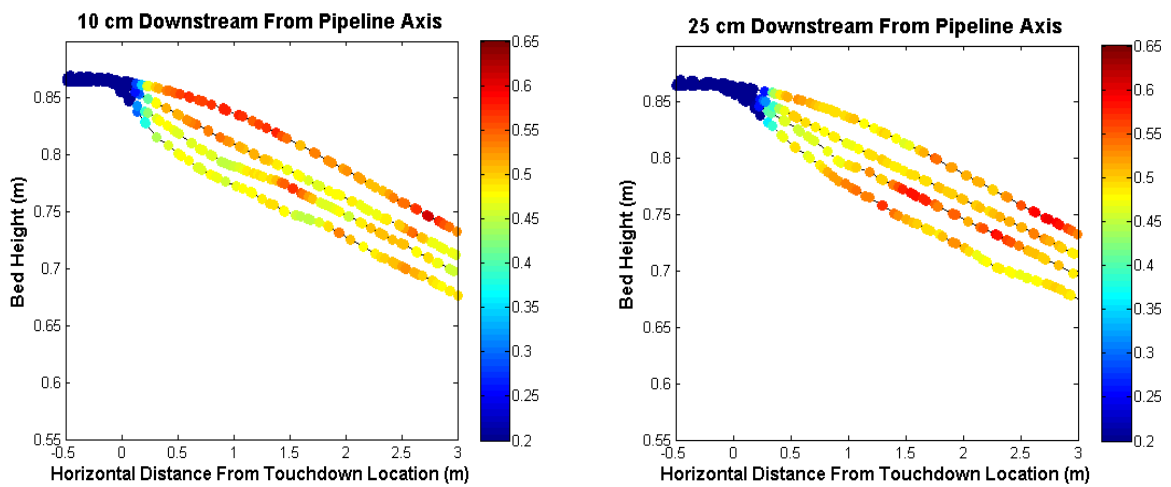


Figure 5-25. Time changing bed shear stress (Pa) profiles for the 50 cm/s simulations at 10 (left), and 25 cm downstream from the pipeline (right).

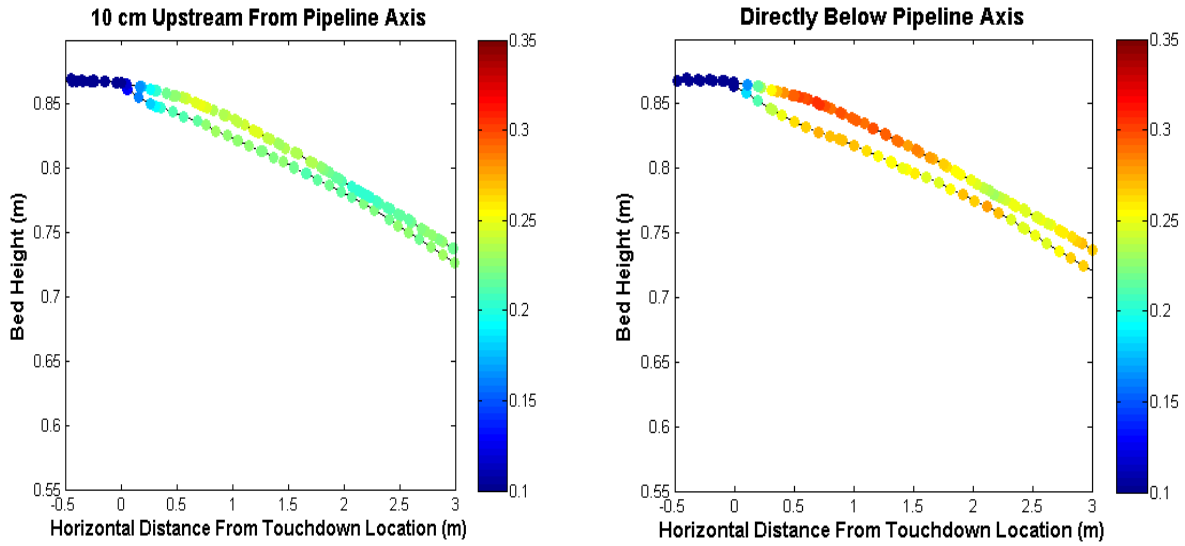


Figure 5-26. Time changing bed shear stress (Pa) profiles for the 35 cm/s simulations at 10 cm upstream from the pipeline axis (left), and directly below the pipeline axis (right).

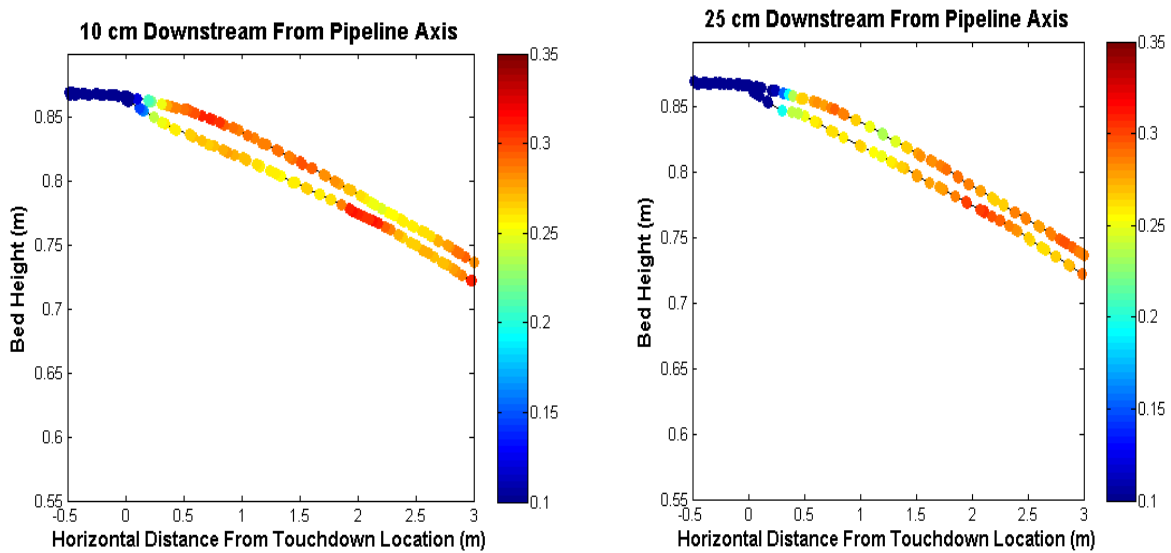


Figure 5-27. Time changing bed shear stress (Pa) profiles for the 35 cm/s simulations at 10 (left), and 25 cm downstream from the pipeline (right)

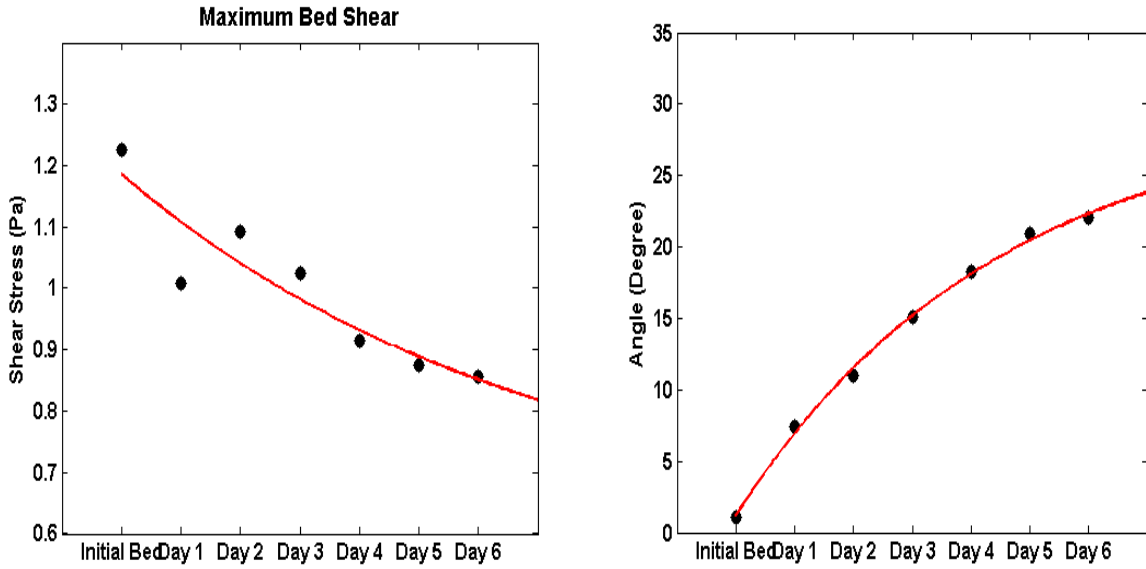


Figure 5-28. Time series of the maximum shear stress (Pa) directly underneath the pipeline (right); and time series of the scour slope (degrees) for the 75 cm/s simulations (left).

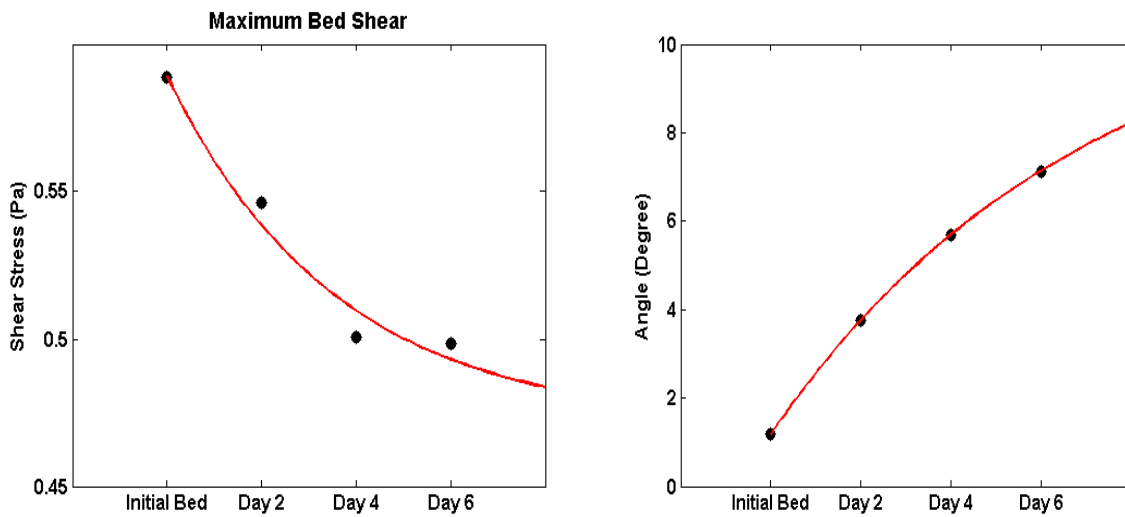


Figure 5-29. Time series of the maximum shear stress (Pa) directly underneath the pipeline (right); and time series of the scour slope (degrees) for the 50 cm/s simulations (left).

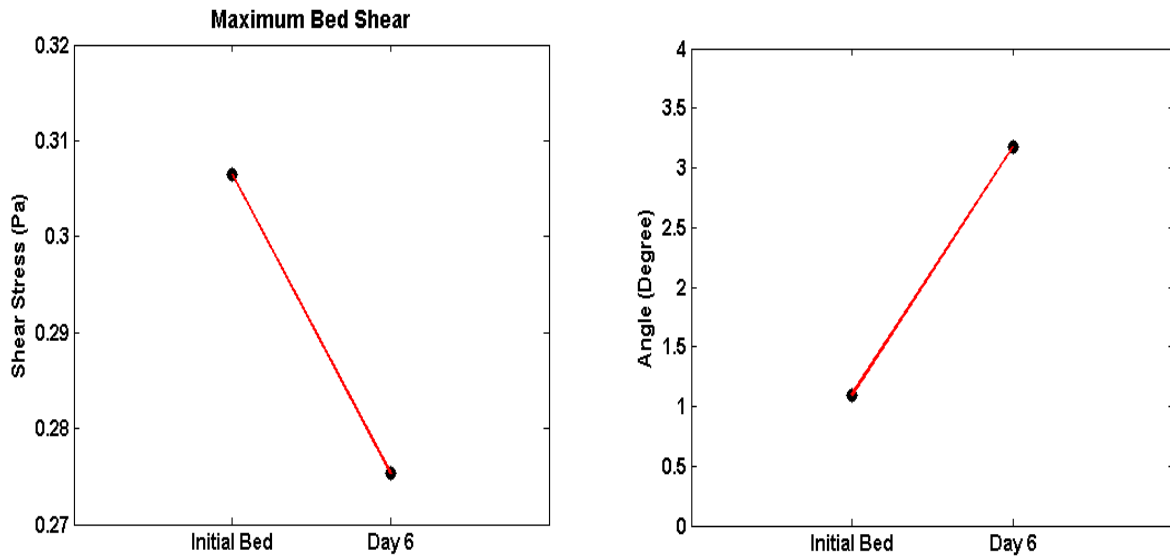


Figure 5-30. Time series of the maximum shear stress directly underneath the pipeline (right); and time series of the scour slope (degrees) for the 35 cm/s simulations (left).

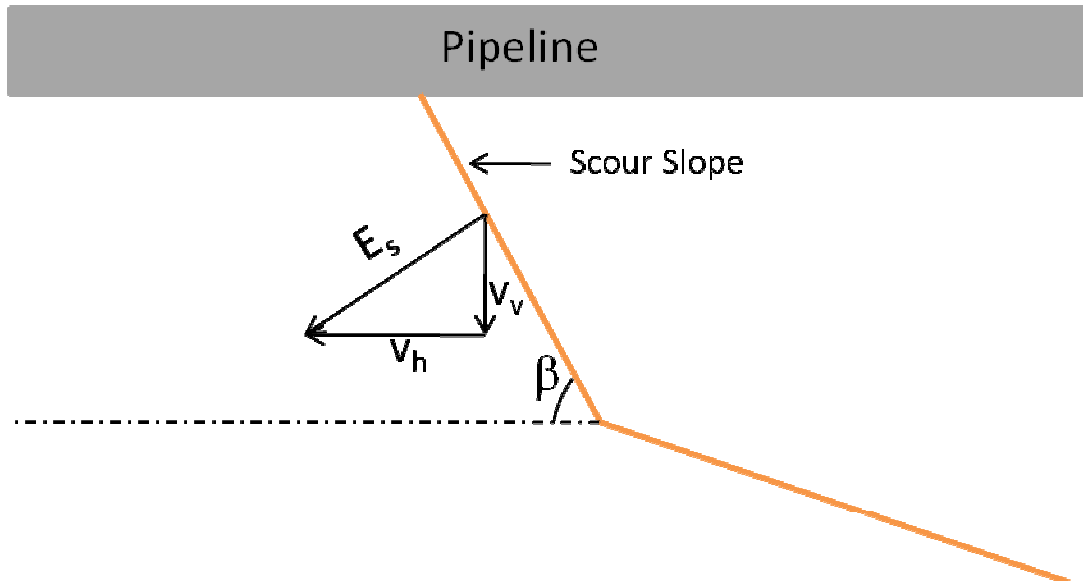


Figure 5-31. Schematic representation of the scour slope relative to the pipeline